UNIVERSIDADE DE LISBOA

FACULDADE DE CIÊNCIAS

DEPARTAMENTO DE QUÍMICA E BIOQUÍMICA

Understanding electronic properties of water: a theoretical approach to the calculation of the adiabatic band gap of liquid water

Paulo Ricardo Castelo Branco
Cabral do Couto

DOUTORAMENTO EM QUÍMICA
(Especialidade em Química Física)

2007

UNIVERSIDADE DE LISBOA

FACULDADE DE CIÊNCIAS

DEPARTAMENTO DE QUÍMICA E BIOQUÍMICA

Understanding electronic properties of water: a theoretical approach to the calculation of the adiabatic band gap of liquid water

Paulo Ricardo Castelo Branco
Cabral do Couto

Tese orientada pelos Professores
Benedito José Costa Cabral
José Artur Martinho Simões

DOUTORAMENTO EM QUÍMICA
(Especialidade em Química Física)

2007

to my Parents,

to Rosário.

Resumo

Apesar de fundamentais para a compreensão do papel desempenhado pela água como participante em reacções químicas e/ou como o meio em que estas ocorrem, as propriedades electrónicas da água em fase condensada são ainda pouco compreendidas. No que diz respeito a propriedades electrónicas, a água líquida pode ser descrita como um isolante ou um semi-condutor e o correspondente potencial de ionização usualmente definido como uma quantidade vertical. Um valor comumente aceite 8.7 ± 0.5 eV. No entanto, a definição de um potencial de ionização para a água líquida depende em ultima análise do conhecimento dos mecanismos elementares de ionização/excitação em fase condensada. Um exemplo bem conhecido e largamente debatido na literatura é a produção de electrões solvatados por fotoabsorção a energias bastante inferiores ($\sim$6.5 eV).

Vários autores sugeriram que a capacidade de reorganização das moléculas de água em torno de espécies neutras e carregadas bem como a natureza reactiva de estados electrónicamente excitados deveriam ser tomados em conta para explicar estas propriedades. Nomeadamente, foi sugerido uma via adiabática para aceder à banda de condução da água líquida, associada à reorganização das moléculas de água em torno do catião hidrónio H_3O^+ e do radical hidroxilo OH, bem como a presença de um electrão deslocalizado. A energia associada a este processo corresponde ao potencial de ionização adiabático da água líquida, $\sim$6.9 eV, J.V. Coe [*Int. Rev. Phys. Chem.* **20**, 33, 2001].

Neste trabalho, é proposta uma estimativa teórica para duas quantidades fundamentais para definir o "band gap" adiabático da água líquida: a entalpia de hidratação do radical hidroxilo e a afinidade electrónica da água liquida. É também avaliada uma metodologia sequencial baseada em métodos do funcional de densidade e simulação Monte Carlo. Como o potencial de ionização adiabático para a água líquida é definido por quantidades macroscópicas, foi também realizado um estudo das popriedades electrónicas de pequenos agregados de moléculas de água como verificação microscópica do quadro adiabático proposto por J.V. Coe.

Abstract

Electronic properties of condensed phase water are not very well understood. They are, however, of fundamental importance for a molecular level understanding of the properties of water as well as the role of water, both as participant and medium where chemical reactions occur. It is generally accepted that bulk water can be described as a lone pair amorphous insulator or a large gap lone-pair amorphous semiconductor and the condensed phase ionization potential defined as a vertical quantity. A usually accepted value is 8.7 $\pm$ 0.5 eV. However, a definition of condensed phase properties such as the condensed phase ionization potential is not straightforward and ultimately dependent our understanding of the elementary mechanisms for ionization/excitation in condensed phase water. A longstanding issue is the concearns the fact that hydrated electrons are produced by photoabsorption at $\sim$6.5 eV.

It has recently been pointed out that the ability of water to reorganize about charged (and neutral) molecules, as well as the reactive nature of electronically excited water molecules, should be taken into account in explaining observed aqueous anion thermochemical and photochemical properties. Moreover, it has been shown that an adiabatic route for accessing the conduction band of liquid water can be defined and that the bottom of the conduction band is characterized by the reorganization of the water molecules around the H_3O^+ cation and OH radical as well as by the presence of a delocalized or quasi-free electron. A $\sim$6.9 eV value was proposed by J.V. Coe [*Int. Rev. Phys. Chem.* 20, 33, 2001], based on known aqueous anion thermochemical and photochemical properties,

The present work presents a theoretical estimate for two key reference quantities required for the quantitative estimate of the adiabatic band gap of pure liquid water as defined by J.V. Coe: the hydration energy of the hydroxyl radical and the electron affinity of liquid water. The hydration of the hydroxyl radical was investigated by microsolvation modeling and statistical mechanics Monte Carlo simulation. The electron electronic density of states and affinity of liquid water was investigated trough a sequential Quantum Mechanical / Monte Carlo methodology. Finally, as the adiabatic approach for a definition of a band gap for pure liquid water is based on macroscopic quantities, a molecular level verification of the adiabatic picture was also undertaken.

Acknowledgments

I am deeply grateful to my supervisors for their inspiring scientific insight and expertise as well as their support, guidance and availability. The scientific stance of both my supervisors has provided me a long sought reference, one which to look up to and strive for in the future. The frequent and long held discussions on ongoing or prospective work were particularly appreciated. I have found these discussions to be the most valuable experience of my formative period as a PhD student.

I am indebted to Professors Hermínio Pires Diogo, José Nuno Canongia Lopes and Manuel Minas da Piedade for welcoming me as a undergraduate student in Centro de Química Estrutural at Instituto Superior Técnico and for patiently waiting for the completion of this thesis to resume unfinished work.

I would also like to thank my colleagues Rita Guedes, Sofia Godinho and Sílvia Estácio for fruitful colaborations and frienship which, along with newly arrived students Nuno Galamba, Filipe Agapito and Margarida Mateus as well as students from other groups, Rosário Ramos, Maria João Oliveira, Pamela Pacciani, Alexandra Spire, Dominique Bang, and Etienne Grossman, have greatly contributed to make these last few years an enriching personal and scientific experience.

Our IT Guru José Esteves cannot be left unmentioned for his help and availability no matter how late in the evening or early in the morning.

I would also like to express my deepest gratitude to Rui Meira, Jacqueline Mercado, the Meira and Azevedo family for their friendship, caring, and for always making me feel I had a home away from home.

I am also grateful to my former workplace colleague Miguel Campos for his friendship, advice, and inspiring ethical and professional standards.

My thanks to Sílvia, Margarida and Filipe for help on this last strech.

The financial support of Fundação para a Ciência e Tecnologia is gratefully aknowledged.

Publication list

Publications included in this thesis

- Paper I - "The hydration of the OH radical: Microsolvation modeling and statistical mechanics simulation", P. Cabral do Couto, R.C. Guedes, B.J. Costa Cabral, J.A. Martinho Simões, *Journal of Chemical Physics* 119, 7344-7355, 2003.

  The author performed all $OH(H_2O)_n$ quantum chemical calculations and related analysis, actively participated in the analysis of Monte Carlo simulation results, planning, bibliographic research and writing of the manuscript.

- Paper II - "The Kohn-Sham density of states and band gap of water: From small clusters to liquid water", P. Cabral do Couto, S.G. Estácio, B.J. Costa Cabral, *Journal of Chemical Physics* 123, 054510, 2005.

  The author performed all quantum chemical calculations and related analysis, planning, bibliographic research, and actively participated in the writing of the manuscript.

- Paper III - "Electronically excited water aggregates and the adiabatic band gap of water", P. Cabral do Couto, B.J. Costa Cabral, *Journal of Chemical Physics* 126, 014509, 2007.

  The author performed all quantum chemical calculations and related analysis, planning, bibliographic research and actively participated in the writing of the manuscript.

Publications not included in this thesis

- "Electron binding energies of water clusters. Implications for the properties of liquid water", P. Cabral do Couto, B.J. Costa Cabral, S. Canuto, *Chemical Physics Letters* 429, 129-135, 2006.

- "S-H bond dissociation enthalpies: The importance of a complete basis set approach", P. Cabral do Couto, B.J. Costa Cabral, J.A. Martinho Simes, *Chemical Physics Letters* 421, 504-507, 2006.

- "The enthalpy of formation of the pentane-2,4-dionate radical: A complete basis set approach", P. Cabral do Couto, B.J. Costa Cabral, J.A. Martinho Simões, *Chemical Physics Letters* 419, 486-491, 2006.

- "Photochemistry of AgCl-water clusters: Comparison with Cl^--water clusters", S.S.M.C. Godinho, P. Cabral do Couto, B.J. Costa Cabral, *Chemical Physics Letters* 419, 340-345, 2006.

- "Polarization effects and charge separation in AgCl-water clusters", S.S.M.C. Godinho, P. Cabral do Couto, B.J. Costa Cabral, *Journal of Chemical Physics* 122, 044316, 2005.

- "Charge separation and charge transfer to solvent (CTTS) in NaCl-water clusters", S.S.M.C. Godinho, P. Cabral do Couto, B.J. Costa Cabral, *Chemical Physics Letters* 399, 200-205, 2004.

- "The energetics of the intramolecular hydrogen bonding in di-substituted benzene by the ortho-para method", S.G. Estácio, P. Cabral do Couto, B.J. Costa Cabral, M.E. Minas da Piedade, J.A. Martinho Simões, *Journal of Physical Chemistry A* 108, 10834-10843, 2004.

- "Homolytic dissociation in hydrogen-bonding liquids: Energetics of the phenol O-H bond in methanol and the water O-H bond in water", S.G. Estácio, P. Cabral do Couto, R.C. Guedes, B.J. Costa Cabral, J.A. Martinho Simões, *Theoretical Chemistry Accounts* 112, 282-289, 2004.

- "The density of states and band gap of liquid water by sequential Monte Carlo / Quantum Mechanics simulation", P. Cabral do Couto, R.C. Guedes, B.J. Costa Cabral, *Brazilian Journal of Physics* 34, 42-47, 2004.

- "Binding energy, structure, and vibrational spectra of $(HCl)_{2-6}$ and $(HF)_{2-10}$ clusters by Density Functional Theory", R.C. Guedes, P. Cabral do Couto, B.J. Costa Cabral, *Journal of Chemical Physics* 118, 1272-1281, 2003.

- "Phenol O-H bond dissociation in water clusters", P. Cabral do Couto, R.C. Guedes, B.J. Costa Cabral, J.A. Martinho Simões, *International Journal of Quantum Chemistry* 86, 297-304, 2002.

Other publications

- "An all-atom force field for metallocenes", J.N. Canongia Lopes, P. Cabral do Couto, M.E. Minas da Piedade, *Journal of Physical Chemistry A* 110, 13850-13856, 2006.

Foreword

The work presented in this thesis was carried out in the Mathematical Physics Group and Molecular Energetics Group, under the supervison of Prof. Benedito José Costa Cabral and Prof. José Artur Martinho Simões.

The body of the present thesis rests on three selected papers, framed within a specific context: the electronic structure of liquid water. The topics covered in the remaining papers, also published during my formative period as a PhD student, mirror the diverse and stimulating scientific environment I was fortunate to find on both groups. Although not focused in one particular subject, I have found this open approach to chemistry has worked to my advantage since the understanding gained as each chemical problem got worked out was proven, more often than not, to result in new opportunities and fresh insight into other chemical problems. Naturally, the perspective by which the subject of the present thesis is approached draws on much of this work. It is however an incomplete view on this subject due to the endless ways the relation between electronic structure, intermolecular interactions and properties can be explored.

This thesis is structured as follows:

- A brief overview of hydrogen bonding, hydrogen bonding in water as well as its consequences on bulk water electronic structure is presented in Chapter 1. A brief discussion on the electronic properties of liquid water as discussed by J.V. Coe [*Int. Rev. Phys. Chem.* **20**, 33, 2001] is also presented. This provides the necessary background based on which the scope and purpose of the present thesis is presented.

- A brief outline of computational methods is presented in Chapter 2. Although an effort has been made to be succinct, and at the same time, cover the relevant issues and methodologies, many aspects and details have inevitably been left out.

- A brief introduction and relevant results in each paper I-III are presented in Chapters 3-5.

- In Chapter 6, a summary of the main results and a brief discussion on future perspectives is presented.

A deliberate effort was made to avoid duplication of information or discussions already contained in Papers I-III. Emphasis was placed on background information required to a clear understanding of the goals and motivation of the present thesis.

Contents

List of Figures

Chapter 1

General introduction

> "Water's H2O, hydrogen two parts, oxygen one, but there's also a third thing, that makes it water and nobody knows what that is."
>
> D.H. Lawrence, Pansies, 1929

Understanding and predicting the chemical and physical transformations of matter in terms of its constituent atoms and molecules, or in other words, bridging quantum and classical reality, is one of the major challenges in chemical sciences [1–6]. In the case of water, the motivation is particularly clear: although it is phenomenologically well known that water is implicated in geological, biological, and chemical scale processes [7], a molecular level understanding of such phenomena is yet to be fully attained [8–14]. This is clearly illustrated by the current status of computer simulation of water: the construction of a simple model, able to accurately predict the properties of water in a broad range of environments and thermodynamic conditions has proven to be an elusive goal [14–21]. Condensed matter properties are size dependent [22–24], and thus arise from the collective behavior of a critical number of atoms or molecules, below which, such properties are not observed [2]. The question of whether and how properties depend on system size, originally posed by Lord Kelvin in 1871 regarding the melting temperature of small particles (clusters or finite aggregates of $2-10^4$ atoms or molecules), can be reformulated in a broader context as: "What is the minimal cluster size for which its properties become size invariant and do not differ in any significant way from those of the macroscopic sample of the same material?" [23]. The answer obviously depends on the property under consideration and the chemical species involved [23–25]. An illustrative example of size-dependence is the transition from disordered to bulk-like structural patterns in clusters: the onset of structural order in water clusters requires a few hundred molecules [26], whereas it occurs for a few tenths of molecules in CO_2 clusters [26], and does not seem to occur up to $\sim 10^5$ atoms in argon clusters [27]. Conversely, as the result of collective behavior, the properties of the interacting species are modified, as illustrated by the increase of the molecular dipole moment in water clusters as cluster size increases [28].

This cyclic causality relationship highlights a well known fact: the description of intermolecular interactions and its consequences on both molecular and macroscopic properties is ultimately an electronic many-body problem [5,6].[1] Therefore, a detailed knowledge of the relation between hydrogen bonding and ground/excited state electronic structure, both from a molecular [29–31] and macroscopic [32–35] perspective, is of fundamental importance for an understanding of the properties of water as well as its role, both as participant and medium where chemical reactions occur [36, 37].

[1] The many-body problem may be defined as the study of the effects arising from the interaction between n particles (molecules or electrons) on the behaviour of a n-particle system, e.g. a drop of water or a water molecule, in terms of its constituent water molecules or electrons and nuclei, respectively. In either case, the behaviour of such systems cannot be easily described since the number of degrees of freedom increases rapidly with system size.

1.1 Hydrogen bonding

The concept of hydrogen bonding is usually associated to the early work of Huggins [38, 39], Lewis [40], Latimer and Rodebush [41], as well as Pauling [42]. Due to its central role in the properties of both molecular liquids [8, 9] and crystals [43, 44], biomolecules [44,45] and both the properties and reactivity of molecules in solution [10, 46], the hydrogen bond has long been the subject of continued and intense experimental and theoretical work [47–51].

1.1.1 Definition and nature of the hydrogen bond

According to the International Union of Pure and Applied Chemistry (IUPAC), the hydrogen bond is currently defined as [52]:

> "A particular type of *multicenter (three center - four electron bond)* X−H$\cdots$Y in which the central hydrogen atom covalently linked to an electronegative atom X (C,N,O,S$\cdots$) forms an additional weaker bond with atom Y (N,O,S$\cdots$) in the direction of its lone electron pair orbital. The energy of hydrogen bonds, which is usually in the range of 3-15 kcal/mol (12-65 kJ/mol), results from the electrostatic interaction and also from the *orbital interaction* of the *antibonding* σ^*(X−H)MO of the molecule acting as the hydrogen donor and the *nonbonding* lone electron pair $MO n_Y$ of the hydrogen acceptor molecule."

The energy of an hydrogen bond is not a physical observable and consequently its absolute value cannot be directly measured. However, unlike intramolecular hydrogen bonds [53–56],[2] the energy of a intermolecular hydrogen bond can be derived from the temperature dependence of the equilibrium constant for the association of 1:1 hydrogen-bonded complexes in the gas phase [57]. From the theoretical standpoint, the interaction energy (or binding energy) of two hydrogen-bonded molecules can be obtained within the supermolecular approach [58], where the reference state corresponds to the energy of the non-interacting configuration:

$$\mathrm{X-H+Y} \longrightarrow \mathrm{X-H\cdots Y} \tag{1.1}$$

$$\Delta E = E[\mathrm{X-H\cdots Y}] - E[\mathrm{X-H}] - E[\mathrm{Y}] \tag{1.2}$$

The formation of a hydrogen bond is associated with the change of specific structural, vibrational and electronic properties, the extent of which is usually correlated with hydrogen bond strenght and taken as general criteria for its existence [48, 50].

[2] The theoretical and experimental determination of the energy of an intramolecular hydrogen bond is a challenging problem on its own. Discussions on this subject can be found in Lipkowski et al. [53], Estácio et al. [54], Gromak [55] and Buemi [56].

The red-shift of the ν(X−H) stretch frequency is interpreted as the result of charge transfer from the proton acceptor lone pair MOn_Y to the anti-bonding σ^* (X−H) proton donor molecular orbital, weakening (and thus lengthening) the X−H covalent bond. The extent of red-shift and X−H bond lengthening has been shown to correlate with hydrogen bonding strength. Other structural consequences, such as the shortening of the X$\cdots$Y and the XH$\cdots$Y distances, have also been found to correlate with hydrogen bond strength [48,50]. The electron density redistribution induced by hydrogen bonding leads to a reduction of the electron density associated with the bridging hydrogen. The corresponding NMR ^{1}H downfield shift is found to correlate with the X$\cdots$Y distance [48,50].

Although the concept of hydrogen bonding is almost a century old, the precise definition of what constitutes an hydrogen bond is still under discussion [59–63]. Exceptions to definitions or criteria for the existence of an hydrogen bond are widely known [64–66]. The difficult task of producing an accurate yet comprehensive definition reflects the composite nature of the hydrogen bond [61], which stems from the interplay of interactions that differ in their nature, magnitude, additivity, and both angular and distance dependence [6].

From a theoretical standpoint, the hydrogen bond energy can be partitioned[3] into a pairwise additive term (electrostatic), that arises as if molecular electron distribution remains unchanged upon hydrogen bonding, and non-additive terms (exchange repulsion, polarization, charge transfer and dispersion), which arise from changes in the electronic density induced by intermolecular interaction [67–70]. The focal point of the longstanding controversy on the nature of hydrogen bonding is the relative importance of charge transfer interactions [59,60], often interpreted as covalent. There are however instances where the importance of charge transfer is not disputed, e.g. strong symmetric, single well, three-center four-electron hydrogen bonds as found in enol forms of β-diketones and dicarboxylic acids [71,72], or charged species such as the $[F\text{-}H\text{-}F]^-$ anion [73]. In such cases, proton donor and acceptor become indistinguishable and the distinction between an intermolecular interaction and a chemical bond becomes ambiguous. As hydrogen bonding weakens, it becomes increasingly dispersive [62,74].

Within these borders, theoretical [75–77] and experimental [78–82] results suggest that hydrogen bonding is best described as the result of a continuum of relative contributions from electrostatic, exchange repulsion, dispersion, polarization, and charge transfer interactions, which in turn spans a continuum of energies and properties [61]. A reevaluation of the concept of hydrogen bonding and its relation to intermolecular interactions is well underway [63].

[3] As is the case for the energy of an hydrogen bond, the quantities into which it may be partitioned are not physical observables and their definition is ambiguous. It is thus difficult to determine which partition scheme provides a realistic picture of the nature of hydrogen bonding.

1.1.2 Hydrogen bonding and cooperativity

Cooperative behavior is usually referred to as the deviation from a strictly pairwise additive behavior [6, 50, 83], the latter only observed when the molecular electron density remains unchanged upon intermolecular interaction. For a molecular cluster of size n, the extent of redistribution of molecular electronic density induced by hydrogen bonding (Figure 1.1), hence the extent of non-additivity, can be qualitatively represented by the electronic density difference, $\rho_{D,n}(r)$,

$$\rho_{D,n}(r) = \rho_n(r) - \sum_{i=1}^{n} \rho_i(r) \tag{1.3}$$

where the electron densities of the non-interacting monomers in the equilibrium geometry of the cluster $\rho_i(r)$ are taken as the reference state and ρ_n(r) is the density associated with a cluster of size n [84, 85].

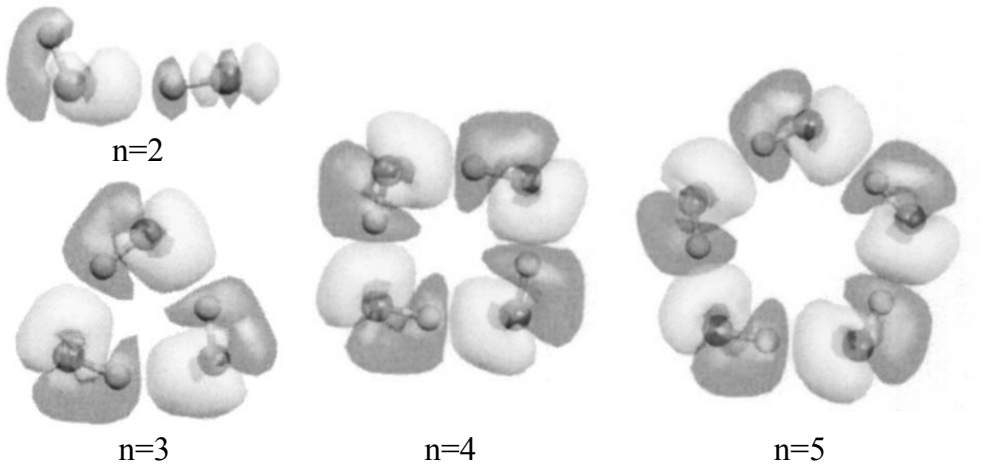

Figure 1.1: Electron density difference for cyclic $(HF)_{2-5}$ clusters. The isosurfaces for $\rho_{D,n}(r)$ correspond to -0.001 (dark) and +0.001 (white) eÅ^{-3} and represent the overall effect of charge depletion (dark) and accumulation (white) induced by hydrogen bonding, relative to the non-interacting monomers. It should be noted that maxima for $\rho_{D,n}(r)$ are size-dependent: 0.03 ($n = 2$), 0.07 ($n = 3$), 0.10 ($n = 4$), 0.08 ($n = 5$), 0.12 ($n = 6$), 0.12 ($n = 7$), 0.12 ($n = 8$) in eÅ^{-3}.

As consequence of electron density redistribution induced by intermolecular interactions, the ability of an hydrogen-bonded molecule to form a hydrogen bond is altered by already existing hydrogen bonds [86], e.g. the electron redistribution in the HF dimer (n=2, Figure 1.1), enhances the proton acceptor and proton donor capabilities of the proton donating and accepting HF molecules respectively .

Manifestations of cooperative behavior are apparent in the size dependence of the stepwise binding energy $\Delta E_{n,n-1}$ (Figure 1.2a), defined as the energy increase per hydrogen bond resulting from the insertion of a monomer into a $n-1$ molecule cluster:

$$(\mathrm{HF})_{n-1} + \mathrm{HF} \longrightarrow (\mathrm{HF})_n \tag{1.4}$$

$$\Delta E_{n,n-1} = E[(\mathrm{HF})_n] - E[(\mathrm{HF})_{n-1}] - E[\mathrm{HF}] \tag{1.5}$$

The variation of $\Delta E_{n,n-1}$ with cluster size (Figure 1.2a) is accompanied by the corresponding trends for structural and vibrational properties (Figure 1.2b), known to be correlated with hydrogen bond strength [50, 83]. It should be noted that in the absence of cooperative effects, $\Delta E_{n,n-1}$ would be a constant and identical to the binding energy of the dimer.

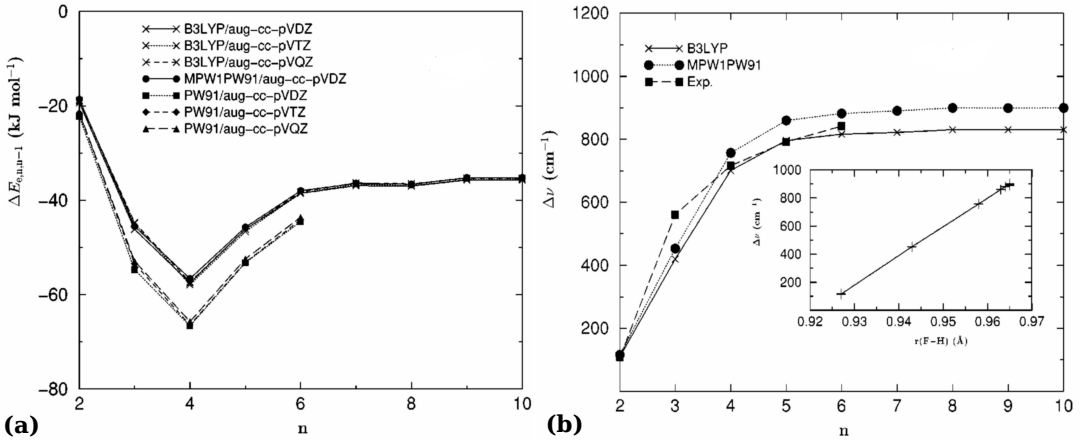

Figure 1.2: a) Stepwise binding energy $\Delta E_{n,n-1}$ (kJ mol^{-1}) vs cluster size n for $(\mathrm{HF})_{2-10}$ cyclic clusters b) Average F−H stretching frequency shift $\Delta\nu$ (cm^{-1}) vs cluster size n in $(\mathrm{HF})_{2-10}$ cyclic clusters. The experimental curve for $\Delta\nu$ vs n was derived from the frequencies reported in Andrews et al., J. Chem. Phys. 84, 3452, 1984. The inset shows $\Delta\nu$ vs the average F−H bond length in Å.

Non-additivity in a cluster of n hydrogen-bonded molecules can be quantitatively accounted for through the decomposition of the total interaction energy ΔE_n into a sum of n-body interaction terms [6, 83]:

$$\Delta E_n = \left\{ \sum_{i=1}^{n} E(i) - nE_{mon} \right\} + \sum_{i<j}^{n} \Delta^2 E(ij) + \sum_{i<j<k}^{n} \Delta^3 E(ijk) + \cdots \tag{1.6}$$

The first term, corresponds to the sum of the energetic cost of monomer geometry deformation, where E_{mon} is the energy of a non-interacting monomer in its minimum energy geometry and $E(i)$ corresponds to the energy of the non-interacting

monomer i in the geometry of the cluster. The second term corresponds to the sum of unique two-body interaction energies $\Delta^2 E(i,j)$, defined as:

$$\Delta^2 E(i,j) = E(ij) - \{E(i) + E(j)\} \tag{1.7}$$

where $E(ij)$ is the total energy of an ij dimer in the geometry of the cluster. $E(i)$ and $E(j)$ are the energies of the corresponding non-interacting monomers also in the geometry of the cluster. Similarly, the third term corresponds to the sum of unique three-body $\Delta^3 E(ijk)$ interactions:

$$\Delta^3 E(ijk) = E(ijk) - \{E(i)+E(j)+E(k)\} - \{\Delta^2 E(ij)+\Delta^2 E(ik)+\Delta^2 E(jk)\} \tag{1.8}$$

Analogous expressions can be readily written for the remaining n-order terms. In a recent energy decomposition study of the interaction energy for $(HF)_{2-8}$ cyclic clusters [87], the calculated total monomer deformation energy for $n = 3-8$ accounts for 3% to 15% of the total interaction energy. Most importantly, the total contribution of non-additive interactions accounts for 21% ($n = 3$) to as much as 56% ($n = 8$) of the total interaction energy.

Many-body or cooperative effects, and the ensuing deviation from a strictly pairwise additive behavior, constitutes a departure from the classical electrostatic picture of hydrogen bonding interactions. The accurate description of such effects is a fundamental requirement for the prediction and understanding of the properties of hydrogen bonded systems [6, 43, 50, 83].

1.1.3 Hydrogen bonding in water

The lack of a clear picture for the nature of hydrogen bonding and the high cost of an accurate account of many-body effects inevitably leads to an incomplete understanding of condensed phase properties of hydrogen bonded systems. Such shortcomings are also apparent in the understanding of the properties of condensed phase water [13–15]. Such an understanding requires a quantitative knowledge of how both molecular properties and interactions, evolve onto bulk properties, with the degree of association and thermodynamic conditions.

The water molecule

The water molecule belongs to the C_{2v} symmetry group, i.e. it has a two-fold rotation axis (x axis) and two mirror planes: a xy plane, where each hydrogen atom is covalently bonded to oxygen, and a xz plane perpendicular to the molecular plane. The experimental gas phase O−H bond length and H−O−H angle is 0.95718 Å and 104.474°, respectively [9]. The total electron density has an uneven distribution along the two-fold symmetry axis, mainly centered around the oxygen

atom, giving rise to a dipole moment of 1.854 D [88]. Upon condensation, the average intramolecular covalent O−H bond length and bond angle in liquid water increase to 0.970 Å and 106.1° [89]. The molecular dipole moment is estimated to be 2.9±0.6 D based on X-ray and neutron diffraction data [90]. Theoretical estimates range from 2.43 to 3.0 D [91–96].

The ground state molecular orbital configuration of an isolated water molecule is $(1a_1)^2(2a_1)^2(1b_2)^2(3a_1)^2(1b_1)^2$ [9] (Figure 1.3). The two lowest occupied molecular orbitals $1a_1$ (core) and $2a_1$ (inner valence) correspond mainly to contributions from the atomic O1s, O2s and H1s atomic orbitals respectively. In the outer valence region, the two lowest energy occupied molecular orbitals, $1b_2$ and $3a_1$, the result of a linear combination of O2p_y and O2p_x with H1s atomic orbitals respectively, are bonding in character, whereas the highest energy occupied molecular orbital $1b_1$ (HOMO) corresponds to the O2p_z atomic orbital and is thus nonbonding in character. The two lowest energy unoccupied orbitals, $4a_1$ (LUMO) and $2b_2$, correspond to the antibonding counterparts of the occupied valence orbitals $2a_1$ and $1b_2$ respectively.

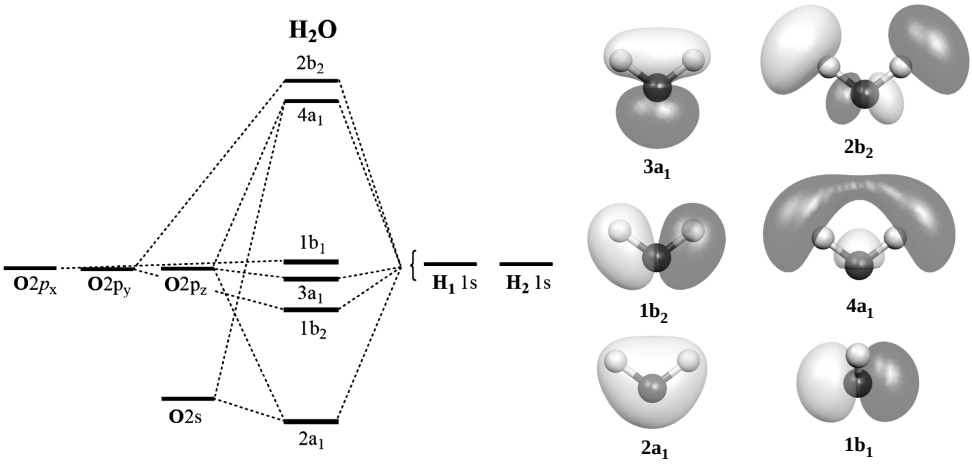

Figure 1.3: Electron isodensity surfaces for valence and unoccupied molecular orbitals of the water molecule.

The continuous charge distribution around oxygen [97] allows effective hydrogen bonding from tetrahedral to trigonal local geometries [98]. This structural versatility is apparent, as one progresses from a nearly perfect tetrahedral local geometry, ∼109.47° in ice Ih [99], to an average near tetrahedral geometry in liquid water, where water molecules are connected by a random three-dimensional macroscopic hydrogen bond network, giving rise to a broad distribution of local hydrogen bonding configurations with strained or broken hydrogen bonds [100]. Interpretations of experimental data from X-ray and neutron diffraction spectroscopy [100, 101]

and X-ray absorption spectroscopy [31, 102, 103] range from a continuous distribution of local hydrogen bonding configurations ("symmetrical" model, tetrahedral coordination) [101], to the prevalence of specific local hydrogen bond configurations ("asymmetrical" model, chain and/or rings) [31]. The prevailing view is that although liquid water fluctuates through a wide variety of local hydrogen bonding environments, the overall tetrahedral structure is maintained [101]. This view is supported by classical and ab-initio molecular dynamics calculations which predict the observed X-ray absorption spectra and simultaneously an average tetrahedral local structure for liquid water [104–106].

Nature and cooperativity

Water clusters constitute the link between the "bare" hydrogen bond between two water molecules in the gas phase and hydrogen bonding in the condensed phase, and consequently the subject of extensive theoretical and experimental studies [12]. Given the wealth of experimental and theoretical information available, small water clusters also constitute the ideal benchmark system for quantum chemical theoretical models [107–110] and provide the information on which classical potential models can be built and/or tested [111–113].

The nature of hydrogen bonding in water has often been discussed in terms of the partition of the interaction energy of the water dimer [67–70]. However, two-body interactions account for only 70% to 80% of the total interaction energy in larger clusters [114–116] (Figure 1.4 and 1.5).

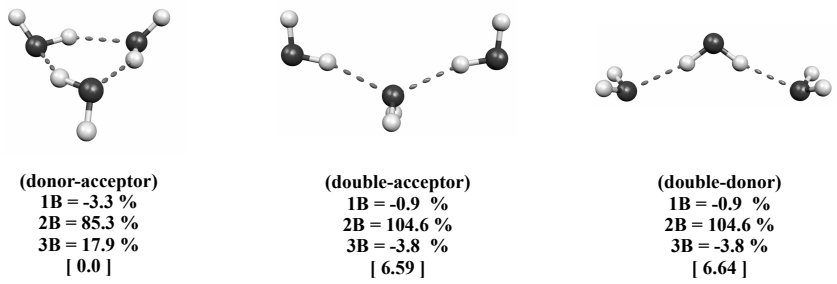

Figure 1.4: Relative stability (square brackets) in kcal mol^{-1} and relative contributions of n-body (nB) interaction terms to the total interaction energy for minimum energy water trimers. Repulsive interactions are presented as a negative percentual. 2B contributions larger than 100% are the result of repulsive nB and 1B contributions. Geometry optimization and many-body decomposition was performed at the B3LYP/6-31+G(d,2p) theory level.

Three-body interactions are found to be by far the largest non-additive contributions which, together with one- and two-body interactions, account for most

of the interaction energy [116]. From the partition of three-body interactions in cyclic water clusters, cooperativity is found to originate from polarization and/or charge-transfer intermolecular interactions [117, 118]. Most importantly, the relative stability of small water clusters and also the magnitude of non-additive interactions depends on the hydrogen bond topology and cluster size [116, 119, 120]. Single donor-acceptor hydrogen bonding patterns are found to be the most stable up to the water pentamer [116] (Figure 1.4 and 1.5). Despite the additional hydrogen bond, the double acceptor-double donor water pentamer minimum energy structure leads to a decrease in the magnitude of three-body interactions and also to lower interaction energies when compared to the corresponding single donor-acceptor cyclic structure (Figure 1.5). A tetrahedral arrangement of five water molecules is also found to be less stable [119].

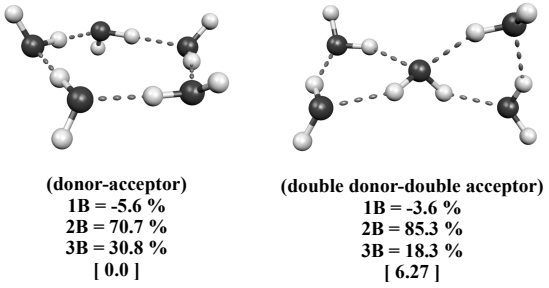

Figure 1.5: Relative stability (square brackets) in kcal mol^{-1} and relative contributions of n-body (nB) interaction terms to the total interaction energy for minimum energy water pentamers. Repulsive interactions are presented as a negative percentual. 2B contributions larger than 100% are the result of repulsive nB and 1B contributions. Geometry optimization and many-body decomposition was performed at the B3LYP/6-31+G(d,2p) theory level.

A discussion on the nature and cooperativity of hydrogen bonding in liquid water in terms of the stability, many-body decomposition, and subsequent partition of n-body interaction energies of minimum energy small water clusters is not straightforward. While some molecular properties are known to converge rapidly to bulk values, e.g. the average hydrogen bond energy, other properties, e.g. the average binding energy per water molecule, show a slow convergence [108]. Such properties have a specific size dependence that leads to a non-monotonous variation of cluster properties with size [23, 24]. Moreover, the statistical nature of the liquid phase implies that hydrogen-bonded molecules are likely to be found far from the minimum energy configurations. Hence interaction energies, magnitude and relative contributions of many-body interactions are expected to decrease when compared with minimum energy structures [121–124].

As initially stated, an understanding of hydrogen bonding and properties of the bulk phase requires a quantitative and detailed knowledge of both intermolecular interactions and molecular properties as well as their dependence with size. Although the study of small water clusters, either in their minimum energy geometries or sampled from simulation, provide valuable information on the underlying physical effects at play in hydrogen bonding and constitute means of insight into the properties of liquid water, the actual picture is far more complex. An understanding of condensed phase water properties, cooperative behaviour and the nature of hydrogen bonding in liquid water requires a quantitative knowledge of how many-body interactions depend on thermal disorder [125] and cluster size [126].

Experimental results suggest some degree of covalency in condensed phase water [81, 82], interpreted as electron sharing between a_1 symmetry valence orbitals or coordinate-covalent bonding [30] or as the result of charge transfer from the lone pair orbital $1b_1$ to empty anti-bonding ($4a_1$ or $2b_1$) orbitals of neighboring water molecules [127, 128]. The current perception is that $3a_1$ and/or $1b_1$ molecular orbitals are involved in hydrogen bonding.

1.2 Hydrogen bonding and electronic structure

Hydrogen bonding and cooperative behavior in condensed phase water can be understood in terms of the electron density redistribution induced by intermolecular interactions and its dependence on local hydrogen bonding patterns [115, 116]. Therefore, changes in the electronic structure of interacting water molecules are dependent on the local hydrogen bonding environment [29,30,102]. Consequently, when compared with the gas phase, electronic energy levels in liquid water are broadened, as observed by photoelectron emission spectroscopy [32, 33] and computer simulation [129–132] (Figure 1.6). Broadening of electronic energy levels can be understood as the result of:

- Electronic broadening: electronic energy level splitting due to electron density redistribution induced by intermolecular interactions.
- Thermal broadening: the statistical distribution of local hydrogen bonding environments in liquid water.

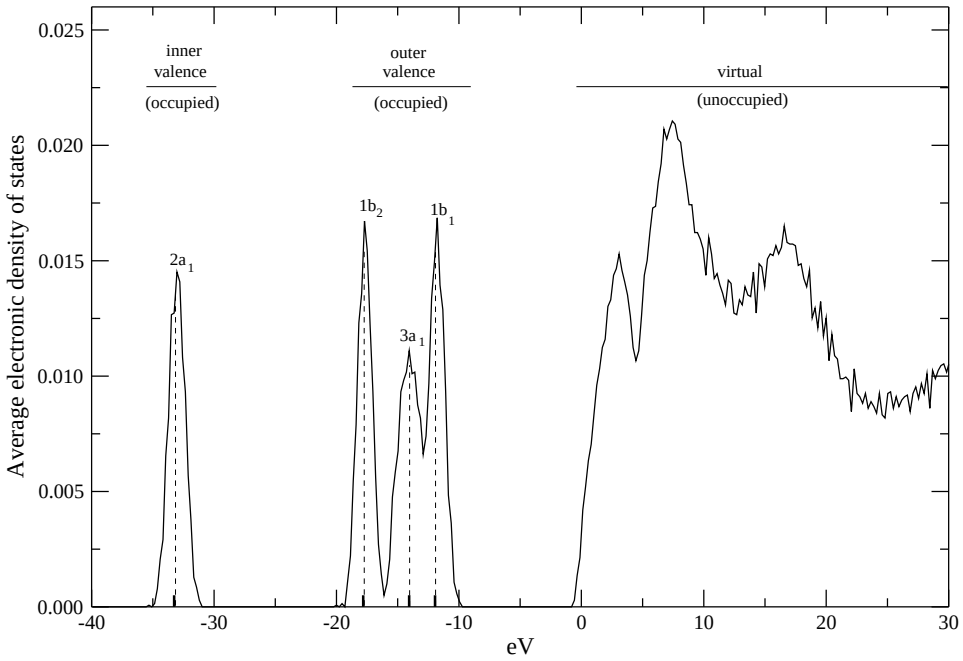

Figure 1.6: Theoretical electronic density of states for valence (occupied) and virtual (unoccupied) states averaged over 50 uncorrelated $(H_2O)_{30}$ configurations sampled from liquid water Monte-Carlo simulation using the TIP5P intermolecular potential (solid lines). The inner and outer valence electronic energy levels for an isolated water molecule in the TIP5P geometry are represented as dotted lines.

Calculations by Hunt et al. [129], suggest that electronic broadening is dominant, although thermal broadening is found to be of comparable magnitude. Band (or peak) positions associated to each valence molecular orbital are also red-shifted, when compared with the gas phase. The experimental gas-liquid shifts are 1.45±0.05 ($1b_1$), 1.34±0.12 ($3a_1$), 1.46±0.06 ($1b_2$), and 1.72±0.16 ($2a_1$) eV and broadenings are 4.0, 2.1, 1.3 and 1.2 times those in the gas phase [32,33]. The different extent of the specific band peak shift, broadening and overlap underlines the different role each molecular orbital plays in hydrogen bonding [30,32,33].

1.2.1 An optical energy diagram for liquid water

The electronic structure of pure liquid water can be approximately described by a simple band structure, as a lone-pair amorphous insulator or a large gap lone-pair amorphous semi-conductor [34,133,134], where the highest valence electronic energy state (valence band edge) is separated from the lowest virtual electronic energy state (conduction band edge) by a large energy gap (band gap) E_g, as illustrated in Figure 1.7.

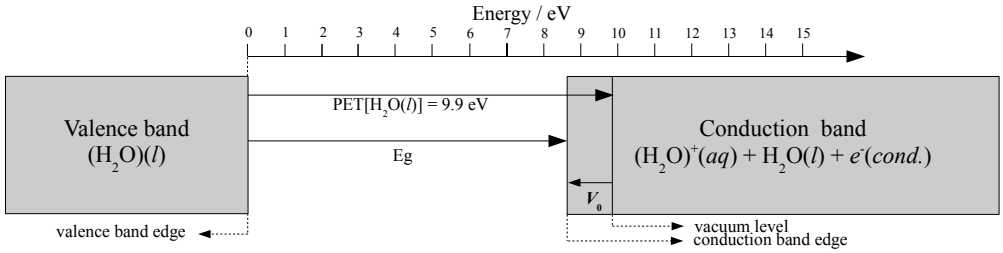

Figure 1.7: A generic semiconductor energy diagram for liquid water. The valence band edge and conduction band edge can be viewed as the condensed phase analog of the highest energy occupied molecular orbital (HOMO) and lowest energy unoccupied molecular orbital (LUMO). The band gap is thus the condensed phase analog of the HOMO-LUMO gap.

The photoemission threshold of pure liquid water PET[$H_2O(l)$] corresponds to the minimum energy required to eject an electron from a liquid water molecule (valence band edge) into vacuum with zero kinetic energy (vacuum level) [32,33]. In common practice, the vacuum level is defined relative to the valence band edge by the photoemission threshold of the pure liquid. A typical reference value is 10.04 eV [135]. A recent estimate based on the extrapolation of the experimental electron binding energies for the $1b_1$ band tail yields an estimate of 9.9 eV [32]. Above the photoemission threshold, at or near the surface of liquid water, the corresponding process can be described as:

$$2H_2O(l) \rightarrow H_2O^+(aq) + H_2O(l) + e^-(g) \tag{1.9}$$

The conduction band edge V_0, is defined relative to the vacuum level, as the energy needed to take a zero kinetic energy electron from vacuum into the conduction band edge as a delocalized quasi-free or conducting electron $e^-(cond.)$. A usual reference value is -1.2±0.1 eV based on photoionization of aqueous indole [133, 136]. A recent estimate based on the extrapolation of hydrated electron cluster ionization data towards bulk, suggests lower values (-0.12$\leqslant V_0 \leqslant$ 0) [35, 137]. Since V_0 is defined relative to the vacuum level, the quantity $-V_0$ is usually referred to as the electron affinity of liquid water.

The optical band gap, E_g, is defined as the energy required to promote an electron from the valence band edge to the conduction band edge as a localized quasi-free or conducting electron $e^-(cond.)$, leaving behind an ionized water molecule $H_2O^+(aq)$ in the geometry of a neutral liquid water molecule.

$$2H_2O(l) \rightarrow H_2O^+(aq) + H_2O(l) + e^-(cond.) \tag{1.10}$$

Within this optical approach E_g is usually associated with the vertical ionization potential of pure liquid water and computed as:

$$E_g = PET[H_2O(l)] + V_0 \tag{1.11}$$

Depending on the value chosen for V_0 and $PET[H_2O(l)]$, the vertical band gap for pure liquid water can be placed within the $8.7-10.04$ eV range. A generally accepted value is 8.7±0.5 eV [138].

1.2.2 The anion problem

Similarly to crystalline semi-conductors, the band gap in liquid water can be occupied by defects such as the hydrated electron $e^-(aq)$ [139] or the hydroxide anion $OH^-(aq)$ [35, 137]. Within an "optical" generic semiconductor energy diagram, anionic defects can be readily located below vacuum level by the corresponding photoemission thresholds. However, the attempt to reconcile known aqueous anion thermochemical and photochemical properties within an "optical" generic semiconductor energy diagram leads to well known inconsistencies.

Removal of an electron from an anionic defect $X^-(aq)$, leaves the resulting neutral species, $X(aq)$, far from its minimum energy structure. The final state resulting from the complete relaxation of solvent molecules about $X(aq)$ defines the vacuum level, whereas the adiabatic reattachment of an electron to this vacuum level structure, restoring the initial anionic defect structure, corresponds to the bulk adiabatic electron affinity $AEA_\infty[X(aq)]$. Accordingly, an anionic defect $X^-(aq)$ (X= e^-, I^-, Br^-, Cl^-, F^-, OH^-) can be located below vacuum level by the bulk adiabatic electron affinity of the corresponding neutral species, $AEA_\infty[X(aq)]$ trough a thermodynamical cycle, as described by Coe et al. [35]:

$$\begin{array}{ccccc} \mathrm{X}^-(g) & \xrightarrow{\mathrm{AEA}[\mathrm{X}(g)]} & \mathrm{X}(g) & + & e^-(g) \\ \downarrow \Delta E_{hyd}[\mathrm{X}^-] & & \downarrow \Delta E_{hyd}[\mathrm{X}] & & \\ \mathrm{X}^-(aq) & \xrightarrow{\mathrm{AEA}_\infty[\mathrm{X}(aq)]} & \mathrm{X}(aq) & + & e^-(g) \end{array}$$

where $\Delta E_{hyd}[\mathrm{X}^-]$ is the hydration energy of the anion defect, $\Delta E_{hyd}[\mathrm{X}]$ the hydration energy and $\mathrm{AEA}[\mathrm{X}(g)]$ the gas phase adiabatic electron affinity of the corresponding neutral species.

$$\mathrm{AEA}_\infty[\mathrm{X}(aq)] = -\Delta E_{hyd}[\mathrm{X}^-] + \mathrm{AEA}[\mathrm{X}(g)] + \Delta E_{hyd}[\mathrm{X}] \tag{1.12}$$

From Eq.(1.12), using experimental values for $\mathrm{AEA}[\mathrm{OH}(g)] = 1.83$ eV [140], $\Delta E_{hyd}[\mathrm{OH}^-] \approx \Delta H_{hyd}[\mathrm{OH}^-] = -4.970$ eV [141] and the semiempirical estimate for $\Delta E_{hyd}[\mathrm{OH}] = -0.37$ eV by Coe et al. [35], the $\mathrm{OH}^-(aq)$ anionic defect can be placed 6.43 eV below vacuum level (Figure 1.8). Based on this value, the experimental $\mathrm{PET}[\mathrm{OH}^-(aq)] = 8.45$ eV [142] would reach the conduction band ~2 eV above vacuum level.

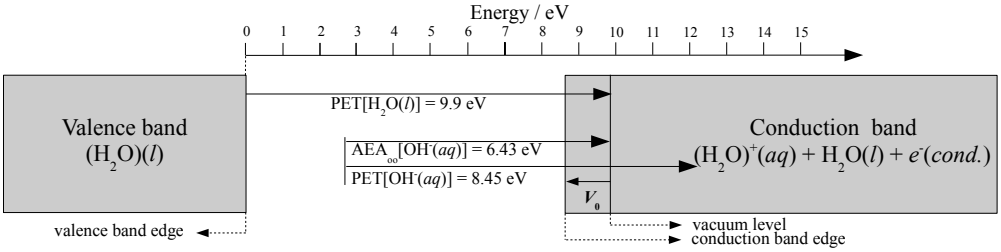

Figure 1.8: Location of the $\mathrm{OH}^-(aq)$ anionic defect below vacuum level.

As $\mathrm{AEA}_\infty[\mathrm{e}^-] = -\Delta E_{hyd}[e^-]$, taking $\Delta E_{hyd}[e^-] \approx \Delta H_{hyd}[e^-] = -1.72$ eV [143], the hydrated electron anionic defect can be placed 1.72 eV below vacuum level [35, 137]. Based on this value, $\mathrm{PET}[\mathrm{e}^-(aq)] = 2.4$ eV [35] would also reach the conduction band above vacuum level (Figure 1.9).

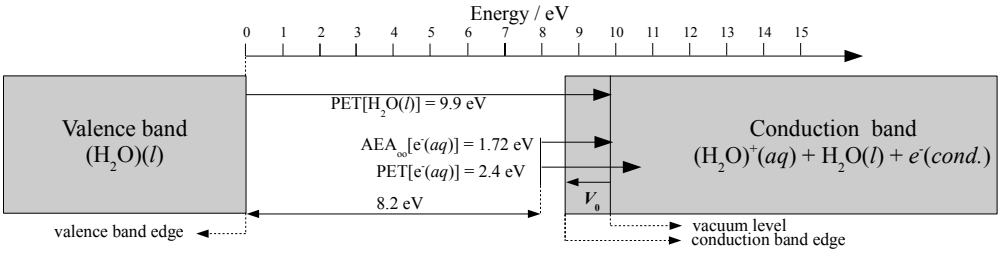

Figure 1.9: Location of the $e^-(aq)$ anionic defect below vacuum level.

Moreover, based on a ∼10 eV PET for pure liquid water, an hydrated electron should only be produced from pure liquid water above ∼8.2 eV. It is however well known that electrons can be produced by photoabsorption at ∼6.5 eV [144, 145]. These and similar discrepancies found for $I^-(aq)$, $Br^-(aq)$, $Cl^-(aq)$ and $F^-(aq)$ anionic defects [35, 137] are collectively known as the anion problem, and show that unlike usually assumed, photoemission thresholds do not determine the vacuum level of pure liquid water.

1.2.3 An adiabatic energy diagram for liquid water

The ability of water molecules to reorganize about charged and neutral defects and the reactive nature of ionized or electronically excited states of water molecules [138, 145–147], suggest that an adiabatic route can be used to define the band gap for for pure liquid water [35, 137]. In order to reconcile known photochemistry and thermochemistry of both pure water and anion aqueous solution, Coe et al. [35, 137] proposed an alternate definition for the band-gap of pure liquid water, (Figure 1.10) where the position of anionic defects depends on a solvent relaxation coordinate and the reactive nature of ionized or electronically excited states is taken into account.

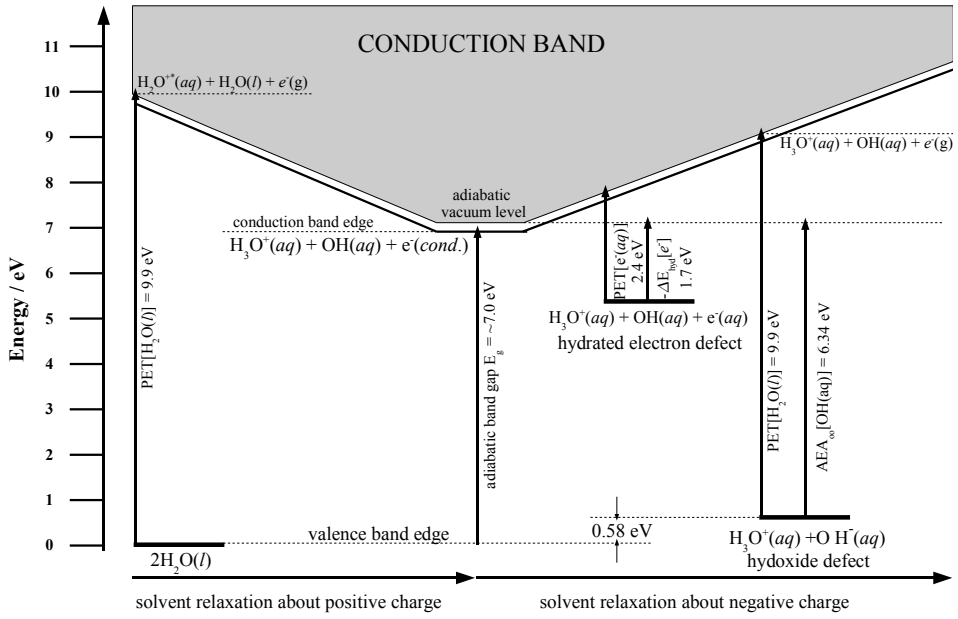

Figure 1.10: An adiabatic semi-conductor bulk energy diagram of water, adapted from Coe et al.. The left-hand side represents the situation already depicted in Figure 1.7: no solvent relaxation or dissociation of the vertically ionized water molecule is considered.

The unstable water cation produced by the vertical ionization/excitation of a valence band water molecule (Figure 1.10, lefthand) undergoes a proton transfer reaction with neighboring water molecules [145, 146].

$$H_2O^+(aq) + H_2O(l) + e^-(cond.) \rightarrow H_3O^+(aq) + OH(aq) + e^-(cond.) \quad (1.13)$$

The adiabatic conduction band edge (Figure 1.10, center) is thus associated with solvent relaxation about the $H_3O^+(aq)$ cation and the $OH(aq)$ radical and the minimum kinetic energy of a delocalized quasi-free conducting electron $e^-(cond.)$. It should noted that there is no solvent relaxation around a quasi-free electron in the conduction band, which otherwise would lead to localization and hence to the electron anionic defect $H_3O^+(aq)$+$OH(aq)$+$e^-(aq)$ (Figure 1.10, righthand) [35, 137].

Since the timescale of solvent relaxation is much larger than the vertical process, the adiabatic conduction band edge is not vertically accessible from the valence band edge, i.e. an adiabatic band-gap cannot be directly measured. However, as much of both thermochemistry and photochemistry of anionic defects is known experimentally, the adiabatic band gap, E_{gap}, can be calculated from their relative energies to the valence band edge and adiabatic band gap of pure liquid water, e.g. as the energy required to get to the hydroxide anionic defect (Figure 1.10, righthand) from the conduction band edge (Figure 1.9, center),

$$H_3O^+(aq) + OH(aq) + e^-(cond) \xrightarrow{E_{gap}} H_3O^+(aq) + OH^-(aq) \quad (1.14)$$

taking into account that the hydroxide anionic defect can be placed 0.58 eV above the valence band edge of pure water by virtue of the temperature dependence of K_W [35, 140] .

$$2H_2O(l) \xrightarrow{\Delta E_r \approx \Delta H_r = 0.58\ eV} H_3O^+(aq) + OH^-(aq) \quad (1.15)$$

Since full solvent relaxation occurs about the hydronium cation in both the conduction band edge and the hydroxide defect, Eq.(1.14) can be rewriten as:

$$OH(aq) + e^-(cond) \xrightarrow{E_{gap}} OH^-(aq) \quad (1.16)$$

The adiabatic bandgap, E_{gap}, can then be readily determined trough a thermodynamic cycle:

$$\begin{array}{ccccc} OH(g) & + & e^-(g) & \xrightarrow{-EA[OH(g)]} & OH^-(g) \\ \downarrow \Delta E_{hyd}[OH] & & \downarrow V_0 & & \downarrow \Delta E_{hyd}[OH^-] \\ OH(aq) & + & e^-(cond) & \xrightarrow{E_{gap}} & OH^-(aq) \end{array}$$

$$E_{gap} = \Delta E_{hyd}[\mathrm{OH}] + V_0 + AEA[\mathrm{OH}(g)] - \Delta E_{hyd}[\mathrm{OH}^-] + 0.58 \approx 7.0e\mathrm{V} \quad (1.17)$$

Although a ~ 7 eV adiabatic band gap is compatible with known pure water and anion defect thermochemistry and photophysics, this estimate rests on two quantities not yet settled: the hydration energy of the hydroxyl radical ($\Delta \mathrm{E}_{hyd}[\mathrm{OH}]$) and the conduction band edge of liquid water (V_0).

1.3 Motivation of this thesis

From the brief overview presented the previous sections, it can be easily seen that the relation between electronic structure, intermolecular interactions and condensed phase properties is a fundamental one and pertains to much of what is understood as chemistry. Since a thourough discussion this subject is beyond the scope of a PhD thesis, we have instead focused on two specific although important aspects which define the motivation and scope of the work developed troughout the present thesis:

- The evaluation of a computationally viable approach for the quantitative prediction of core and valence electron binding energies in liquid water based on density functional methods [130, 148, 149].
- A reevaluation of the two unknowns in Eq.(1.17), namely the hydration energy $\Delta \mathrm{E}_{hyd}[\mathrm{OH}]$ and enthalpy $\Delta \mathrm{H}_{hyd}[\mathrm{OH}]$ of the OH radical as well as the conduction band edge V_0.

Up to this point, although the arguments for an adiabatic picture are founded on a microscopic perspective, the quantitative estimate of the adiabatic bandgap is entirely based on macroscopic properties. However, the question whether the adiabatic picture also holds at the molecular level presents itself naturally. Consequently, a molecular level study of finite size analogs of the valence band edge, conduction band edge and the hydrated electron anionic defect was carried out as a molecular level verification of the adiabatic picture proposed by J.V. Coe.

Chapter 2

Computational methods

Scientific computing has lead to a profound transformation of scientific practice and reasoning, from which the digital computer has emerged as an instrument of research alongside with experiment and theory [4, 150]. In chemistry, those aspects of molecular research that are expedited or rendered practical by the use of computers, can be grouped under the heading of computational chemistry [151].

Computational chemistry methodologies are based on theoretical models, defined as approximate but well defined mathematical procedures [152], that when implemented as a computer program [153, 154], make it possible to quantitatively describe chemical systems [155–165]. According to their theoretical foundations, computational chemistry methods can ultimately be grouped as quantum chemical and simulation methods.

- Quantum chemical methods describe the properties of matter in terms of their constituent electrons and nuclei according to quantum theory, where computations seek approximate solutions to the Schrödinger equation, based on molecular orbital theory [159, 160] or density functional theory [161, 162].

- Simulation methods describe the properties of matter in terms of their constituent atoms or molecules under the rules of classical statistical mechanics, where computations are aimed at predicting macroscopic properties, based on the statistical averaging over the possible microscopic states of the system [163, 164].

Computational chemistry thus spans from microscopic to macroscopic scale, providing a molecular level interpretation of experimental data [31, 166], estimates for properties difficult to obtain from experiment [54, 98] and the testing grounds for theory [167]. The synergy between computation, experiment and theory has accelerated progress in every aspect of chemical sciences and established computational chemistry as an integral part of basic and applied research [150]. Widespread aknowledgement came with the 1998 award of the Nobel prize in chemistry to John Pople for his development of computational methods in quantum chemistry [152] and Walther Kohn for his development of the density functional theory [168].

2.1 Quantum chemical methods

Quantum chemical methods [155–162] seek approximate solutions for the time-independent, non-relativistic molecular Schrödinger eigenvalue equation,

$$\hat{H}\Psi = E\Psi \tag{2.1}$$

where $\hat{H}$ is the Hamiltonian, the wavefunction Ψ one of its eigenfunctions and the energy E the corresponding eigenvalue. In atomic units [52], the Hamiltonian is,

$$\hat{H} = -\sum_{i=1}^{N}\frac{1}{2}\nabla_i^2 - \sum_{A=1}^{M}\frac{1}{2M_A}\nabla_A^2 - \sum_{i=1}^{N}\sum_{A=1}^{M}\frac{Z_A}{r_{iA}} + \sum_{i=1}^{N}\sum_{j>i}^{N}\frac{1}{r_{ij}} + \sum_{A=1}^{M}\sum_{B>A}^{M}\frac{Z_A Z_B}{R_{AB}} \tag{2.2}$$

where i, j refer to electrons and A, B to nuclei, ∇^2 is the Laplace operator, M is the nuclear mass in multiples of the mass of an electron, Z the atomic number, r and R distances between particles. The first two terms are electronic and nuclear kinetic energy operators whereas the remaining terms are potential energy operators which describe Coulomb electron-nuclei, electronic and nuclear interactions.

The central approximation in quantum chemical methods is the adiabatic Born-Oppenheimer approximation [169, 170], where electronic and nuclear motion is decoupled based on the large difference in the mass of nuclei and electrons: the latter move much more rapidly and thus considered to move in the field generated by stationary nuclei. Neglecting nuclear kinetic energy, and taking nuclear repulsion as constant, the original problem is simplified to:

$$\hat{H}_e\Psi_e(\{\mathbf{R}\}) = E_e(\{\mathbf{R}\})\Psi_e(\{\mathbf{R}\}) \tag{2.3}$$

$$\hat{H}_e = \sum_{i=1}^{N}\hat{h}(i) + \sum_{i=1}^{N}\sum_{j>i}^{N}\frac{1}{r_{ij}} \qquad \hat{h}(i) = -\frac{1}{2}\nabla_i^2 - \sum_{A=1}^{M}\frac{Z_A}{r_{iA}} \tag{2.4}$$

where $\{\mathbf{R}\}$ denotes a parametric dependence on nuclear coordinates. The total energy of the system $E_{tot}\{\mathbf{R}\}$, defines a potential energy surface for nuclear motion which holds information on all possible minimum energy structures and all their interconnecting pathways.

$$E_{tot}\{\mathbf{R}\} = E_e\{\mathbf{R}\} + \sum_{A=1}^{M}\sum_{B>A}^{M}\frac{Z_A Z_B}{R_{AB}} \tag{2.5}$$

This provides the fundamental relation between energy and structure, properties, dynamics and reactivity [96, 98, 171]. Consequently, quantities derived from quantum chemical calculations depend on how accurately potential energy surfaces are described.

The ultimate aim of quantum chemical methods can thus be restated as the search for approximate solutions for the electronic Schrödinger equation Eq.(2.3) [172], as implemented in molecular orbital [159, 160] and density functional [161, 162] theory based methods. Subscripts will be dropped henceforth.

2.1.1 Wavefunction methods

Wavefunction methods seek approximate solutions $\tilde{\Psi}$ to Eq.(2.3), based on an expansion of the exact wavefunction Ψ in terms of a superposition of N-electron wavefunctions $\{\Phi_a\}$,

$$\tilde{\Psi} = \sum_a c_a \Phi_a \tag{2.6}$$

each of which expressed as a Slater determinant [173], defined as the antisymmetrized product of orthonormal one-electron wavefunctions $\{\chi_N\}$,

$$\Phi_a = |\chi_1 \cdots \chi_K\rangle = \frac{1}{\sqrt{N!}} \begin{vmatrix} \chi_1(\mathbf{x}_1) & \chi_2(\mathbf{x}_1) & \cdots & \chi_N(\mathbf{x}_1) \\ \chi_1(\mathbf{x}_2) & \chi_2(\mathbf{x}_2) & \cdots & \chi_N(\mathbf{x}_2) \\ \vdots & \vdots & \vdots & \vdots \\ \chi_1(\mathbf{x}_N) & \chi_2(\mathbf{x}_N) & \cdots & \chi_N(\mathbf{x}_N) \end{vmatrix} \tag{2.7}$$

where $1/\sqrt{N!}$ is a normalization constant and $\mathbf{x} = (\mathbf{r}, \omega)$ refers to electronic space and spin coordinates. A Slater determinant describes a system with N indistinguishable electrons (rows) occupying $\chi_1 \cdots \chi_N$ spin orbitals (columns), also referred to as molecular orbitals, each defined as the product of a one-electron spatial function $\psi(\mathbf{r})$ and one of two orthonormal spin functions ($\alpha(\omega)$ or $\beta(\omega)$). The properties of determinants enforce the antisymmetry principle since the exchange of any two rows changes its sign and also the Pauli exclusion principle given that if any two rows are identical the determinant vanishes.

Using Slater-Condon rules [173, 174] and Dirac notation [175], the energy expression for a Slater determinant Φ_a can be written in terms of spin orbitals:

$$E_a = E\left[\{\chi_i\}\right] = \langle \Phi_a | \hat{H} | \Phi_a \rangle = \sum_{i=1}^{N} \langle i | \hat{h} | i \rangle + \sum_{i=1}^{N} \sum_{j>i}^{N} \left[\langle ij | ij \rangle - \langle ij | ji \rangle \right] \tag{2.8}$$

where

$$\langle i | \hat{h} | i \rangle = \int \chi_i^*(\mathbf{x}_1) \hat{h}(\mathbf{x}_1) \chi_i(\mathbf{x}_1) d\mathbf{x}_1 = \mathbf{H}_{ii} \tag{2.9}$$

$$\langle ij | ij \rangle = \int \chi_i^*(\mathbf{x}_1) \chi_j^*(\mathbf{x}_2) r_{12}^{-1} \chi_i(\mathbf{x}_1) \chi_j(\mathbf{x}_2) d\mathbf{x}_1 d\mathbf{x}_2 = \mathbf{J}_{ij} \tag{2.10}$$

$$\langle ij | ji \rangle = \int \chi_i^*(\mathbf{x}_1) \chi_j^*(\mathbf{x}_2) r_{12}^{-1} \chi_j(\mathbf{x}_1) \chi_i(\mathbf{x}_2) d\mathbf{x}_1 d\mathbf{x}_2 = \mathbf{K}_{ij} \tag{2.11}$$

The first term in Eq.(2.8) is a sum of one-electron core integrals $\mathbf{H}_{ii}$ which collects all electronic kinetic energy and Coulomb electron-nuclei attraction potential energy. The second term is a sum of two-electron Coulomb $\mathbf{J}_{ij}$ and exchange $\mathbf{K}_{ij}$ integrals, which collect all electronic repulsion potential energy.

Computational strategies are based on the variation principle [159], which states that if the energy $E[\tilde{\Psi}]$ of an approximate wavefunction $\tilde{\Psi}$ is stationary with respect to an arbitrary variation $\delta\tilde{\Psi}$, then the wavefunction is an eigenfunction of the hamiltonian $\hat{H}$. The corresponding energy $E[\tilde{\Psi}]$ is an upper bound to the exact ground state energy E_0,

$$E[\tilde{\Psi}] = \frac{\langle\tilde{\Psi}|\hat{H}|\tilde{\Psi}\rangle}{\langle\tilde{\Psi}|\tilde{\Psi}\rangle} = \frac{\int \tilde{\Psi}^* \hat{H} \tilde{\Psi} d\mathbf{x}}{\int \tilde{\Psi}^* \tilde{\Psi} d\mathbf{x}} = \frac{\sum_a \mid c_a \mid^2 E_a}{\sum_a \mid c_a \mid^2} \geq E_0 \tag{2.12}$$

where $E[\tilde{\Psi}] = E_0$ only if $\tilde{\Psi} = \Psi_0$. The equality in Eq.(2.12) holds for an expansion over the complete (infinite) set $\{\Phi_a\}$ of eigenfunctions of $\hat{H}$. Altough the variational principle is mostly invoked for the ground state it also applies for excited states, where $E[\tilde{\Psi}_a]$ is an upper bound to the exact energy E_a of the corresponding excited state [176]. In practice a finite expansion is used and approximate solutions are found by making $E[\tilde{\Psi}]$ stationary with respect to variations of the expansion parameters.

The Hartree-Fock approximation

Minimization of $E\left[\{\chi_i\}\right]$ Eq.(2.8) with respect to the choice of spin orbitals, constrained to remain orthonormal, leads to N coupled one-electron eigenvalue equations known as the Hartree-Fock equations [177–180],

$$\underbrace{\left[\hat{h}(\mathbf{x}_1) + \sum_j \left(\hat{J}_j(\mathbf{x}_1) - \hat{K}_j(\mathbf{x}_1)\right)\right]}_{\hat{f}(\mathbf{x}_1)} \chi_i(\mathbf{x}_1) = \varepsilon_i \chi_i(\mathbf{x}_1) \tag{2.13}$$

where the Fock operator $\hat{f}(\mathbf{x}_1)$ is the corresponding one-electron Hamiltonian. The Coulomb operator, $\hat{J}_j$, corresponds to an effective local one-electron repulsion potential due to the average distribution of an electron in the j^{th} spin orbital. As consequence each electron moves in the field generated by the average distribution of all other electrons.

$$\hat{J}_j(\mathbf{x}_1)\chi_i(\mathbf{x}_1) = \left[\int |\chi_j(\mathbf{x}_2)|^2 r_{12}^{-1} d\mathbf{x}_2\right] \chi_i(\mathbf{x}_1) \tag{2.14}$$

The exchange operator, $\hat{K}_j$, corresponds to a non-local potential that arises from the antisymmetric nature of a single determinant wavefunction, associated to the

correlated motion of same spin electrons. Since α and β spin functions are orthogonal, all but same spin integrals $\mathbf{K}_{ij}$ vanish in Eq.(2.8). As exchange integrals $\mathbf{K}_{ij}$ are always positive, the repulsive potential energy $(\mathbf{J}_{ij} - \mathbf{K}_{ij})$ for same spin electrons is lower than for those of different spin. This reflects the reduced probability of finding same spin electrons close to one another. The exchange potential can thus be viewed as a correction to the Coulomb potential due to the Pauli exclusion principle.

$$\hat{K}_j(\mathbf{x}_1)\chi_i(\mathbf{x}_1) = \left[\int \chi_j^*(\mathbf{x}_2) r_{12}^{-1} \chi_i(\mathbf{x}_2) d\mathbf{x}_2\right] \chi_j(\mathbf{x}_1) \tag{2.15}$$

The total electron repulsion potential in Eq.(2.13) is usually denoted as V_{eff}. Since V_{eff}, and thus $\hat{f}$ depends on yet to be determined $N-1$ occupied orbitals, solutions are found via an iterative procedure, starting from an initial guess χ_i from which V_{eff} can be known, Eq.(2.13) solved, and V_{eff} built from the resulting orbitals. Iteration proceeds until the initial and final orbitals differ by less than a predefined threshold, at which point are considered to be eigenfunctions of the Fock operator. The ground state energy can then be readily evaluated by Eq.(2.8) or by Eq.(2.16) where eigenvalues of the Fock operator ε_i are interpreted as orbital energies.

$$E(\mathrm{HF}) = \sum_{i=1}^{N} \varepsilon_i - \frac{1}{2} \sum_{i=1}^{N} \sum_{j=1}^{N} \left[\langle ij|ij\rangle - \langle ij|ji\rangle\right] \tag{2.16}$$

Orbital energies can be related to physical quantities via Koopmans theorem [181], under the assumption that molecular orbitals remain unchanged upon subtraction or addition of an electron. The N lowest energy spin orbitals χ_i are termed as occupied and $-\varepsilon_i$ is interpreted as an approximate vertical ionization potential whereas the remaining higher energy orbitals χ_r are termed as virtual and $-\varepsilon_r$ interpreted as an approximate vertical electron affinity.

$$\varepsilon_i = \langle \chi_i|\hat{f}|\chi_i\rangle = \langle i|\hat{h}|i\rangle + \sum_{j}^{N} \left[\langle ij|ij\rangle - \langle ij|ji\rangle\right] \approx -\mathrm{IP}_i \tag{2.17}$$

$$\varepsilon_r = \langle \chi_r|\hat{f}|\chi_r\rangle = \langle r|\hat{h}|r\rangle + \sum_{i}^{N} \left[\langle ri|ri\rangle - \langle ri|ir\rangle\right] \approx -\mathrm{EA}_i \tag{2.18}$$

Agreement with experiment is dependent on error cancellation, which is most effective for outer valence orbitals, particularly for the highest energy occupied molecular orbital, which corresponds to the molecular ionization potential [182].

The Hartree-Fock approximation thus simplifies the original N-electron eigenvalue equation Eq.(2.3) to N one-electron coupled eigenvalue equations Eq.(2.13) at the cost of an approximate description of electron motion Eq.(2.14). Computational implementations are based on numerical methods, and applications restricted to atoms or small diatomic molecules [183].

The Roothaan-Hall approximation

An efficient computational implementation of the Hartree-Fock approximation is achieved trough the expansion of the spacial component $\psi_i(\mathbf{r})$ of the unknown molecular orbitals χ_i as linear combinations of already known atom-centered one-electron basis functions $\phi_\mu(\mathbf{r})$, often taken as atomic orbitals,

$$\psi_i(\mathbf{r}) = \sum_{\mu=1}^{K} C_{\mu i}\phi_\mu(\mathbf{r}) \tag{2.19}$$

for which Slater functions ($\propto e^{-r}$) are the optimal functional form [184, 185]. Actual implementations make use of gaussian (primitive) functions $\phi^{pgto}(\mathbf{r})$ and linear combinations (contractions) thereof $\phi^{cgto}(\mathbf{r})$, as an approximation to Slater functions and the correct radial behaviour [186]:

$$\phi_\mu^{pgto}(\zeta_\mu, j, k, l, \mathbf{r}) = N(x - x_A)^j(y - y_A)^k(z - Z_A)^l e^{-\zeta_\mu(\mathbf{r}-\mathbf{R_A})^2} \tag{2.20}$$

$$\phi_\mu^{cgto}(\mathbf{r}) = \sum_{p=1}^{L} d_{p\mu}\phi_p^{pgto}(\zeta_{p,\mu}, \mathbf{r}) \tag{2.21}$$

where N is a normalization constant and R_A nuclear coordinates. The exponent parameter ζ defines the size and the integers j, k, l the shape of a primitive gaussian. Since valence orbitals are the most affected by chemical bonding and intermolecular interactions, the contraction scheme can be structured in such a way that the greatest flexibility is allocated to the valence region by assigning multiple contractions to each valence orbital and a single contraction to each core orbital as implemented in segmented [187] split-valence basis sets [188, 189]. The introduction of polarization functions [189, 190], higher angular moment primitives, is also required to describe electron redistribution in a molecular environment, e.g. d- and f-type primitives are used as polarization functions for p-type contractions. Diffuse functions [191, 192], usually small exponent s- or p-type primitives are often necessary, namely for an adequate descrition of lone pairs, anions and excited states. More details on can be found in Ref. [193, 194]. A public repository of gaussian basis sets is available at the Basis Set Exchange database [195].

Expansion of the energy expression of a restricted closed-shell Slater determinant in terms of the atomic basis $\{\phi_\mu\}$ and minimization of the total energy with respect to the variation of the expansion coefficients leads to the Roothaan-Hall matrix equations [196–198].[1]

$$\sum_{\nu=1}^{K} F_{\mu\nu}C_{\nu i} = \varepsilon_i \sum_{\nu=1}^{K} S_{\mu\nu}C_{\nu i} \tag{2.22}$$

[1] or to the Pople-Nesbet equations for a open-shell unrestricted Slater determinant [199]

The resulting set of $(K \times K)$ equations is usually presented in compact matrix notation as

$$\mathbf{FC} = \mathbf{SC}\varepsilon \tag{2.23}$$

where the Fock matrix $\mathbf{F}$ is the representation of the Fock operator in the atomic basis $F_{\mu\nu} = \langle\phi_\mu|\hat{f}|\phi_\nu\rangle$ and $\mathbf{S}$ the overlap matrix between non-orthogonal atomic basis functions $S_{\mu\nu} = \langle\phi_\mu|\phi_\nu\rangle$. The expansion coefficient matrix $\mathbf{C}$ spans the full set of K solutions, where each column $\{C_{\nu i}\}$ corresponds to the expansion coefficients of each doubly occupied molecular orbital ψ_i and ε is a diagonal $K \times K$ square matrix of the corresponding orbital energies ε_K. Solutions are found trough an iterative procedure similar to the already described for the Hartree-Fock approximation, the difference being that the overlap matrix is orthogonalized in intermediate steps in order to bring Eq.(2.23) into true eigenvalue form. An infinite expansion of the molecular orbitals, yields the lowest possible energy within the Hartree-Fock approximation, referred to as the Hartree-Fock limit E_∞(HF) [200].

Therefeore, the Roothaan-Hall approximation simplifies the numerical problem posed by the Hartree-Fock equations to a matrix eigenvalue problem Eq.(2.23), ammenable to efficient computational implementation, at the cost of an approximate description of molecular orbitals Eq.(2.19).

Electron Correlation

The motion of any two electrons is said to be correlated when the joint probability of finding two electrons $\rho(\mathbf{x}_1, \mathbf{x}_2)$ at two given locations is not equal to the product of the individual probability densities $\rho(\mathbf{x}_1)\rho(\mathbf{x}_2)$. Consequently, the two events are not independent. The difference between these two quantities can be ascribed to electron correlation, usually subdivided into Coulomb and Exchange correlation.

- Coulomb correlation is the consequence of instantaneous electron repulsion, which leads to a reduced probability of finding a second electron in the immediate vicinity of another, irrespective of spin.

- Exchange correlation is the consequence of the Pauli exclusion principle, which leads to a reduced probability of finding a second electron in the immediate vicinity of an electron with the same spin.

The more accurately electron correlation is described, the lower the electron repulsion potential energy and the closer the total energy is to the exact value from above, as expected from the variational principle. The energy associated with the correlated motion of electrons is thus a negative quantity and usually defined as the difference between the energy of a system calculated as the minimal value within the Hartree-Fock approximation (i.e. the Hartree-Fock limit) and the exact

nonrelativistic energy of that system [201].

$$E_{corr} = E_{exact} - E_{\infty}(\mathrm{HF}) \tag{2.24}$$

As exchange correlation is already accounted for Eq.(2.15), the above energy difference concearns (dynamic) Coulomb correlation Eq.(2.16). Often, a distinction is made between dynamic and static correlation [202]. Contributions to Eq.(2.24) may also arise from the inadequacy of a single determinant wavefunction, where a single configuration does not provide a qualitatively correct description of electronic structure for degenerate or near-degenerate systems [203]. As such effects are unrelated to short range instantaneous electron repulsion, it is refered to as static or non-dynamic correlation. While dynamic correlation is by definition always present, the contribution from static correlation depends on the chemical problem at hand [204]. Non-degeneracy is assumed troughout the present work.

In wavefunction methods, electron correlation is introduced by the admixture of virtual orbitals into the wavefunction. As the total energy depends only on occupied orbitals Eq.(2.16), electron correlation accounted for by expanding the exact wavefunction as a superposition states, each built by the promotion of electrons from occupied ($\chi_{i,\ldots}$) to virtual ($\chi_{r,\ldots}$) orbitals of the ground state Hartree-Fock wavefunction Φ_0.[2]

Post Hartree-Fock methods

Electron correlation is introduced in a straightforward way in Configuration Interaction (CI) methods [205–209], where the exact wavefunction is expressed as a linear combination of the ground state Hartree-Fock determinant Φ_0 and all unique determinants corresponding to single (S) Φ_i^r, double (D) Φ_{ij}^{rs}, triple (T) Φ_{ijk}^{rst} and higher excitations.

$$\Psi = c_0\Phi_0 + \sum_{i}^{occ}\sum_{r}^{virt} c_i^r\Phi_i^r + \sum_{r<s}^{virt} c_{ij}^{rs}\Phi_{ij}^{rs} + \sum_{i<j<k}^{occ}\sum_{r<s<t}^{virt} c_{ijk}^{rst}\Phi_{ijk}^{rst} + \cdots \tag{2.25}$$

The ground state energy and wavefunction is found by variational minimization of the energy with respect to the expansion coefficients $\{c_0, c_{i\ldots}^{r\cdots}\}$, under the normalization constraint. This leads to the CI matrix eigenvalue equation,

$$\begin{bmatrix} \langle\Phi_0|\hat{H}|\Phi_0\rangle & 0 & \langle\Phi_0|\hat{H}|D\rangle & 0 & \cdots \\ 0 & \langle S|\hat{H}|S\rangle & \langle S|\hat{H}|D\rangle & \langle S|\hat{H}|T\rangle & \cdots \\ \langle D|\hat{H}|\Phi_0\rangle & \langle D|\hat{H}|S\rangle & \langle D|\hat{H}|D\rangle & \langle D|\hat{H}|T\rangle & \cdots \\ 0 & \langle T|\hat{H}|S\rangle & \langle T|\hat{H}|D\rangle & \langle T|\hat{H}|T\rangle & \cdots \\ \vdots & \vdots & \vdots & \vdots & \ddots \end{bmatrix} \begin{bmatrix} c_0 \\ c_i^r \\ c_{ij}^{rs} \\ c_{ijk}^{rst} \\ \vdots \end{bmatrix} = E \begin{bmatrix} c_0 \\ c_i^r \\ c_{ij}^{rs} \\ c_{ijk}^{rst} \\ \vdots \end{bmatrix} \tag{2.26}$$

[2] The single determinant picture, where electrons occupy well defined molecular orbitals with energy ε_i must be abandoned once the wavefuntion is expanded.

where $\langle\Phi_0|\hat{H}|S\rangle = \langle S|\hat{H}|\Phi_0\rangle = 0$ as from Brilouin's theorem [159], singly excited determinants do not mix directly with the ground state. Also, as $\hat{H}$ is a two-electron operator, all contributions to the energy from matrix elements that differ in more than two orbitals are zero [159]. The remaining non-vanishing terms, weighed by the corresponding expansion coefficients, constitute a correlation energy correction. The lowest eigenvalue of the CI matrix is the CI ground state energy and the corresponding eigenvector the expansion coefficients for the CI ground state wave function. In turn, the second lowest eigenvalue corresponds to the CI energy for the first excited state, etç.

Expansion over all possible Slater determinants, within the limits of a finite one-electron basis, is termed as Full CI. The exact energy corresponds to Full CI in the limit of a complete one-electron basis. A computationally viable approach to electron correlation usually requires truncation of both N-electron and one-electron expansion. While on one hand truncated CI methods are variational, which ensures that successive improvement as the CI expansion converges to Full CI from above, on the other, truncation results in incorrect scaling of the correlation energy with system size. In a size-extensive method, correlation energy should scale linearly with the number of interacting particles. While FCI is size-extensive, truncated CI methods are not, due to the absence corrections involving higher excitations, increasingly important as the number of electrons increases. Consequently, the fraction of exact correlation recovered in truncated CI methods decreases as system size increases, leading to incomplete error cancellation in relative energy calculations.

Size-extensive alternatives to CI also involve truncation of the wavefunction expansion at some point. However, truncation of the wavefunction expansion is done so that correct scaling of the correlation energy with system size is enforced. In Coupled Cluster (CC) methods [210–213], all excited Slater determinants are generated by an exponential expansion of the cluster operator $\hat{T}$, defined as a sum of N-fold excitation operators $\hat{T}_N$, where N is the number of electrons.

$$\Psi = e^{\hat{T}}\Phi_0 = \left(1 + \hat{T} + \tfrac{1}{2!}\hat{T}^2 + \tfrac{1}{3!}\hat{T}^3 \cdots \tfrac{1}{n!}\hat{T}^n + \cdots\right)\Phi_0 \tag{2.27}$$

$$\hat{T} = \hat{T}_1 + \hat{T}_2 + \cdots + \hat{T}_N \qquad \hat{T}_N\Phi_0 = \sum_{i<\cdots}^{occ}\sum_{r<\cdots}^{virt} t_{i\cdots}^{r\cdots}\Phi_{i\cdots}^{r\cdots} \tag{2.28}$$

The unknown cluster amplitudes $t_{i\cdots}^{r\cdots}$ are the equivalent to the coefficients in the CI expansion. Each type of correction (S, D, T, ...) is included, trough the amplitudes of (connected) $\hat{T}_N$ and product (disconnected) $\hat{T}_N^n$ excitations. From the expansion of the full cluster operator, and grouping terms according to the associated overall

excitation,

$$\begin{aligned} e^{\hat{T}} =& 1 + \hat{T}_1 + \underbrace{\left(\hat{T}_2 + \tfrac{1}{2}\hat{T}_1^2\right)}_{\texttt{double excitations}} + \underbrace{\left(\hat{T}_3 + \hat{T}_2\hat{T}_1 + \tfrac{1}{6}\hat{T}_1^3\right)}_{\texttt{triple excitations}} \\ &+ \underbrace{\left(\hat{T}_4 + \hat{T}_3\hat{T}_1 + \tfrac{1}{2}\hat{T}_2^2 + \tfrac{1}{2}\hat{T}_2\hat{T}_1^2 + \tfrac{1}{24}\hat{T}_1^4\right)}_{\texttt{quadruple excitations}} + \cdots \end{aligned} \tag{2.29}$$

the advantage of a non-linear expansion is evident. The cluster expansion ensures size-extensivity as truncation eliminates contributions from higher (connected) terms while at the same time retaining contributions from higher excitations trough the amplitudes of lower (disconnected) product terms.

A complementary approach is the Møller-Plesset perturbation method [214,215], where the exact Hamiltonian $\hat{H}$ is partitioned into a unperturbed term $\hat{H}_0$, defined as a sum of one-electron Fock operators and a perturbation potential $\hat{V}$, taken as electron correlation,

$$(\hat{H}_0 + \lambda\hat{V})\Psi = E\Psi \tag{2.30}$$

where λ defines the extent of the perturbation. The exact wavefunction and energy are given as a power series of the perturbation parameter λ.

$$\begin{aligned} \Psi &= \Psi_0 + \lambda^1\Psi_1 + \lambda^2\Psi_2 + \lambda^3\Psi_3 + \cdots + \lambda^n\Psi_n + \cdots \\ E &= E_0 + \lambda^1 E_1 + \lambda^2 E_2 + \lambda^3 E_3 + \cdots + \lambda^n E_n + \cdots \end{aligned} \tag{2.31}$$

Inserting Eq.(2.31) into Eq.(2.30) and collecting the terms of the same order in λ^n yields a set of perturbation equations which can be solved recursively for up to any order n for all (S, D, T, ...) corrections. The order to which energy is corrected defines a hierarchy of methods denoted as MPn. Truncation of the perturbation series also results in a size-extensive method.

Although convergence to Full CI is assumed as the cluster operator expansion Eq.(2.29) or the perturbation series Eq.(2.31) is successively improved, both methods are not variational. Consequently, improvement may not lead to better results and the energy does not necessarily converge to the exact value from above, as is the case of Møller-Plesset methods, where convergence of the perturbation series has been sown to be non monotonic [216, 217].

The possibility of systematic improvement in wavefunction methods allows the prediction of accurate energies (and thus properties) up to any accuracy within the Born-Oppenheimer nonrelativistic time independent approximation, the only limitation being computational power available. However, the introduction of electron correlation brought about by the expansion of the wave function comes at a high price due to the factorial growth of the number of determinants to be evaluated. Usually both the N-electron Eq.(2.25) and one-electron Eq.(2.19)

expansion is truncated. The corresponding error is defined as the error relative to the exact solution whereas, in the limit of complete one-electron basis, the remaining error defines the error associated with an incomplete expansion of the wave function, i.e. the intrinsic error of the theoretical method [218].

2.1.2 Density functional methods

An entirely different approximation to the electron correlation problem is based on Density Functional Theory (DFT) [161, 162], where in contrast with wavefunction methods, the central variable is the electron density $\rho(\mathbf{r})$,

$$\rho(\mathbf{r}) = N \int |\Psi(\mathbf{x}_1, \ldots, \mathbf{x}_N)|^2 d\omega_1 d\mathbf{x}_2 \ldots d\mathbf{x}_N \tag{2.32}$$

which determines the probability of finding any of the N electrons in the volume element $d\mathbf{r}_1$. Such an approach constitutes a considerable simplification since $\rho(\mathbf{r})$ depends on 3 coordinates, independently of N, whereas in wavefunction methods one has to deal explicitely with $4N$ coordinates. The theoretical foundation of density functional methods rests on the Hohenberg-Kohn theorems [219], which demonstrate that any ground state property, e.g. energy, is a functional[3] of the ground state electron density ρ_0,

$$E_0 = F[\rho_0] = E[\rho_0] \tag{2.33}$$

and that the energy of any approximate electron density function $\tilde{\rho}(\mathbf{r})$ is an upper bound to the true ground state energy,

$$E[\tilde{\rho}] \geq E[\rho_0] \tag{2.34}$$

where $E[\tilde{\rho}] = E[\rho_0]$ only if $\tilde{\rho} = \rho_0$. The equality holds for the exact ground state energy if the exact energy functional is known, in which case Eq.(2.34) is equivalent to the variational principle. However, as the first Hohenberg-Kohn theorem Eq.(2.33) only provides proof of the existence of an exact functional, the problem at hand is thus to determine the unknown energy functional $E[\rho]$ and invoke the variational principle in order to determine the ground state energy.

In the approach adopted by Kohn and Sham [220], in which current density functional methods are based, the total energy is regarded as a deviation from a reference, ficticious system of non-interacting electrons, moving in an external potential V_S chosen so that the overall electron density $\rho_S(\mathbf{r})$ is the same as that

[3] Broadly defined, a functional is a function whose domain is a set of functions and denoted as $F[f(x)]$. This concept was implicitely invoked earlier in Eq.(2.12) as the energy can be viewed as a functional of the wavefunction $E[\Psi]$.

of the ground state of the fully interacting system $\rho_0(\mathbf{r})$. Accordingly, the exact reference wavefunction is written as a Slater determinant $\Theta = |\varphi_1 \cdots \varphi_N\rangle$ Eq.(2.7) and spin orbitals $\varphi_i(\mathbf{r})$ are determined by,

$$\hat{h}_{KS}\varphi_i(\mathbf{r}) = \left(-\frac{1}{2}\nabla^2 + V_S(\mathbf{r})\right)\varphi_i(\mathbf{r}) = \varepsilon_i\varphi_i(\mathbf{r}) \tag{2.35}$$

where

$$\rho_S(\mathbf{r}) = \sum_i \sum_\omega |\varphi_i(\mathbf{r},\omega)|^2 = \rho_0(\mathbf{r}) \tag{2.36}$$

The total energy for the fully interacting system can be written as a sum of the electronic kinetic energy $T[\rho]$, electron-nuclei attraction potential $V_{ne}[\rho]$ and electron repulsion potential energies $V_{ee}[\rho]$, each expressed as a functional of the electron density. Relative to the reference system, this sum can be rewritten as,

$$E[\rho] = T[\rho] + V_{ne}[\rho] + V_{ee}[\rho] = T_S[\rho] + V_{ne}[\rho] + V_{ee}[\rho] + \underbrace{\Delta T[\rho] + \Delta V_{ee}[\rho]}_{E_{xc}[\rho]} \tag{2.37}$$

where $T_s[\rho]$ is the kinetic energy of the non-interacting electrons and the exchange-correlation energy $E_{xc}[\rho]$ is defined as the sum of $\Delta T[\rho]$ and $\Delta V_{ee}[\rho]$ which correspond to the deviation of the kinetic energy and electron repulsion energy of the fully interacting system from that of the reference system, respectively.

As the total density of both the reference system and the fully interaction system is chosen to be the same via V_S, the energy functional can be written in terms of the spin orbitals of the reference system,

$$\begin{aligned} E[\rho] =& T_S[\rho] + V_{ne}[\rho] + V_{ee}[\rho] + E_{xc}[\rho] \\ =& T_S[\rho] + \int V_{ne}\rho(\mathbf{r})d\mathbf{r} + \frac{1}{2}\int \frac{\rho(\mathbf{r}_1)\rho(\mathbf{r}_2)}{r_{12}}d\mathbf{r}_1 d\mathbf{r}_2 + E_{xc}[\rho] \\ =& -\frac{1}{2}\sum_i^N \langle\varphi_i|\nabla^2|\varphi_i\rangle - \sum_i^N \int \sum_A^M \frac{Z_A}{r_{1A}}|\varphi_i(\mathbf{r}_1)|^2 d\mathbf{r}_1 \\ &+ \frac{1}{2}\sum_i^N \sum_j^N \int \frac{|\varphi_i(\mathbf{r}_1)|^2|\varphi_j(\mathbf{r}_2)|^2}{r_{12}}d\mathbf{r}_1 d\mathbf{r}_2 + E_{xc}[\rho] \end{aligned} \tag{2.38}$$

where $E_{xc}[\rho]$ is the unkonw exchange-correlation energy functional. Variational minimization of $E[\rho]$ with respect to the choice of spin orbitals, under the constraint that they remain orthogonal, leads to the Kohn-Sham equations,

$$\underbrace{\left[-\frac{1}{2}\nabla_1^2 - \sum_A^M \frac{Z_A}{r_{1A}} + \int \frac{\rho(\mathbf{r}_2)}{r_{12}}d\mathbf{r}_2 - V_{xc}(\mathbf{r}_1)\right]}_{\hat{h}_{KS}}\varphi_i = \varepsilon_i\varphi_i \tag{2.39}$$

which can be regarded as the equivalent of Eq.(2.13) and $\hat{h}_{KS}$ the equivalent of the one-electron operator Fock operator. From Eq.(2.35) and Eq.(2.39), V_S is

$$V_S = -\sum_{A}^{M} \frac{Z_A}{r_{1A}} + \int \frac{\rho(\mathbf{r}_2)}{r_{12}} d\mathbf{r}_2 - V_{xc}(\mathbf{r}_1) \tag{2.40}$$

where $V_{xc}(\mathbf{r}_1)$ is the unknown exchange-correlation potential, for which the E_{xc} is the expectation value.

$$V_{xc}(\mathbf{r}) = \frac{\delta E_{xc}[\rho(\mathbf{r})]}{\delta \rho(\mathbf{r})} \tag{2.41}$$

Similarly to the Hartree-Fock equations, the Kohn-Sham equations are solved iteratively since V_S and thus $\hat{h}_{KS}$ depends on the yet to be determined total electron density. Starting from a initial guess for $\rho(\mathbf{r})$ from which V_S can be known, Eq.(2.39) solved and V_S built from the resulting total electron density Eq.(2.36). Iteration proceeeds until the initial and final densities differ by less than a predefined threshold. The energy is then readily obtained from Eq.(2.38) Also, in the same spirit of the Roothaan-Hall approximation, the introduction of a basis set Eq.(2.19) leads to the equivalent matrix equation Eq.(2.23), which allows a computationally efficient implementation of the Kohn-Sham approach. Also, the eigenvalues ε_i can be interpreted as molecular orbital energies, and the highest occupied orbital energy as the ionization potential, provided that the exact exchange-correlation functional is used [221].

Unfortunately, the major drawback of density functional methods is that the explicit form of $E_{xc}[\rho]$ is unknown and as consequence, so is the exchange-correlation potential $V_{xc}(\mathbf{r})$. Therefore approximations must be made, the most simple of which is the local density approximation (LDA), where it is assumed that the density can be treated locally as a uniform electron gas [219, 220, 222, 223]. However, as in molecular systems the electron density is inhomogeneous, this approach does not yield accurate results. Further improvement is obtained if besides the electron density, the exchange-correlation functional is also made to depend on the gradient of the density. This approach is known as the generalized gradient approach (GGA), based on which the B88 [224] exchange functional or P86 [225], PW91 [226], and LYP [227] correlation functionals were developed.

As coulomb repulsion for the ith electron, Eq.(2.39) third term on the l.h.s, is determined from the total electron density, an electron experiences repulsion of its own density. This self-interaction energy should be offset by an exact exchange-correlation functional. This problem does not arise in the Hartree-Fock approximation as $\mathbf{J}_{ii} = \mathbf{K}_{ii}$ Eq.(2.10-11) both terms cancel out in Eq.(2.16). As exchange contributions are larger than those arising form correlation, accurate exchange energy is a attribute for an exchange-correlation functional. The adiabatic connection

method [228] provides the theoretical framework for the introduction of exact exchange as a way to improve on the results of GGA functionals [229–233]. Exchange energy is usually taken as a combination of LDA, the corresponding gradient correction term and exact exchange where the optimal weigth of each contribution is usually found trough a fit to experimental data [230] or theory [233]. This leads to improvement over GGA functionals as the introduction of exact exchange leads to a partial correction of the self-interaction error [161]. However, although globally leading to accurate results, the amount of exact exchange required for accurate results has been shown not to be the same for all species [234, 235].

Density functional methods recover electron correlation for the same computational cost as the Hartree-Fock method, which extends the range of application of quantum chemical methods to systems that are too large for wavefunction based methods. Unfortunately, there is no systematic way to improve accuracy in density functional methods. Consequently, it is not possible to clearly define the error associated with a given calculation without reference to experimental data or accurate wavefunction methods. Comparison between theory and experiment can be found at the NIST Computational Chemistry Comparison and Benchmark Database [236]

2.1.3 Singly excited states

The basic approach to singly electronically excited states in wavefunction methods is the configuration interaction singles method (CIS) [237–239], where the wavefunction is now expanded as a linear combination of singly excited determinants.

$$\Psi_{CIS} = \sum_{i}^{occ} \sum_{r}^{virt} c_i^r \Phi_i^r \tag{2.42}$$

The corresponding eigenvalue equation can be written in matrix notation as

$$\mathbf{AX} = \omega \mathbf{X} \tag{2.43}$$

where $\mathbf{A}$ is the representation of the Hamiltonian in the singly excited N-electron basis, $\mathbf{X}$ is the matrix of the CIS expansion coefficients and ω is the diagonal matrix of the excitation energies. The general expression for the total energy of a singly excited state is expressed in terms of orbital energies and integrals over molecular orbitals,

$$E_{CIS} = E_{HF} + \sum_{i}^{occ} \sum_{r}^{virt} (c_i^r)^2 (\varepsilon_r - \varepsilon_i) + \sum_{i}^{occ} \sum_{r}^{virt} \sum_{j}^{occ} \sum_{s}^{virt} (c_i^r)(c_j^s)(ir||js) \tag{2.44}$$

where two-electron integrals $(ir||js)$ are represented in mulliken notation. As virtual orbital energies are computed in the average field generated by the ground

state charge distribution of all N electrons Eq.(2.18), excitation energies are usually overestimated from 0.5 to 2 eV when compared with experiment [237, 240]. However, CIS geometries have been shown to yield reliable geometries [241].

Although originally developed in a time-independent formalism, density functional theory was extended to include the description of time-dependent phenomena, where the first Hohenberg-Kohn theorem was generalized to include time-dependent densities and potentials [242]. Similarly to the time-independent formalism, $V_S(\mathbf{r}, t)$ is chosen so that the overall time-dependent electron density of the reference system $\rho_S(\mathbf{r}, t)$ is the same as that of the fully interacting system $\rho(\mathbf{r}, t)$. The corresponding time-dependent Kohn-Sham orbitals $\varphi(\mathbf{r}, t)$ satisfy the time-independent Kohn-Sham equations,

$$i\frac{\partial\varphi(\mathbf{r},t)}{\partial t} = \left[-\frac{1}{2}\nabla^2 + V_S(\mathbf{r},t)\right]\varphi(\mathbf{r},t) \tag{2.45}$$

where

$$\rho(\mathbf{r},t) = \sum_{i}^{N} |\varphi(\mathbf{r},t)|^2 \tag{2.46}$$

Usually the exchange correlation potential is taken as a functional of the density at fixed time t,

$$V_{xc}\left[\rho\right](\mathbf{r},t) \approx V_{xc}\left[\rho_t\right](\mathbf{r}) \tag{2.47}$$

which enables the use of exchange-correlation functionals developed for time-independent density functional theory. Excitation energies are determined within linear response theory [239], namely from the evaluation of the mean dynamic polarizability $\langle\alpha\rangle_\omega$, which describes the response of the dipole moment to a time-dependent electric field, where ω is the frequency of the fluctuation [243].

$$\langle\alpha\rangle_\omega = \sum_{i\neq 0}^{states} \frac{\langle\Psi_0|\mathbf{r}|\Psi_i\rangle^2}{\omega - (E_i - E_0)} \tag{2.48}$$

The numerator of each term term in the summation corresponds to the transition dipole moment whereas in the denominator E_i is the energy of the ith excited state and E_0 the energy of the ground state. In practice, $\langle\alpha\rangle_\omega$ is determined trough the linear response of the charge density to the time-dependent electric field, which diverges when ω is equal to the difference in energy between an excited state and the ground state, i.e. the excitation energy. The photoabsorption spectrum is thus determined as the poles of the dynamic polarizability, which in turn is a function of the frequency of the applied field. Time dependent density functional methods have been proven to be reliable for low-lying valence-excited states [239, 243]. However, the quality of the results strongly depends on the choice of the exchange-correlation functional [239, 244]. Therefore as is the case of the ground state, comparison with experiment or accurate theory is required.

2.2 The sequential approach

Molecular simulation methods provide the means for the prediction of the properties and behaviour of a macroscopic collection of atoms or molecules based on statistically averaging over the possible microscopic states of the system as it evolves under the rules of classical mechanics. In molecular dynamics simulation [164], the microscopic states of the system are generated by solving the classical equations of motion as a function of time, using forces calculated by either quantum chemical methods [96, 98] or classical interaction potentials [245]. In Monte Carlo simulation , equilibrium configurations are generated according to the probabilities known from classical statistical mechanics, using energies calculated by either quantum chemical methods [246] or classical interaction potentials [245].

A fundamental requirement in both methods is an accurate representation of the potential energy surface of the system so that the dynamics or the relative populations of equilibrium configurations are adequatly described. While on one hand, the use of quantum chemical methods in molecular simulation provides accurate potential energy surfaces at a substancial computational cost, on the other, classical interaction potentials are computationally inexpensive but less accurate. In the latter, the "effective" pairwise-additive approach for interactions between *neutral* water molecules in liquid water is adopted and many-body effects are *implicitly* taken into account, since the intermolecular potential parametrization is set to reproduce bulk properties, e.g. structure or vaporization enthalpy, usually at ambient conditions [245, 247]. Consequently, "effective" classical interaction potentials, e.g. SPC [247] or TIP5P [245] models, based on rigid and/or geometry independent and partial charges, are not expected to describe accurately both liquid and solid phase [17, 19, 248]. The inherent shortcomings of effective pairwise-additive potentials are more striking in complex heterogeneous systems such as surfaces, clusters, and aqueous solutions, [249, 250] which require an explicit inclusion of many-body effects and a flexible intra-molecular potential [19, 248]. Nevertheless, effective pairwise additive potentials are quite successful in the prediction of the properties for which they were parametrized [251–253], and are therefore a usefull tool, provided the range of applicability is kept in mind [18, 100, 254].

Throughout this thesis, both approaches, classical and quantum mechanical, were adopted according to their intrinsic limitations, computational demands and the property to be predicted. In particular, the electronic density of states of liquid water was obtained trough a sequential methodology where electronic energy levels were averaged over configurational space, using configurations appropriately sampled from Monte Carlo simulation. This significantly decreases computational cost, while at the same time retaining the relevant statistical information and allows the recovery of the electronic degrees of freedom trough subsequent quantum chemical calculations on a small number of statistically uncorrelated configura-

tions [255, 256]. Sampling of liquid water configurations, usually a supramolecular structure containing a few tens of molecules, raises the problem of surface effects: although in a liquid-like configuration, the environment for each molecule differs from that of bulk, this difference being more pronounced the closer water molecules are to the surface of the supramolecular structure. Hence, to study bulk properties, e.g. the electronic density of states, this problem must be addressed. This effect was mitigated by retaining the TIP5P charge distribution of the nearest 200 molecules in each configuration. This approach not only partially introduces a correction for surface effects trough static polarization but also introduces the effects of the thermal fluctuation of the interactions with surrounding the molecules as both explicit molecules and TIP5P charges are sampled from the same statistical distribution.

Within this approach, the only property that has to be reliably estimated by classical simulation is liquid water structure. As it is known to be adequatly described by pairwise additive intermolecular potentials, e.g. TIP5P [100], this constitutes a reliable methodology within the limitations of a rigid molecule model.

Chapter 3

Paper I: The missing piece

The $OH\cdots H_2O$ interaction [257–259] and small $OH(H_2O)_n$ clusters [260, 261] had already been the subject of theoretical studies. However, available theoretical estimates for bulk hydration energetics of the OH radical were based on extrapolated results of OH binding energies for $OH(H_2O)_n$ minimum energy clusters using semi-empirical [35] or ab initio methods [261] . In view of the lack of an experimental or theoretical reference value for $\Delta E_{hyd}[OH]$ or $\Delta H_{hyd}[OH]$ and limited theoretical data for $OH(H_2O)_n$ clusters, the purpose of Paper I was threefold:

- A microsolvation study of the properties of $OH(H_2O)_{1-6}$ clusters as well as a proposal of global minima using density functional methods. These calculations also serve a second purpose: the parametrization of the SPC intermolecular potential [262] for $OH\cdots H_2O$ Coulomb interactions.

- A theoretical estimate for $\Delta E_{hyd}[OH]$ and $\Delta H_{hyd}[OH]$, by Monte Carlo simulation using the previously parametrized potential for $OH\cdots H_2O$ interactions.

- An estimate for E_{gap}, as defined in Eq.(1.17), using our result for $\Delta E_{hyd}[OH]$.

From microsolvation studies it is found that the most stable minimum energy geometries for $OH(H_2O)_{n=2-5}$ clusters were found to be single donor-acceptor structures, whereas other isomers, irrespective of the number of hydrogen bonds, were found to be less stable. This enhanced stability of single donor-acceptor structures can be understood under the same reasoning presented for the enhanced stability of neutral water clusters (Figure 1.4) [116]. In general, the binding energies of the OH radical and the water molecule were found to be very close for the most stable geometries, the exception being the enhanced stability of the $OH\cdots OH_2$ complex relative to the water dimer, as already noted by Wang et al. [259]. Although some effort was devoted to the search for a global minimum for $(H_2O)_{n=6}$, the number of possible isomers was found to be too large for a systematic search. Hence a tentative global minimum is proposed for $(H_2O)_{n=6}$. As the most stable structures were derived from $(H_2O)_n$ clusters by the removal of a dangling hydrogen, the present

results suggest this might constitute a possible route for a systematic search for minimum energy geometries of larger $OH(H_2O)_n$ clusters [263].

The hydration enthalpy of the hydroxyl radical estimated from Monte Carlo simulation, ΔH_{hyd}[OH] =-39.1±3.9 kJ mol^{-1}, is similar to the hydration enthalpy of water as already hinted by similar binding energies in the previous microsolvation study. This result was later found to be in agreement with experiment (-38.1±6.3 kJ mol^{-1}) [264]. Altough the hydration structure of the hydroxyl radical has been discussed in subsequent molecular dynamics studies [265–269], a theoretical estimate for the hydration enthalpy has not been proposed.

The hydration energy of the hydroxyl radical estimated from Monte Carlo simulation, ΔE_{hyd}[OH] =-36.6 kJ mol^{-1}, is close to the value predicted by Coe et al. (-35.7 kJ mol^{-1}) [35]. This agreement may be fortuitous as the latter estimate was based on a semi-empirical method and relies on a extrapolation of the binding energy of the hydroxyl radical onto bulk for minimum energy structures. From Eq.(1.17), taking $V_0 = -0.12$ eV and our estimate for the hydration energy of the hydroxyl radical, the adiabatic band gap of liquid water is 6.88 eV, in excellent agreement with the result reported by Coe et al. (6.9 eV) [35].

The hydration of the OH radical: Microsolvation modeling and statistical mechanics simulation

P. Cabral do Couto, R. C. Guedes, and B. J. Costa Cabral[a)]
Departamento de Química e Bioquímica, Faculdade de Ciências, Universidade de Lisboa, 1749-016 Lisboa, Portugal and Grupo de Física Matemática da Universidade de Lisboa, Av. Professor Gama Pinto 2, 1649-003 Lisboa, Portugal

J. A. Martinho Simões
Departamento de Química e Bioquímica, Faculdade de Ciências, Universidade de Lisboa, 1749-016 Lisboa, Portugal

(Received 12 June 2003; accepted 15 July 2003)

The hydration of the hydroxyl OH radical has been investigated by microsolvation modeling and statistical mechanics Monte Carlo simulations. The microsolvation approach was based on density functional theory (DFT) calculations for $OH-(H_2O)_{1-6}$ and $(H_2O)_{1-7}$ clusters. The results from microsolvation indicate that the binding enthalpies of the OH radical and water molecule to small water clusters are similar. Monte Carlo simulations predict that the hydration enthalpy of the OH radical, $\Delta_{hyd}H(OH,g)$, is $-39.1\ kJ\,mol^{-1}$. From this value we have estimated that the band gap of liquid water is 6.88 eV, which is in excellent agreement with the result of Coe *et al.* [J. Chem. Phys. **107**, 6023 (1997)]. We have compared the structure of the hydrated OH solution with the structure of pure liquid water. The structural differences between the two systems reflect the strong role played by the OH radical as a proton donor in water. From sequential Monte Carlo/DFT calculations the dipole moment of the OH radical in liquid water is 2.2 ± 0.1 D, which is ~33% above the experimental gas phase value (1.66 D). © *2003 American Institute of Physics.*
[DOI: 10.1063/1.1605939]

I. INTRODUCTION

The interaction of the hydroxyl radical with biological molecules, including amino acids, peptides, and proteins, is of great interest due to the deleterious effects of the radical on biological systems.[1–4] For example, high concentrations of the hydroxyl (OH) radical in the cell cytoplasm have been associated with Parkinson's disease.[5] The OH radical is also important in the chemistry of earth's atmosphere, where its role in hydrogen abstraction reactions determines the atmospheric lifetime of many hydrofluorocarbons.[6–8] Most of the reactions involving the OH radical occur in aqueous environment or in small water aggregates that can act as catalysts in some atmospheric reactions.[9] The study of OH radical hydration is therefore very important because the oxidation mechanisms of organic molecules by aqueous OH will depend strongly on the structural and energetic properties of the hydrated radical.[10,11] Another relevant issue concerns the electronic properties of liquid water, where the adiabatic band gap of the liquid, which can be determined over thermochemical cycles involving the OH^- defect state in water, depends on the OH radical hydration energy.[12]

Several works have been carried out to analyze the interactions of the OH radical with the water molecule[13–16] and the microsolvation of the radical in water clusters.[12,17] In the present paper we report a theoretical study of the hydration of the OH radical. To carry out this study two approaches have been adopted: microsolvation modeling and Monte Carlo statistical mechanics simulations. Initially, we have analyzed the microsolvation of the OH radical in water (W) by carrying out density functional theory (DFT) calculations for $OH-W_N$ clusters ($N=1-6$), where N is the number of water molecules. From these calculations, several properties, including the structure, energetics, vibrational spectrum, and charge distribution have been determined and compared with the properties of water clusters W_{N+1} ($N=1-6$). Monte Carlo simulations were then carried out to analyze the structure of the hydrated hydroxyl solution and to predict the OH radical enthalpy of hydration, $\Delta_{hyd}H(OH,g)$. Finally, sequential Monte Carlo/DFT calculations over uncorrelated configurations[18,19] of the solution have been performed to investigate the electronic polarization of the hydroxyl radical in liquid water.

II. COMPUTATIONAL DETAILS

To analyze the structure, vibrational spectrum, and energetics of $OH-W_N$ ($N=1-6$) clusters, where $W=H_2O$ and N is the number of water molecules, we have carried out density functional theory calculations with the Adamo and Barone[20–22] Becke style one-parameter hybrid functional, using a modified Perdew–Wang exchange[22] and PW91 correlation[23] (MPW1PW91). The geometries of $OH-W_N$ and W_{N+1} clusters ($N=1-6$) have been fully optimized with Dunning's correlation consistent polarized valence double

a)Author to whom all correspondence should be addressed. Electronic mail: ben@adonis.cii.fc.ul.pt

zeta basis set augmented with diffuse functions (aug-cc-pVDZ).[24] Single-point energy calculations with the aug-cc-pVTZ and aug-cc-pVQZ basis sets[25] are also reported.

The energetics of the $OH–W_N$ clusters can be discussed in terms of the formation and binding energies. The formation energy $\Delta E_{e,N}$ is defined as

$$\Delta E_{e,N} = E[\mathrm{OH–W}_N] - E[\mathrm{OH}] - NE[\mathrm{W}_1], \tag{1}$$

where $E[\mathrm{OH–W}_N]$ is the energy of a cluster with the hydroxyl radical and N water molecules.

The binding energy $\Delta E_{b,N}$ is given by

$$\Delta E_{b,N} = E[\mathrm{OH-W}_N] - E[\mathrm{OH}] - E[W_N]. \tag{2}$$

We also define the binding enthalpy $\Delta H_{b,N}$, which is similar to the binding energy (2) but includes zero point vibrational energy corrections (ZPVE) and thermal corrections. For $N=1$, $\Delta E_{e,1} \equiv \Delta E_{b,1}$. In this case, they will be represented simply by ΔE and ΔH, respectively. Formation energies, $\Delta E_{e,N}$, calculated with the aug-cc-pVDZ basis set were corrected for basis set superposition error by using the counterpoise method[26] with fragment relaxation energy contributions.[27]

We have verified that several properties predicted by MPW1PW91/aug-cc-pVDZ calculations for the water molecule and dimer, and for the isolated hydroxyl radical are in very good agreement with experiment. These results are reported in Table I, where they are compared with experimental data for the dipole moment,[28–30] structure,[31–33] vibrational spectrum,[32,34] and energetic properties.[35,36] For $OH–W_N$ complexes no experimental information seems to be available. Thus, we have compared the properties of the $OH–W_1$ complex predicted by several theoretical methods, including Møller–Pleset perturbation theory[37] at second (MP2) and fourth order (MP4), quadratic configuration interaction (QCI)[38] with the inclusion of single and double substitutions with triples and quadruples contributions to the energy [QCISD(TQ)],[39] and coupled cluster with single and double excitations (CCSD).[40–43] The results of these calculations are reported in Table I, which also includes previous theoretical data for the $OH–W_1$ complex from different works.[14–16] Very good agreement between DFT and *ab initio* results is observed for $OH–W_1$ complexes. We interpret this agreement as a strong indication on the reliability of the MPW1PW91/aug-cc-pVDZ approach to model the properties of larger $OH–W_N$ clusters.

Monte Carlo simulations of the hydroxyl radical in water have been carried out in the isobaric–isothermal (*NPT*) ensemble[44] at $T=298$ K and $P=1$ atm. The interactions between two molecules, a and b, were described by a Lennard-Jones (LJ) plus a Coulomb contribution, with parameters ϵ_i, σ_i, and q_i for each atom:

$$U_{ab} = \sum_{i\in a}\sum_{j\in b} 4\epsilon_{ij}\left[\left(\frac{\sigma_{ij}}{r_{ij}}\right)^{12} - \left(\frac{\sigma_{ij}}{r_{ij}}\right)^{6}\right] + \frac{q_i q_j e^2}{r_{ij}}, \tag{3}$$

where $\epsilon_{ij} = (\epsilon_i \epsilon_j)^{1/2}$ and $\sigma_{ij} = (\sigma_i \sigma_j)^{1/2}$.

The SPC potential proposed by Berendsen *et al.*[45] has been adopted to represent the interactions between the water molecules. For the hydroxyl radical the Lennard-Jones parameters are the same as the SPC model for water.

To model the Coulomb interactions between the solute (hydroxyl radical) and the water molecules the charge distribution of the hydroxyl radical has been determined in the most energetically stable $OH–W_5$ isomer (see Fig. 2). The charge distribution of the water molecules in this cluster was represented by SPC charges and a quantum mechanical DFT calculation at the MPW1PW91/aug-cc-pVDZ level has been carried out to calculated Merz–Kollman–Singh charges[46,47] of the OH radical. This procedure takes into account, at least partially, the polarization of the OH radical by the closest water molecules. The structure of the cluster has been determined by the DFT optimizations previously described. Lennard-Jones parameters, charge distributions, and dipole moments for the OH radical and water molecule are reported in Table II.

The Monte Carlo simulations have been carried out with one solute molecule and $N=250$ water molecules. A cubic cell with periodic boundary conditions was used. The interactions were truncated at a cutoff distance R_c of 9.6 Å. The initial configuration has been generated randomly. We have carried out 10^8 steps for equilibration. Average values have been calculated over 12.5×10^8 additional steps. Each step involves the attempt to move one molecule of the system.

H_{sx} and H^*_{ss} represent, respectively, the total enthalpies of the solution (with one solute molecule) and pure liquid water, for systems with N water molecules. The total enthalpies are defined as

$$H_{sx} = E_{sx} + E_{ss} + PV \tag{4}$$

and

$$H^*_{ss} = E^*_{ss} + PV^*, \tag{5}$$

where E_{sx} is the solute–solvent energy, E^*_{ss} and E_{ss} the solvent–solvent energies in the pure liquid and solution, and V^* and V are, respectively, the volumes of the pure liquid and solution.

The hydration enthalpy of the OH radical $\Delta_{\mathrm{hyd}}H(\mathrm{OH,g})$, can be calculated as

$$\Delta_{\mathrm{hyd}}H(\mathrm{OH,g}) = H_{sx} - H^*_{ss} - RT \tag{6}$$

$$= E_{sx} + (E_{ss} - E^*_{ss}) + P(V - V^*) - RT \tag{7}$$

$$= E_{sx} + \Delta H_R - RT, \tag{8}$$

where

$$\Delta H_R = \Delta E_R + P\Delta V_R = H_{ss} - H^*_{ss} \tag{9}$$

is the solvent relaxation enthalpy. We note that a very large number of configurations is necessary to attain convergence of this quantity, which is calculated as the difference between two large fluctuating numbers.[48–50]

The DFT calculations were carried out with the GAUSSIAN 98 program.[51] The Monte Carlo simulations were carried out with the DICE program.[52]

TABLE I. Theoretical results for water, hydroxyl radical, water dimer, and hydroxyl–water complex. Dipole moment (μ) in D; distances in Å; angles in degrees; frequencies (ν) in cm^{-1}; binding energy (ΔE) and enthalpy (ΔH) in kJ mol^{-1}. MPW1PW91 and MP2 results are from geometry optimizations with the aug-cc-pVDZ basis set. MP4, QCISD(TQ), and CCSD results are single-point energy calculations with the same basis set in the MPW1PW91 geometry.

	H_2O		OH			
	MPW1PW91	Expt.	MPW1PW91	Expt.		
μ	1.872	1.855[a]	1.655	1.66[b]		
d(O–H)	0.961	0.957[c]	0.975	0.970[d]		
A(H–O–H)	104.6	104.5[c]				
ν_1	3968	3756[e]	3750	3738[e]		
ν_2	3855	3657[e]				
ν_3	1630	1595[e]				
	MPW1PW91	MP2(SDTQ)	MP4(SDTQ)	QCISD(TQ)	CCSD	Expt.
$(H_2O)_2$[f]						
μ	2.59	2.02	2.65			2.60[g]
ΔE	−20.1	−22.3	−22.5	−21.9	−20.8	−20.9±0.5[h]
ΔH^{373}	−15.5	−14.6				−15.1±0.5[i]
d(O–O)	2.892	2.911				2.976[j]
OH–(H_2O)DA(1)[f]						
μ	4.02	4.19	4.17			
ΔE	−23.8	−24.9	−24.8	−24.3	−23.3	
	[−24.4][k]	[−24.9][k]		[−23.6][l]		
ΔH^{298}	−18.1	−19.1				
d(O–H)	0.984	0.981				
OH–(H_2O)DA(3)						
μ	1.057	0.734	1.07			
ΔE	−14.3	−15.8	−15.9	−15.99	−14.7	
	[−14.8][k]					
ΔH^{298}	−9.7	−11.0				
d(O–H)	0.976	0.976				
OH–(H_2O)DD(2)						
μ	0.321	0.300				
ΔE	−15.5	−9.4[m]	−11.2	−12.4	−10.5	
	[−19.5][n]					
ΔH^{298}	−10.1					
d(O–H)	0.972					

[a]From Shepard *et al.* (Ref. 28).
[b]From Nelson *et al.* (Ref. 29).
[c]From Benedict *et al.* (Ref. 31).
[d]From Huber *et al.* (Ref. 32).
[e]From Shimanouchi (Ref. 34).
[f]PM3 semiempirical values for binding energies and enthalpies. $(H_2O)_2$: $\Delta E=-14.6$ kJ mol^{-1}; $\Delta H^{298}=-7.3$ kJ mol^{-1}. OH–W_1DA(1): $\Delta E=-16.3$ kJ mol^{-1}; $\Delta H^{298}=-8.1$ kJ mol^{-1}.
[g]From Kuchitsu and Morino (Ref. 30).
[h]From Feyerisen *et al.* (Ref. 36).
[i]From Curtiss *et al.* (Ref. 35).
[j]From Outdola and Dyke (Ref. 33).
[k]B3LYP/6-311++G(2*d*,2*p*) from Wang *et al.* (Ref. 14).
[l]CISD with triple-ζ basis set including two sets of polarization functions (TZ2P). From Xie *et al.* (Ref. 15).
[m]Single-point energy calculation with the geometry optimized at MPW1PW91/aug-ccpVDZ.
[n]B3LYP/6-311++G(2*d*,2*p*) from Zhou *et al.* (Ref. 16).

III. MICROSOLVATION MODELING

A. Energetic properties

The structure of OH–W_N clusters should reflect the ability of the OH radical to form hydrogen bonds at both ends. Thus, energetic properties of OH–W_N clusters will also be related to the energy differences between structures where the radical plays the role of a proton–acceptor and/or a proton–donor species. We will name these structures as donor–acceptor (DA). In addition, there is some indication from the present DFT calculations that other isomers are possible, where both hydrogen atoms of the water molecule interact with the OH radical oxygen and the OH hydrogen

TABLE II. Lennard-Jones (LJ) parameters, charge distribution, and dipole moment for the hydroxyl radical and water.

OH,H_2O	ϵ (kJ mol^{-1})	σ (Å)
O	0.648	3.165
H	0	0
q (a.u.)	OH	H_2O
O	−0.476	−0.820
H	0.476	0.410
μ (D)	2.3[a]	2.27[b]

[a]Calculated at the MPW1PW91/aug-cc-pVDZ level in the OH–W_5(1) conformer. The charges of the water molecules were represented by SPC charges.
[b]SPC water dipole moment.

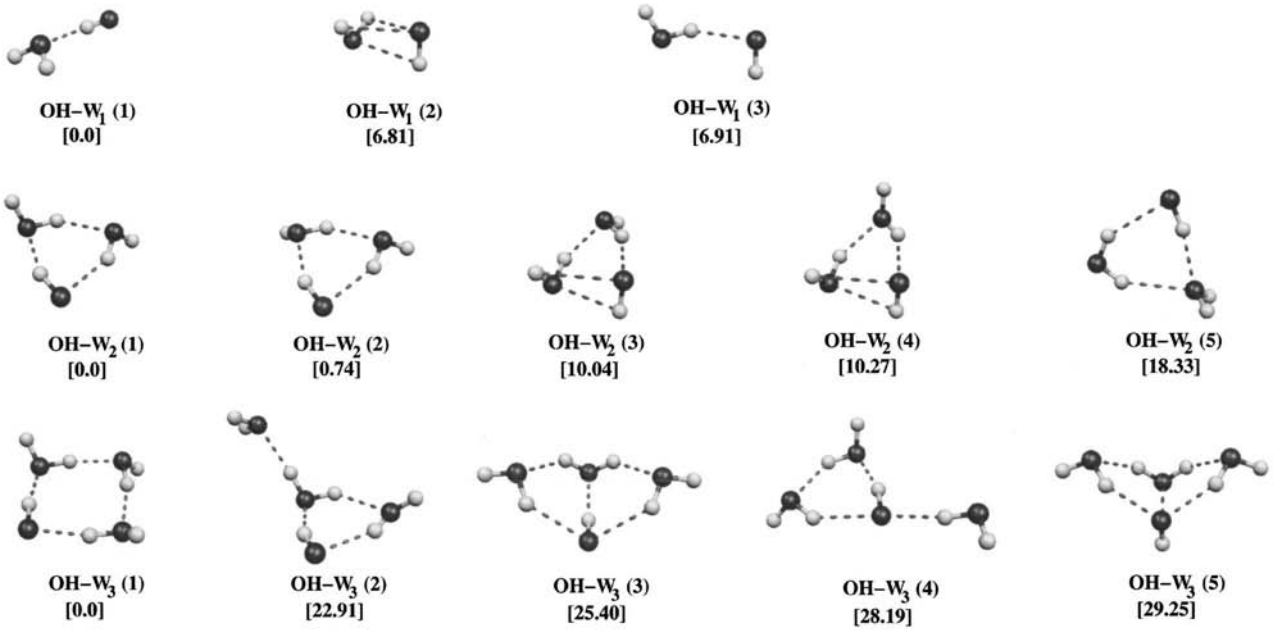

FIG. 1. Structure of the optimized OH–W_N clusters ($N=1-3$). The first structure (1) is the most stable isomer. Energy differences (including ZPVE) in kJ mol^{-1} relative to the isomer (1) are shown in brackets.

forms a weak hydrogen bond with the water oxygen [see the OH–W_1 (2) isomer in Fig. 1]. This class of isomers will be called dipole–dipole structures (DD), since they are clearly stabilized by OH radical–water antiparallel dipolar interactions. The present OH–W_1 DD complex is similar to a local minimum structure from DFT calculations, reported by Zhou *et al.*[16]

The optimized structures of the different OH–W_N isomers are shown in Fig. 1 ($N=1-3$) and Fig. 2 ($N=4-6$). These structures are local minima on the potential energy surface. Energy differences (in kJ mol^{-1}) relative to the most stable isomer (1) are reported in Figs. 1 and 2. They were calculated at the MPW1PW91/aug-cc-pVDZ level and include ZPVE.

Energetic properties for the most stable isomers of the OH–W_N clusters ($N=1-6$) are reported in Table III. We have investigated the importance of basis set superposition error (BSSE) on the evaluation of formation energies, $\Delta E_{e,N}$'s. BSSE is less than ~1% of the uncorrected values at the MPW1PW91/aug-cc-pVDZ level. Thus, BSSE is not significant in the present calculations for the formation energies and binding enthalpies, whose final values are single-point energy calculations with the larger aug-cc-pVTZ and aug-cc-pVQZ basis sets.

Water clusters have been the subject of several theoretical investigations.[53–60] Energetic properties of W_{N+1} clusters ($N=1-6$) are also reported in Table III. The present results for $\Delta E_{e,N}$'s are in very good agreement with those reported by Lee *et al.*,[59] which were based on MP2/TZ2P++ calculations. For example, for the water cyclic hexamer, $\Delta E_{e,n} = -181.0$ kJ mol^{-1} (MPW1PW91/aug-cc-pVQZ), which is in excellent agreement with the MP2/TZ2P++ value reported by Lee *et al.* (-182.1 kJ mol^{-1}).[59] For the heptamer (prism conformer) our $\Delta E_{e,n} = -219.4$ kJ mol^{-1}, which is very close to the value reported by Kim *et al.*[58] (-215.8 kJ mol^{-1}) from MP2/TZ2P++ calculations including full BSSE corrections.

It is interesting to compare binding enthalpies of the OH–W_1 complex and the water dimer. The MPW1PW91/aug-cc-pVQZ result for the water dimerization enthalpy is -12.3 kJ mol^{-1}, which is in very good agreement with the experimental result (-15.0 ± 2 kJ mol^{-1}).[35] For the OH–W_1 complex we predict that the binding enthalpy is -17.3 kJ mol^{-1} (MPW1PW91/aug-cc-pVQZ), which is ~5 kJ mol^{-1} more negative than the water dimerization enthalpy, illustrating the stability of the OH–W_1 complex, where the OH radical plays the role of proton donor. The present value is in excellent agreement with the prediction by Wang *et al.* (-16.9 kJ mol^{-1})[14] based on a Becke3LYP/6-311++G($2d,dp$) calculation for the OH–W_1 binding enthalpy. No experimental value seems to be available for comparison.

A relevant feature characterizing OH–W_N and W_{N+1} clusters is hydrogen bonding co-operativity, i.e., binding energies are strongly dependent on the cluster size, due to the nonadditive polarization effects induced by hydrogen bonding. This is illustrated in Fig. 3, where the binding enthalpy $\Delta H_{b,N}$ of OH–W_N and W_{N+1} are compared. Our results, based on MPW1PW91/aug-cc-pVQZ calculations, show that in OH–W_N clusters, $-\Delta H_{b,N}$ increases from 17.3 kJ mol^{-1} ($N=1$) to 41.3 kJ mol^{-1} ($N=3$), and then decreases to 28.2 kJ mol^{-1} ($N=6$).

In W_{N+1} clusters, $-\Delta H_{b,N}$ increases from 12.3 kJ mol^{-1} ($N+1=2$) to 42.1 kJ mol^{-1} ($N+1=4$) and then decreases to 28.5 kJ mol^{-1} ($N+1=7$). We note the remarkable stability of the water tetramer (W_4) and the OH–W_3 complex relative to other clusters. Moreover, $\Delta H_{b,N}$ for these clusters is very similar (~-41 kJ mol^{-1}). For larger clusters, the difference between $\Delta H_{b,N}$ of OH–W_N and

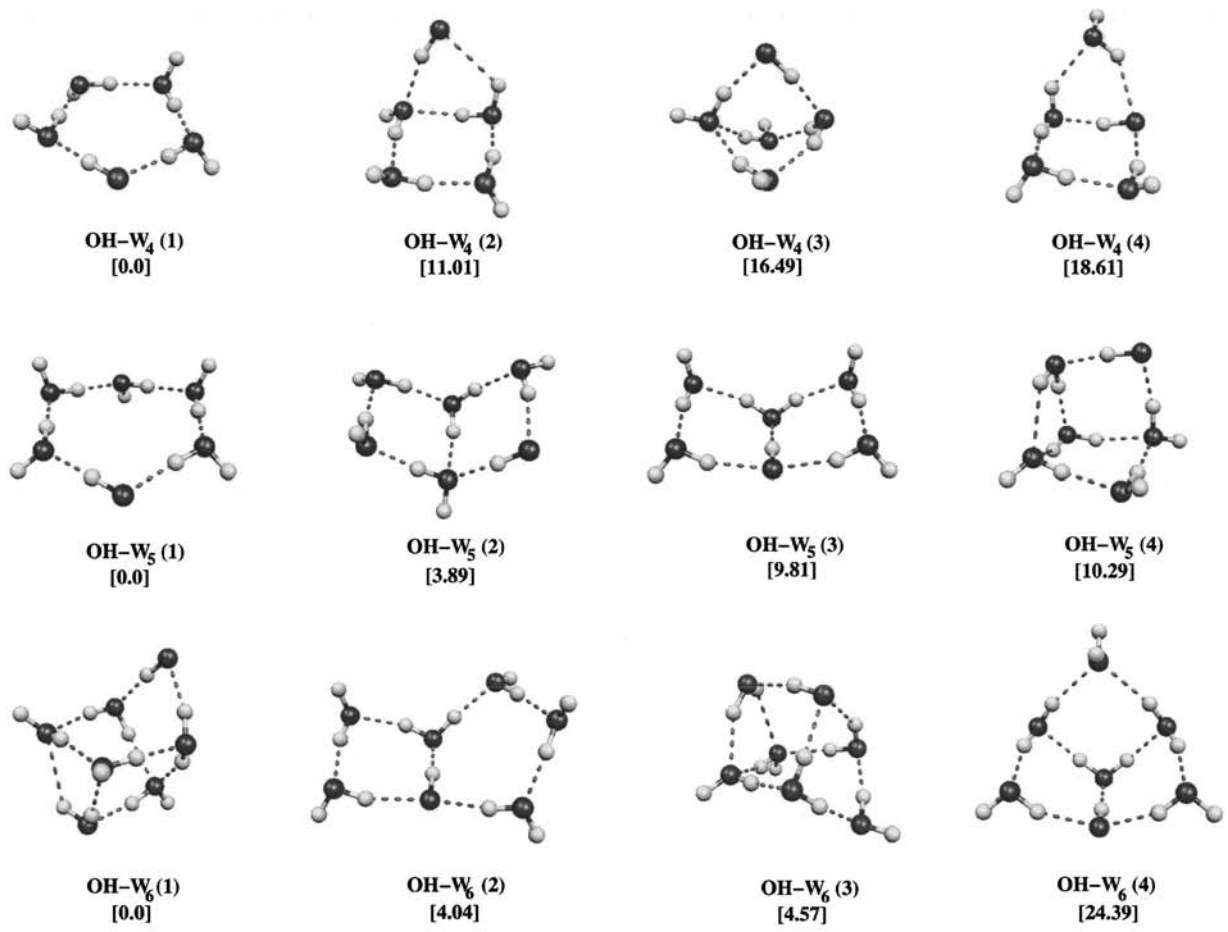

FIG. 2. Structure of the optimized OH–W_N clusters ($N=4-6$). The first structure (1) is the most stable isomer. Energy differences (including ZPVE) in kJ mol^{-1} relative to the isomer (1) are shown in brackets.

W_{N+1} clusters becomes very small. For example, when $N=4$, it is only -1.6 kJ mol^{-1}.

The behavior of $\Delta H_{b,N}$ for $N=5,6$ may suggest a convergence to some limit value close to ~ -30 kJ mol^{-1}, although extrapolations to bulk values from small clusters should be carried out with caution. For instance, the experimental water hydration enthalpy, $\Delta_{\mathrm{hyd}}H(H_2O,g) = -44.0$ kJ mol^{-1},[61] is very close to $\Delta H_{b,N} = -42.1$ kJ mol^{-1} for the W_4 cluster. However, there is a clear dependence of $\Delta H_{b,N}$ on the cluster size. For W_6, $\Delta H_{b,N} = -28.5$ kJ mol^{-1}, which is 16 kJ mol^{-1} above the experimental $\Delta_{\mathrm{hyd}}H(H_2O,g)$.

Binding energies for OH–W_N DD clusters are also reported in Table III. The binding energy of the OH–W_1 complex, -8.4 kJ mol^{-1} (aug-cc-pVQZ), is ~ 9 kJ mol^{-1} above the corresponding DA complex. Higher stability of DA clusters seems to be a general trend when we compare DA and DD isomers. This can be related to the stability of the proton–donor OH–W_1 complex, which is a building unit of all OH–W_N DA clusters.

Very recently, Hamad *et al.*[17] carried out theoretical calculations for OH–W_N clusters ($N=1-4$). They estimate that $\Delta H_{b,N}$ can be extrapolated to -20 or -25 kJ mol^{-1} from gas phase clusters and to -12 or -17 kJ mol^{-1} from a hybrid solvation model.[17] The first values (-20 or -25 kJ mol^{-1}) are in reasonable agreement with our results for OH–W_N ($N=4-6$), which range from -31.1 kJ mol^{-1} ($N=4$) to -28.2 kJ mol^{-1} ($N=6$). The extrapolations from their hybrid solvation model (-12 or -17 kJ mol^{-1}) seem to underestimate $\Delta H_{b,N}$. To discuss the electronic properties of liquid water, Coe *et al.*[12] carried out semiempirical PM3 calculations and evaluated $\Delta E_{b,N}$ for OH–W_N clusters ($N=1-15$). The extrapolated value of this quantity, based on a fitting procedure for water droplets is -35.7 kJ mol^{-1}. For water clusters, the same procedure leads to -37.6 kJ mol^{-1}.[12] The difference between the two quantities is only -1.9 kJ mol^{-1}, in good agreement with our prediction that in small clusters, $\Delta H_{b,N}$ for OH–W_N and W_{N+1} are similar.

B. Structural and vibrational properties

Structural and vibrational properties of the OH–W_N and W_{N+1} clusters are reported in Table IV. In agreement with results for energetic properties, important geometric dependence on the cluster sizes is observed. The most important changes concern the intramolecular O–H distance in the hydroxyl radical, d(O–H), which increases from 0.975 Å in the isolated radical to 1.007 Å in the OH–W_5 DA cluster. The structural changes related to the role played by the hydroxyl radical as hydrogen acceptor, d(HO...HOH), and hy-

TABLE III. Formation and binding energies (kJ mol^{-1}) for the most stable clusters of the hydroxyl radical with N water molecules (OH–W$_N$) and for water clusters (W$_{N+1}$).

DA[a]	OH–W$_1$	OH–W$_2$	OH–W$_3$	OH–W$_4$	OH–W$_5$	OH–W$_6$
			aug-cc-pVDZ			
$\Delta E_{e,N}$	−23.8	−62.0	−111.7	−151.8	−186.5	−229.8
$\Delta H_{b,N}$	−18.1	−35.7	−43.2	−32.7	−29.6	−33.3
			aug-cc-pVTZ[b]			
$\Delta E_{e,N}$	−23.1	−59.7	−108.1	−147.1	−180.7	−219.8
$\Delta H_{b,N}$	−17.4	−34.1	−41.8	−31.5	−28.3	−29.1
			aug-cc-pVQZ[b]			
$\Delta E_{e,N}$	−23.0	−59.1	−107.1	−145.6	−178.9	−217.2
$\Delta H_{b,N}$	−17.3	−33.7	−41.3	−31.1	−28.0	−28.2
			aug-cc-pVDZ(BSSE)			
$\Delta E_{e,N}$	−22.6	−58.8	−106.6	−145.0	−178.1	−216.2
E(BSSE)	1.2	3.2	5.1	6.7	8.4	13.6
DD[c]	OH–W$_1$	OH–W$_2$	OH–W$_3$			
			aug-cc-pVDZ			
$\Delta E_{e,N}$	−15.5	−51.7	−83.0			
$\Delta H_{b,N}$	−10.1	−24.9	−13.0			
			aug-cc-pVTZ[b]			
$\Delta E_{e,N}$	−14.0	−48.3	−77.3			
$\Delta H_{b,N}$	−8.7	−24.7	−9.5			
			aug-cc-pVQZ[b]			
$\Delta E_{e,N}$	−13.7	−47.6	−76.3			
$\Delta H_{b,N}$	−8.4	−24.2	−9.0			
Water clusters	W$_2$	W$_3$	W$_4$	W$_5$	W$_6$	W$_7$
			aug-cc-pVQZ[b]			
$\Delta E_{e,N}$[d]	−19.2	−60.4	−110.0	−146.1	−181.0	−219.4
	(−20.4)	(−63.3)	(−111.9)	(−147.3)	(−182.1)	(−231.4)
						[−215.8]
$\Delta H_{b,N}$	−12.3	−33.1	−42.1	−29.5	−28.2	−28.5

[a]Donor–acceptor OH–W$_N$ structures.
[b]Single-point energy calculation. Geometry optimized at MPW1PW91/aug-cc-pVDZ.
[c]Dipole–dipole OH–W$_N$ structures.
[d]Values in parentheses are MP2/TZ2P++ calculations with half BSSE correction from Lee *et al.* (Ref. 59). Bracketed value for the prism heptamer conformer (MP2/TZ2P++ calculation with full BSSE correction) is from Kim *et al.* (Ref. 58).

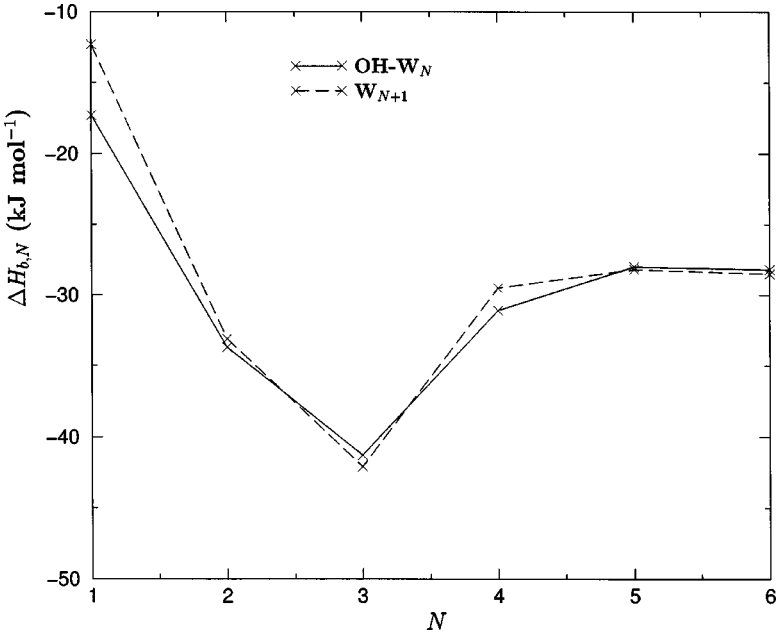

FIG. 3. Binding enthalpy ($\Delta H_{b,N}$ in kJ mol^{-1}) for OH–W$_N$ clusters and for W$_{N+1}$ clusters as a function of N, the number of water molecules (W) in the cluster.

TABLE IV. Structural and vibrational data for hydroxyl–water ($OH–W_N$) and water (W_{N+1}) clusters. Frequencies in cm^{-1}; distances in Å. Results are from MPW1PW91/aug-cc-pVDZ optimizations.

DA[a]	OH	$OH–W_1$ (1)	$OH–W_2$ (1)	$OH–W_3$ (1)	$OH–W_4$ (1)	$OH–W_5$ (1)
ν(O–H)	3750 [3738][b] [3554.1][c]	3562 [3452.2]±0.5[d] [3453.5][e]	3382	3188	3124	3105
d(O–H)[O–H]	0.975	0.984	0.994	1.003	1.006	1.007
d(HO...HOH)			1.996	1.820	1.780	1.762
d(OH...OH_2)		1.870	1.798	1.681	1.643	1.629
d(O–O)		2.854	2.784	2.717	2.693	2.682
(DD)[f]	OH	$OH–W_1$ (2)	$OH–W_2$ (3)	$OH–W_3$ (3)		
ν(O–H)	3750	3782	3795	3820		
d(O–H)[O–H]	0.975	0.972	0.971	0.969		
d(HO...HOH)		2.425	1.915	1.945		
d(OH...OH_2)		2.444	2.293	2.289		
d(O–O)		2.467	2.643	2.785		
	W_1	W_2	W_3	W_4	W_5	W_6
ν(O–H)	3968	3791	3616	3441	3377	3355
d(O–H)	0.961	0.969	0.977	0.985	0.987	0.987
d(HOH...OH_2)		1.929	1.873	1.738	1.706	1.693
d(O–O)		2.892	2.770	2.709	2.691	2.679

[a]Donor–acceptor $OH–W_N$ structures.
[b]Gas phase value from Huber *et al.* (Ref. 32).
[c]OH in argon matrix (Ref. 65).
[d]$OH–W_1$ in argon matrix (Ref. 64).
[e]$OH–W_1$ in argon matrix (Ref. 62).
[f]Dipole–dipole $OH–W_N$ structures. The most stable DD isomer has been selected.

drogen donor, d(OH...OH_2), are very similar and these distances are reduced by ~0.24 Å from $OH–W_1$ to $OH–W_5$. The average O–O distance, d(O–O), changes from 2.854 Å in $OH–W_1$ to 2.682 Å in $OH–W_5$. The same effect is observed in the water clusters where d(O–O) is reduced by 0.21 Å from W_2 to W_6.

The structure of $OH–W_N$ DD clusters shows a very interesting and specific dependency on the cluster size. Although d(O–H) is almost constant when we compare the $OH–W_1$ (0.975 Å) and $OH–W_3$ (0.969 Å) clusters, d(HO...HOH) is reduced by 0.48 Å. In contrast with W_{N+1} and $OH–W_N$ DA structures, the average distance between oxygen atoms in DD structures, d(O–O), increases by 0.32 Å from $OH–W_1$ to $OH–W_3$ clusters.

The present results for $OH–W_N$ and W_{N+1} clusters indicate a strong redshift, $\Delta\nu$, relative to isolated species (OH radical and water molecule) of the vibrational mode associated with the intramolecular O–H stretch frequency. Thus, ν(O–H) changes from 3750 cm^{-1} in the isolated radical to 3105 cm^{-1} in $OH–W_5$. A significant redshift is also observed in water clusters where ν(O–H) changes from 3968 cm^{-1} in the water monomer to 3355 cm^{-1} in W_6.

Frequency shifts ($\Delta\nu$) for the most stable $OH–W_N$ and W_{N+1} isomers as a function of N are shown in Fig. 4. Our results indicate that $\Delta\nu$ is larger in $OH–W_N$ clusters than in water clusters, mainly when $N \geqslant 3$. Experimental results for $OH–W_N$ clusters are relatively scarce although some works on the $OH–W_1$ complex in rare gas matrices have been reported.[62–66] A recent spectroscopic investigation based on the generation of the OH–W complexes in argon matrices[62] suggested that $\nu(O–H) = 3453.5\ cm^{-1}$ should be assigned to the $OH–W_1$ complex. This value is 100 cm^{-1} lower than ν(O–H) for the radical in the matrix (3554.1 cm^{-1}).[65] For $OH–W_1$, we predict that $\Delta\nu = 188\ cm^{-1}$, which is significantly higher than the experimental shift in argon matrix. However, comparison between harmonic gas phase frequencies and data in rare gas matrices is not direct. There is experimental[66] and theoretical[67] evidence that the interactions of the guest species with the matrix atoms may strongly influence the vibrational spectrum.

IV. MONTE CARLO SIMULATIONS

A. Energetics of the OH radical hydration

Thermodynamic properties for the hydrated hydroxyl radical and for pure water, obtained from *NPT* Monte Carlo simulations are reported in Table V. We first note that the densities of the solution of the hydroxyl radical in water and pure liquid water are identical (1.1 $g\,cm^{-3}$). In addition, the solvent relaxation energy induced by the hydration of the OH radical and by the water molecule differ by 7.1 $kJ\,mol^{-1}$. ΔH_R for the hydroxyl radical and water are 38.7±3.9 and 45.8±3.9 $kJ\,mol^{-1}$, respectively.

From Monte Carlo (MC) simulations, the hydration enthalpy of the OH radical, $\Delta_{hyd}H$(OH,g), is −39.1 ±3.9 $kJ\,mol^{-1}$. No experimental result is available for comparison. On the other hand, the MC result for $\Delta_{hyd}H(H_2O,g)$ is −47.9±3.9 $kJ\,mol^{-1}$, in very good agreement with experiment (−44.0 $kJ\,mol^{-1}$).[61] Thus, in keeping with the results based on the microsolvation model, our MC results in-

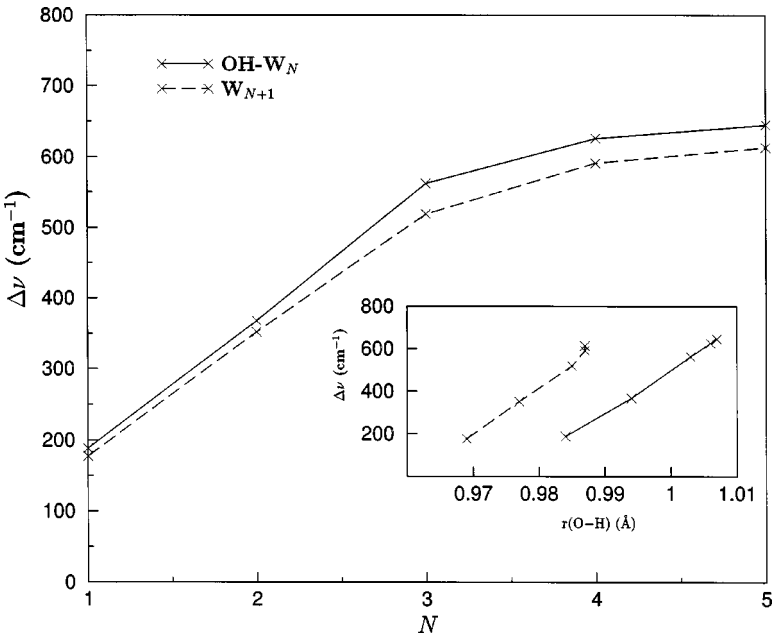

FIG. 4. O–H frequency shift $\Delta\nu$ (in cm^{-1}) vs the number of water molecules (N) in OH–W$_N$ and W$_{N+1}$ clusters ($N=1-5$). The inset shows $\Delta\nu$ vs the O–H bond length (in Å).

dicate that the hydration enthalpy of the OH radical is not very different from the hydration enthalpy of water.

We predict that the hydration energy of the hydroxyl radical, $\Delta_{\text{hyd}}E(\text{OH,g})$ is -36.6 kJ mol^{-1}. Although this result is very close to the extrapolated value of Coe *et al.* (-35.7 kJ mol^{-1}),[12] the agreement may be fortuitous. In fact, their extrapolation was based on PM3 calculations and the energetic properties of OH–W$_1$ and W$_2$ predicted by this method are not in good agreement with experiment (see Table I). Not surprisingly, however, our $\Delta_{\text{hyd}}E(\text{OH,g})$ leads to a value for the band gap of liquid water (6.88 eV) in excellent agreement with the result reported by Coe *et al.* (6.9 eV).[12] The present estimate has assumed that the vacuum level V_0 (minus the energy to promote a delocalized conducting electron of minimal energy into vacuum with zero kinetic energy) is -0.12 eV (see Coe *et al.*[12] for details on the water band gap estimation).

TABLE V. Thermodynamic properties for the hydrated hydroxyl radical and pure water from *NPT* Monte Carlo simulations at $T=298$ K and $P=1$ atm. Energies in kJ mol^{-1}. N is the number of water molecules: R_c (Å) is the cutoff radius for the interactions; ρ and ρ^* are, respectively, the densities (g/cm^3) of pure liquid and solution; E_{sx} is the solute–solvent interaction energy; $H_{ss}=E_{ss}+PV$ is the enthalpy of the water in the solution; $H^*_{ss}=E^*_{ss}+PV^*$ is the enthalpy of pure liquid water, where E^*_{ss} and V^* are the energy and volume of pure liquid water; $\Delta_{\text{hyd}}H(\text{OH,g})$ and $\Delta_{\text{hyd}}H(\text{H}_2\text{O,g})$ are the hydration enthalpies of the hydroxyl radical and water, respectively.

N	250
R_c	9.6
Hydroxyl radical in water	
ρ	1.1
E_{sx}	-75.3 ± 0.2
H_{ss}	-11304.3 ± 2.7
ΔH_R	38.7 ± 3.9
$\Delta_{\text{hyd}}H(\text{OH,g})$	-39.1 ± 3.9
Pure water (SPC model)	
ρ^*	1.1
H^*_{ss}	-11342.9 ± 2.8
ΔH_R	45.8 ± 3.9
$\Delta_{\text{hyd}}H(\text{H}_2\text{O,g})$	-47.9 ± 3.9
	$[-44.0]$[a]

[a]Experimental value from Cox *et al.* (Ref. 61).

B. Structure of the solution

The partial radial distribution functions (RDFs) for the OH radical solvated in water and pure water are shown in Figs. 5–7. Figure 5 shows the $g_{\text{O–O}}(r)$ radial distribution functions in the solution and pure liquid. The O–O RDF for the hydroxyl radical is bimodal, reflecting the hydroxyl oxygen interaction with two water molecules closer to the radical. For the hydroxyl radical this function shows two maxima (1.38 at 2.6 Å and 1.5 at 3.2 Å). Integration up to the first minimum (0.8 at 4.5 Å) yields 13.6, which is the average coordination number or the average number of water molecules in the first coordination shell of the hydroxyl radical. Although the short-range O–O correlation in pure water is quite different from the one observed for the hydrated OH radical, integration of the O–O RDF for pure water up to 4.5 Å also yields 13.6 water molecules. The average coordination numbers related to O–O correlations for the solvated O–H radical, and pure liquid water, are very close for $r \geqslant 3.7$ Å (see the inset of Fig. 5).

Figure 6 shows the $g_{\text{O–H}}(r)$ radial distribution function, which describes the correlations between the OH radical oxygen and water hydrogen atoms. These correlations are related to the role played by the OH radical as a proton acceptor in liquid water. For the hydrated OH radical this function shows a first maximum (0.6 at 1.9 Å) and integration of this function up to the first minimum (0.42 at 2.3 Å) yields 0.6, which is the average number of hydrogen atoms in close interaction with the OH oxygen atom. Comparison with the same function for liquid water shows that here the oxygen atom has a stronger interaction with the water hydro-

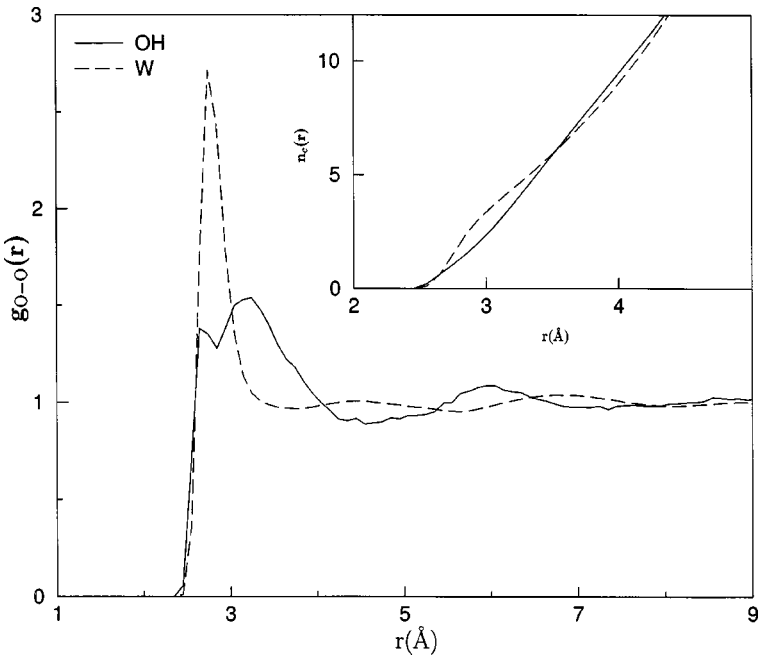

FIG. 5. Partial radial distribution function $g_{O-O}(r)$ for the hydrated OH radical and for liquid water. The inset shows the average coordination number $n_c(r)$.

gen atoms: $g_{O-H}(r)$ shows a first peak (1.3 at 1.7 Å), and integration up to the first minimum (0.25 at 2.3 Å) yields 0.94.

Figure 7 shows the $g_{H-O}(r)$ RDF, which is related to the role played by the OH radical as a proton donor in water. This function shows a sharp maximum (2.8 at 1.65 Å). Integration up to the first minimum (0.05 at 2.3 Å) yields 1.0, which is the average number of water oxygen atoms in close interaction with the OH radical hydrogen. The short-range order in the hydrated hydroxyl solution is consistent with some structural data for $OH-W_N$ clusters (Table IV). For example, $d(OH...OH_2)$ in $OH-W_1$ is 1.87 Å, which is shorter than $d(HOH...OH_2)=1.93$ Å in W_2.

Comparison between $g_{H-O}(r)$ of the hydrated OH radical and pure liquid water confirms that the short-range order is quite different for the two systems. Moreover, this function shows that the OH radical plays a more important role as a proton donor in liquid water than the water molecule. This reflects the stability of the $OH-W_1$ (1) conformer relative to the water dimer.

C. The OH dipole moment in water

Sequential Monte Carlo/DFT calculations have been carried out to analyze the polarization of the OH radical in liquid water. We have selected 50 uncorrelated supermolecular structures[18,19] with the hydroxyl radical and 2, 14, 52, 75, 100, and 125 water molecules. These numbers correspond to including all the water molecules within solvation radii of 2.85, 4.65, 7.05, 8.0, 8.8, and 9.45 Å, respectively.

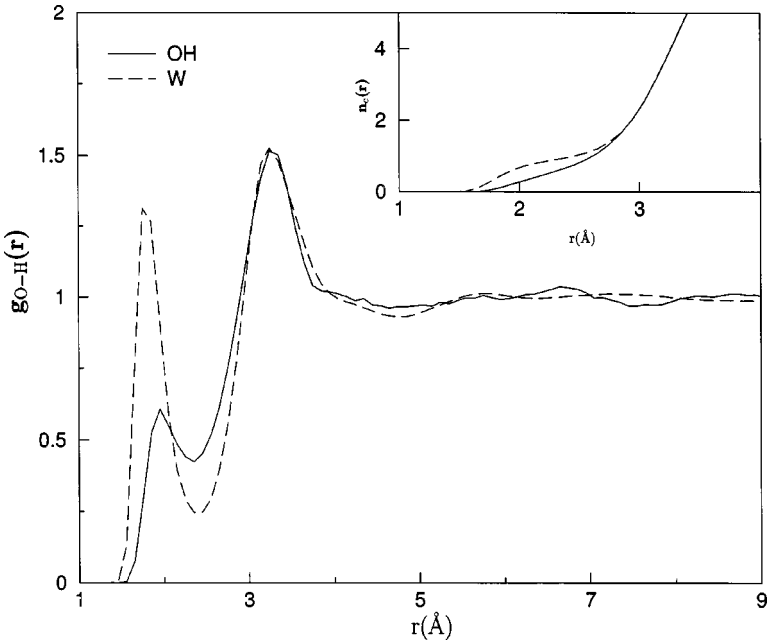

FIG. 6. Partial radial distribution function $g_{O-H}(r)$ for the hydrated OH radical and for liquid water. The inset shows the average coordination number $n_c(r)$.

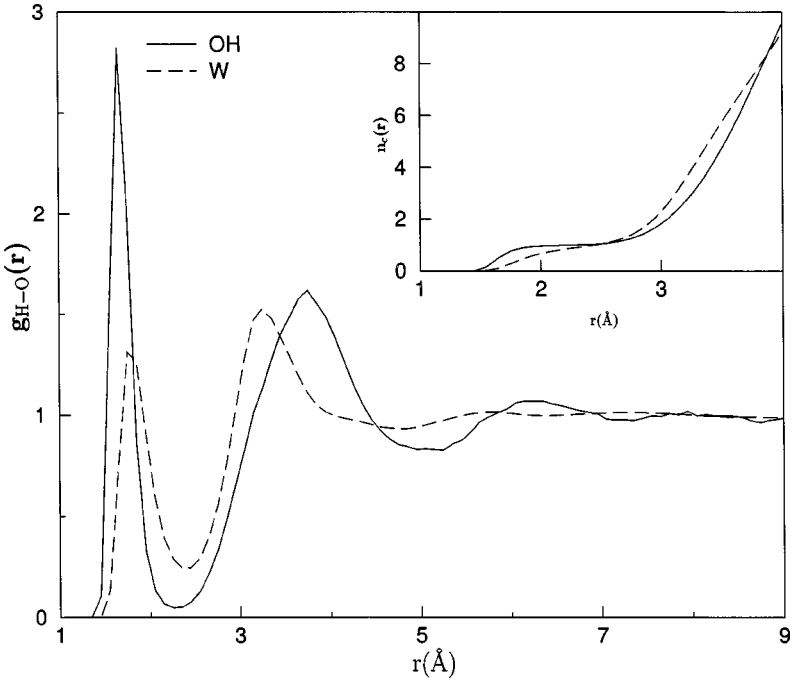

FIG. 7. Partial radial distribution function $g_{H-O}(r)$ for the hydrated OH radical and for liquid water. The inset shows the average coordination number $n_c(r)$.

Note that 14 and 52 represent the average number of water molecules in the first and second coordination shells of the hydroxyl radical. By using SPC charges on the water molecules, the average dipole moment of the solute (OH radical) over 50 uncorrelated configurations has been evaluated at the MPW1PW91/aug-cc-pVDZ level. The behavior of the induced dipole moment as a function of the number of water molecules N and the convergence of the dipole in the solution as a function of the number of uncorrelated configurations is shown in Fig. 8.

We find that the OH induced dipole moment in liquid water is $\sim 0.58 \pm 0.1$ D, which leads to an average dipole of 2.2 ± 0.1 D for the hydroxyl radical in water. This value is consistent with our parametrization of the OH radical charge distribution in the $OH-W_5$ cluster that leads to a dipole moment of 2.3 D (see Table II). It is interesting to compare the result for the OH radical with our recent prediction of the liquid water dipole moment (2.6 ± 0.14 D).[68] If we assume that the dipole moment of the water molecule in the liquid can be calculated by adding the contributions of two polarized OH dipoles of 2.2 D in the experimental geometry of the water molecule, the water dipole moment can be estimated as 2.8 D, which is only 0.2 D above our recent prediction.[68]

V. CONCLUSIONS

This work reports results for the hydration of the OH radical, including, for the first time, a theory-based predic-

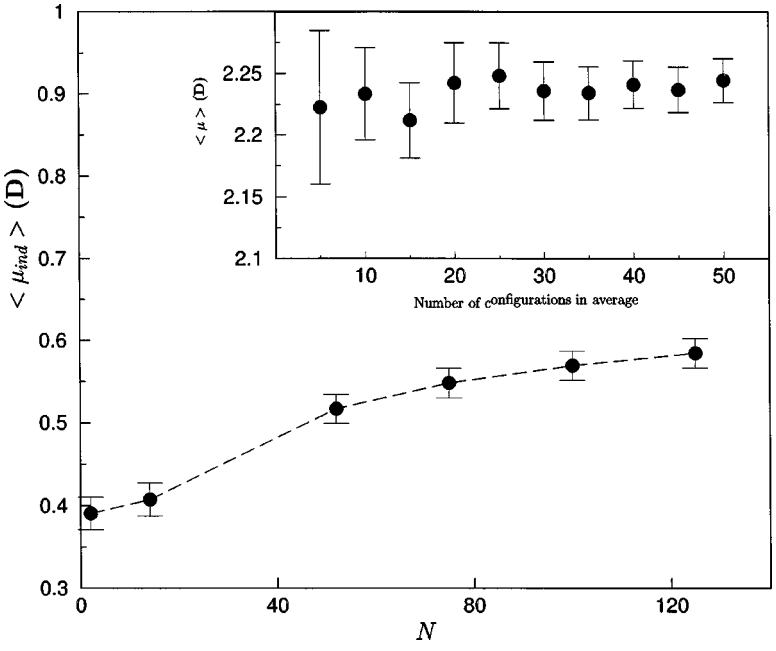

FIG. 8. Average induced dipole moment ($\langle \mu_{ind} \rangle$ in D) of the hydroxyl radical as a function of the number of water molecules N in the liquid. The inset shows the convergence of the OH average dipole moment as a function of the number of uncorrelated MC configurations.

tion for the hydration enthalpy of this species. This quantity is of fundamental interest in several domains, ranging from biochemistry to electronic properties of liquid water. The present study relies on two complementary approaches: microsolvation and statistical mechanics Monte Carlo simulations. From microsolvation modeling we conclude that for small water clusters (W_N), the binding energies of the OH radical to W_N, and of the water molecule to W_N, are very close. This can be related to the stability of the $OH–W_1$ complex, where the radical plays the role of proton donor.

Based on Monte Carlo simulations, our results show that the hydration enthalpies of the OH radical and water differ by less than 10 $kJ\,mol^{-1}$. The enthalpic stabilization of the water molecule in liquid water relative to the OH radical is possibly due to the contribution of long-ranged dipolar interactions and polarization effects. In this sense, other interesting conclusion concerns the polarization of the OH radical in liquid water. We predict that the dipole moment of the OH radical in water (2.2 ± 0.1 D) is increased by $\sim$30% in comparison with the gas phase value (1.66 D). This prediction is based on the SPC intermolecular potential, which is a very simple model. Further investigations with other intermolecular interaction models can be useful to confirm the present predictions. However, we note that our result for the OH radical dipole moment in water is consistent with a recent evaluation of the water dipole moment in liquid water (2.6 ± 0.1 D) by sequential Monte Carlo/quantum mechanics calculations,[68] based on the TIP5P[69] intermolecular potential model.

Our results for the OH radical hydration energy leads to a value for the liquid water band gap (6.88 eV) in excellent agreement with a recent prediction by Coe *et al.*[12]

ACKNOWLEDGMENTS

R.C.G. and P.C.d.C. gratefully acknowledge the support of Fundação para a Ciência e a Tecnologia. (Ph.D. Grant Nos. PRAXIS/XXI/BD/15920/98 and PRAXIS/XXI/BD/6503/2001). This work was partially supported by the Sapiens program of the FCT, Portugal (Grant No. POCTI/43315/QUI/2001).

[1] B. Halliwell and J. H. C. Gutteridge, *Free Radicals in Biology and Medicine* (Oxford University Press, Oxford, 1989).
[2] W. H. Kopenol, Free Radical Biol. Med. **10**, 85 (1991).
[3] E. R. Stadtman, Annu. Rev. Biochem. **62**, 797 (1993).
[4] B. Aygodan, D. T. Marshall, S. G. Stwarts, J. E. Turner, A. J. Boone, N. G. Richards, and W. E. Bolch, Radiat. Res. **157**, 38 (2002).
[5] W. Linert and G. N. L. Jameson, Inorg. Chem. **79**, 319 (2000).
[6] A. K. Chandra and T. Uchimaru, J. Phys. Chem. A **104**, 8535 (2000).
[7] P.-Y. Lien, R.-M. You, and W.-P. Hu, J. Phys. Chem. A **105**, 2391 (2001).
[8] I. W. M. Smith and A. R. Ravishankara, J. Phys. Chem. A **106**, 4798 (2002).
[9] J. E. Headrick and V. Vaida, Phys. Chem. Earth. **26**, 479 (2001).
[10] T. LaVere, D. Becker, and M. D. Sevilla, Radiat. Res. **145**, 673 (1996).
[11] L. Cermenati, P. Pichat, C. Guillard, and A. Albini, J. Phys. Chem. B **101**, 2650 (1997).
[12] J. V. Coe, A. D. Earhart, M. C. Cohen, G. J. Hoffman, H. W. Sarkas, and K. H. Bowen, J. Chem. Phys. **107**, 6023 (1997).
[13] K. S. Kim, H. S. Kim, J. H. Jang, H. S. Kim, and B.-J. Mhin, J. Chem. Phys. **94**, 2057 (1991).
[14] B. Wang, H. Hou, and Y. Gu, Chem. Phys. Lett. **303**, 96 (1999).
[15] Y. Xie and H. F. Schaefer III, J. Chem. Phys. **98**, 8829 (1993).
[16] Z. Zhou, Y. Qu, A. Fu, B. Du, F. He, and H. Gao, Int. J. Quantum Chem. **89**, 550 (2002).
[17] S. Hamad, S. Lago, and J. A. Mejías, J. Phys. Chem. A **106**, 9104 (2002).
[18] S. Canuto and K. Coutinho, Adv. Chem. Phys. **28**, 90 (1997).
[19] K. Coutinho and S. Canuto, J. Chem. Phys. **113**, 9132 (2000).
[20] C. Adamo and V. Barone, Chem. Phys. Lett. **274**, 242 (1997).
[21] C. Adamo and V. Barone, J. Comput. Chem. **19**, 419 (1998).
[22] C. Adamo and V. Barone, J. Chem. Phys. **108**, 664 (1998).
[23] J. P. Perdew and Y. Wang, Phys. Rev. B **45**, 13244 (1992).
[24] D. E. Woon and T. H. Dunning, Jr., J. Chem. Phys. **98**, 1358 (1993).
[25] R. A. Kendall, T. H. Dunning, Jr., and R. J. Harrisson, J. Chem. Phys. **96**, 6796 (1992).
[26] S. F. Boys and F. Bernardi, Mol. Phys. **19**, 553 (1970).
[27] S. S. Xantheas, J. Chem. Phys. **104**, 8821 (1986).
[28] A. C. Shepard, Y. Beers, G. P. Klein, and L. S. Rothman, J. Chem. Phys. **59**, 2254 (1973).
[29] R. D. Nelson, Jr., D. R. Lide, and A. A. Maryott, *Selected Values of Electric Dipole Moments for the Molecules in the Gas Phase* (NSRDS-NBS10, Washington, DC, 1967).
[30] K. Kuchitsu and Y. Morino, Bull. Chem. Soc. Jpn. **38**, 805 (1965).
[31] W. S. Benedict, N. Gailar, and E. K. Plyler, J. Chem. Phys. **24**, 9639 (1956).
[32] K. P. Huber and G. Herzberg, *Molecular Spectra and Molecular Structure. IV. Constants of Diatomic Molecules* (Van Nostrand Reinhold, New York, 1979).
[33] A. Outdola and T. R. Dyke, J. Chem. Phys. **72**, 5062 (1980).
[34] T. Shimanouchi, *Tables of Molecular Vibrational Frequencies* (NSRDS NBS-39, Washington, DC, 1972), Consolidated Vol. 1.
[35] L. A. Curtiss, D. J. Frurip, and M. Blander, J. Chem. Phys. **71**, 2703 (1979).
[36] M. M. Feyerisen, D. Feller, and D. A. Dixon, J. Phys. Chem. **100**, 2993 (1996).
[37] C. Møller and M. S. Pleset, Phys. Rev. **46**, 618 (1934).
[38] J. A. Pople, M. Head-Gordon, and K. Raghavachari, J. Chem. Phys. **87**, 5968 (1987).
[39] K. Raghavachari, J. A. Pople, E. S. Replogle, and M. Head-Gordon, J. Phys. Chem. **94**, 5579 (1990).
[40] J. Cizek, Adv. Chem. Phys. **14**, 35 (1969).
[41] G. D. Purvis and R. J. Bartlett, J. Chem. Phys. **76**, 1910 (1982).
[42] G. E. Scuseria, C. L. Janssen, and H. F. Schafer III, J. Chem. Phys. **72**, 4244 (1980).
[43] G. E. Scuseria and H. F. Schafer III, J. Chem. Phys. **90**, 3700 (1989).
[44] D. Frenkel and B. Smit, *Understanding Molecular Simulation* (Academic, San Diego, 1996).
[45] H. J. C. Berendsen, J. P. M. Postma, W. F. van Gusteren, and J. Hermans, in *Intermolecular Forces*, edited by B. Pullman (Reidel, Dordrecht, 1981), p. 331.
[46] U. C. Singh and P. A. Kollman, J. Comput. Chem. **5**, 129 (1984).
[47] B. H. Besler, K. M. Merz, Jr., and P. A. Kollman, J. Comput. Chem. **11**, 431 (1990).
[48] V. N. Levchuk, I. I. Sheykhet, and B. Ya. Simkin, Chem. Phys. Lett. **185**, 339 (1991).
[49] T. Lazaridis, J. Phys. Chem. B **104**, 4964 (2000).
[50] R. C. Guedes, K. Coutinho, B. J. Costa Cabral, and S. Canuto, J. Phys. Chem. B **107**, 4304 (2003).
[51] M. J. Frisch, G. W. Trucks, H. B. Schlegel *et al.*, GAUSSIAN 98, Gaussian Inc., Pittsburgh, PA, 1998.
[52] K. Coutinho and S. Canuto, DICE: A general Monte Carlo program for liquid simulation, University of São Paulo, Brazil, 2000.
[53] K. S. Kim, M. Dupuis, G. C. Lie, and E. Clementi, Chem. Phys. Lett. **131**, 451 (1986).
[54] K. S. Kim, B. J. Mhin, and K. S. Kim, J. Chem. Phys. **97**, 6649 (1992).
[55] J. Kim, J. Y. Lee, S. Lee, B. J. Mhin, and K. S. Kim, J. Chem. Phys. **102**, 310 (1995).
[56] M. W. Feyereisen, D. Feller, and D. A. Dixon, J. Phys. Chem. **100**, 2993 (1996).
[57] M. Schütz, S. Brdarski, P.-O. Widmark, R. Lindh, and G. Karlström, J. Chem. Phys. **107**, 4597 (1997).
[58] J. Kim, D. Majumdar, H. M. Lee, and K. S. Kim, J. Chem. Phys. **110**, 9128 (1999).
[59] H. M. Lee, S. B. Suh, J. Y. Lee, P. Tarakeshwar, and K. S. Kim, J. Chem. Phys. **112**, 9759 (2000).
[60] K. S. Kim, P. Tarakeshwar, and J. Y. Lee, Chem. Rev. (Washington, D.C.) **100**, 4145 (2000).

[61] *CODATA Key Values for Thermodynamics*, edited by J. D. Cox, D. D. Wagman, and V. A. Medvedev (Hemisphere, New York, 1989).
[62] A. Engdahl, G. Karlström, and B. Nelander, J. Chem. Phys. **118**, 7797 (2003).
[63] P. D. Cooper, H. G. Kjaergaard, V. S. Langford, A. J. McKinley, T. I. Quickenden, and D. P. Schofield, J. Am. Chem. Soc. **125**, 6048 (2003).
[64] V. S. Langford, A. J. McKinley, and T. I. Quickenden, J. Am. Chem. Soc. **122**, 12859 (2000).
[65] L. Khriachtchev, M. Pettersson, S. Touminen, and M. Räsänen, J. Chem. Phys. **107**, 7252 (1997).
[66] J. Goodman and L. E. Brus, J. Chem. Phys. **67**, 4858 (1977).
[67] J. P. Prates Ramalho, B. J. Costa Cabral, and F. M. S. Silva Fernandes, Chem. Phys. Lett. **184**, 53 (1991).
[68] K. Coutinho, R. C. Guedes, B. J. Costa Cabral, and S. Canuto, Chem. Phys. Lett. **369**, 345 (2003).
[69] M. W. Mahoney and W. L. Jorgensen, J. Chem. Phys. **112**, 8910 (2000).

Chapter 4

Paper II: A bulk view

As already explored in previous work [130], one of the motivations of the present work is the quantitative prediction of the electronic density of states for liquid water. A further motivation was that theoretical estimates for the optical band gap of liquid water, E_g, were scarce and ranged from 3.6 to 6.5 eV [91, 130, 270], at odds with experimental evidence which pointed to much higher values ∼8.9 eV [138]. Also, estimates for the conduction band edge V_0 ranged from -1.2 to 0.0 eV [35, 133]. The purpose of paper II was thus fourfold:

- The reparametrization of a one-parameter hybrid exchange-correlation functional, for the quantitative account of electron binding energies for the water dimer [149].
- The evaluation of a sequential MC/QM approach [255, 256] for the quantitative determination of the electronic density of states of liquid water.
- An estimate for V_0 based on the calculated electronic density of states.
- An estimate of E_{gap} based on our results for V_0 and ΔE_{hyd}[OH].

Electronic energy levels were calculated using the one parameter mPW1PW91 hybrid functional, reparametrized to reproduce the first ionization potential of the water dimer in its minimum energy geometry. It should be noted that, as found in previous work, the reparametrization of a hybrid density functional for the reproduction of the electronic properties of single water molecule does nor yield the correct optical gap. The optimal amount of exact exchange was found to be 62.5%. In order to run these calculations using Gaussian 03, the IOP(3/76=0375006250) keyword must be included in the route section. Using the notation in paper II, Eq.(1), $(1 - \alpha) = 0.625$ and $\alpha = 0.375$.

The size dependence of the electronic density of states, the optical band gap and V_0 of water was studied within a sequential quantum chemical / Monte Carlo methodology for statistically uncorrelated $(H_2O)_n$, $(n = 2, 4, 8, 15, 20, \ldots, 30)$ configurations, generated from liquid water Monte Carlo simulation. The optimal

number configurations to be sampled from Monte Carlo simulation and the required cluster size for the size convergence of the electronic density of states had already been established in earlier work [130].

For $n = 30$, with the exception of the $2a_1 1$ orbital, a good agreement between experimental binding energies for liquid water and theoretical results is observed. For the $1b_1$ and $3a_1$ orbitals, experimental electron binding energies are in better agreement with theoretical results for free water clusters, although the differences are quite small. More important, the redshift of electron binding energies, which is a condensed-phase effect, is qualitatively in keeping with experimental information: the red shift of electron binding energies is $\sim$0.9 and 0.7 eV for the $1b_1$ and $3a_1$ orbitals, respectively. The experimental values are $\sim$1.3 eV. The only significant discrepancy relative to experiment concerns the $2a_1$ orbital for which theoretical calculations predict a small blueshift $\sim$0.4 eV, whereas a 1.7 eV redshift is predicted by experiment.

Extrapolation of V_0 to bulk yields 0.17$\pm$0.05 eV, in good agreement with the recent estimate by Coe et al. (-0.12 eV) [35] but significantly smaller than the value reported by Grand et al. (1.2$\pm$0.1 eV) [133]. From Eq.(1.17), taking our previous Monte Carlo result for ΔE_{hyd}[OH] =-0.38 eV, and the present estimate of V_0, the adiabatic band gap for pure liquid water E_g is 6.83$\pm$0.05 eV Eq.(1.17), again in agreement with the value reported by Coe and co-workers [35].

The Kohn-Sham density of states and band gap of water: From small clusters to liquid water

P. Cabral do Couto, S. G. Estácio, and B. J. Costa Cabral[a)]
Departamento de Química e Bioquímica, Faculdade de Ciências, Universidade de Lisboa, 1749-016 Lisboa, Portugal and Grupo de Fýsica Matemýtica da Universidade de Lisboa, Avenida Professor Gama Pinto 2, 1649-003 Lisboa, Portugal

(Received 27 April 2005; accepted 1 June 2005; published online 9 August 2005)

Electronic properties of water clusters $(H_2O)_n$, with $n=2$, 4, 8, 10, 15, 20, and 30 molecules were investigated by sequential Monte Carlo/density-functional theory (DFT) calculations. DFT calculations were carried out over uncorrelated configurations generated by Monte Carlo simulations of liquid water with a reparametrized exchange-correlation functional that reproduces the experimental information on the electronic properties (first ionization energy and highest occupied molecular orbital-lowest unoccupied molecular orbital gap) of the water dimer. The dependence of electronic properties on the cluster size (n) shows that the density of states (DOS) of small water clusters $(n>10)$ exhibits the same basic features that are typical of larger aggregates, such as the mixing of the $3a_1$ and $1b_1$ valence bands. When long-ranged polarization effects are taken into account by the introduction of embedding charges, the DOS associated with $3a_1$ orbitals is significantly enhanced. In agreement with valence-band photoelectron spectra of liquid water, the $1b_1$, $3a_1$, and $1b_2$ electron binding energies in water aggregates are redshifted by ~ 1 eV relative to the isolated molecule. By extrapolating the results for larger clusters the threshold energy for photoelectron emission is 9.6 ± 0.15 eV (free clusters) and 10.58 ± 0.10 eV (embedded clusters). Our results for the electron affinity ($V_0=-0.17\pm0.05$ eV) and adiabatic band gap ($E_{G,\mathrm{Ad}}=6.83\pm0.05$ eV) of liquid water are in excellent agreement with recent information from theoretical and experimental works. © *2005 American Institute of Physics*. [DOI: 10.1063/1.1979487]

I. INTRODUCTION

Water is the most important liquid for life and chemical reactivity in liquid water is a fundamental process characterizing the behavior of many living organisms. Therefore, the structure, energetics, and electronic properties of liquid water were the subject of numerous investigations.[1–7] Some properties of liquid water are unique, fascinating, and worth referring: the structure of water is characterized by a complex hydrogen (H)-bond network which leads to a very specific dependence of the density on the thermodynamic state and to the water density anomaly at $T=4\ ^\circ\mathrm{C}$;[8] the strong polarizability of liquid water, which is related to cooperative effects induced by H bonding, determines its dielectric properties as well as the significant increase of the water molecule dipole moment from 1.85 D in the gas to ~ 2.6 D in the liquid phase.[9,10] In comparison with its energetics and structure, the electronic properties of liquid water[3,11–22] are apparently not well understood. One specific aspect concerns the band gap of water.[3,11,14,16,17,19,20] It is generally accepted that water can be described as a very large band-gap amorphous semiconductor.[11,17] However, it is not obvious that the band gap of liquid water can be uniquely associated with an optical (vertical) excitation process, where the gap is defined simply as the highest occupied molecular orbital-lowest unoccupied molecular orbital (HOMO-LUMO) energy difference. As recently pointed out by Coe *et al.*,[3] the reactive nature of electronically excited water molecules,[18] the reorganization of water molecules around charged species in liquid phase, and the observed photophysics of anionic defects (known as the anion problem)[4] strongly indicate that an adiabatic route can be defined for accessing the conduction-band edge in liquid phase. Moreover, given that the time scale of the solvent relaxation is much larger than the vertical process, the adiabatic band gap of liquid water cannot be determined vertically.

From the theoretical point of view, electronic properties of liquid water were the subject of several studies.[3,23–26] It is well known that *ab initio* molecular dynamics (ABMD) simulations are of great interest for investigating the electronic properties in condensed phase. Although the complexity of liquid water makes a first-principles approach rather difficult, several ABMD simulations were carried out[27–34] and some of them also reported results for the HOMO-LUMO gap and the density of states (DOS).[27,32,33] However, only few works on the adiabatic band gap of liquid water were reported.[3,4] Another aspect of interest concerns the relationship between H bonding and the electronic properties of water.[35–40] In this sense, specific issues including the size dependence of the electronic properties, the influence of surface effects on the DOS, and water band gap certainly deserve further attention.

The present article is focused on the electronic properties of water, in particular, on its density of states (DOS),

[a)]Author to whom correspondence should be addressed. Electronic mail: ben@adonis.cii.fc.ul.pt

HOMO-LUMO gap (E_G), and adiabatic band gap ($E_{G,\mathrm{Ad}}$). A sequential Monte Carlo/quantum mechanics approach[41,42] was adopted. From uncorrelated supermolecular structures generated by Monte Carlo simulations for liquid water, density-functional theory (DFT) calculations were carried out to study the electronic properties of water aggregates of different sizes. Surface effects were then minimized and long-ranged electrostatic interactions were taken into account by the introduction of embedding charges, as an approximation to the liquid environment.

DFT calculations were carried out with a reparametrization of the Adamo and Barone modified exchange-correlation functional (MPW1PW91).[43–45] The reparametrized functional reproduces experimental information on the electronic properties of the water dimer. The article is organized as follows. Initially, we describe the generation of the aggregates by the Monte Carlo method and the reparametrization of the MPW1PW91 functional. A detailed analysis of size dependence and surface effects is then reported. Finally, extrapolated results for larger water aggregates (free and embedded in a charge distribution) are reported and compared with experimental information and theoretical predictions for liquid water from other studies. We conclude by placing emphasis on the difference between the optical and the adiabatic band gap of liquid water.

II. COMPUTATIONAL DETAILS

A. Monte Carlo simulations

The interactions between water molecules were described by the TIP5P potential.[46] This model, which has been designed to reproduce the water density anomaly at $T=4\ ^\circ\mathrm{C}$,[46] predicts the structural and thermodynamic properties of liquid water in excellent agreement with experiment. The TIP5P charge distribution is described by two negatively charged ($-0.241\ e$) sites located symmetrically along the lone pair directions and a positive charge ($+0.241\ e$) on each hydrogen site.[46] It is important to observe that this model predicts a dielectric constant of water ($\epsilon=81.5\pm1.5$) in very good agreement with experiment ($\epsilon=79.3$). Monte Carlo (MC) simulations of water were carried out in the isobaric-isothermal (npT) ensemble[47] at $T=298$ K and $p=1$ atm in a cubic box with periodic boundary conditions. The number of water molecules is $n=500$ and the interactions are truncated at a cutoff radius of 9.0 Å. We carried out 10^8 MC steps for equilibration. This run was followed by 1.25×10^9 additional MC steps. Each step involves the attempt to move one molecule of the system. From the configurations generated by the MC procedure $N=50$ uncorrelated configurations were selected by determining a correlation time over the MC Markov chain.[41,42] We note that successive configurations generated by the Metropolis algorithm[48] are strongly correlated. When the property of interest involves a high computational effort, the use of uncorrelated structures is of crucial importance for evaluating the averages over a relatively small number of representative configurations.[41,42]

Each uncorrelated configuration corresponds to a supermolecular structure (water cluster) including explicitely n molecules. The structure of the clusters corresponds to the liquid-phase structure at $T=298$ K and no geometry optimization of the aggregates was carried out. Size dependence was investigated by carrying out calculations with $n=1$, 2, 4, 8, 10, 15, 20, 30. Surface effects and long-ranged corrections to polarization effects were investigated by embedding the clusters in the TIP5P charge distribution of the surrounding water molecules. Thus, no periodic boundary conditions were applied for evaluating the electronic properties. The number of embedding water molecules is represented by n_c. We have taken $n_c=200$. Some calculations based on the Kirkwood-Onsager model,[49] where the clusters are placed in a spherical cavity surrounded by a continuum dielectric medium, were also carried out.

B. Density-functional theory calculations

The electronic properties of the clusters were determined by performing DFT calculations over uncorrelated MC configurations. Although the physical meaning of Kohn-Sham (KS) orbital energies remains a controversial issue in the literature,[50,51] several works provided evidence that DFT can correctly predict electron binding energies.[52–61] The disagreement between KS electron binding energies predicted by the widely used exchange-correlation functionals and experiment is related to the self-interaction error in DFT.[62] An interesting possibility is to parametrize the exchange-correlation functional for reproducing experimental electron binding energies.[53,57] The present approach to study the electronic properties of water is based on the following semiempirical procedure. The modified Perdew-Wang functional (MPW1PW91) proposed by Adamo and Barone[43–45] has been reparametrized to reproduce the electronic properties of the water dimer. The reparametrization was based on the representation of the exchange-correlation functional as[43–45]

$$E_{\mathrm{xc}}=(1-\alpha)E_x^{\mathrm{HF}}+\alpha(E_x^{\mathrm{Slater}}+\Delta E_x^{\mathrm{mPW}})+E_c^{\mathrm{local}}+\Delta E_c^{\mathrm{PW91}}, \tag{1}$$

where $\Delta E_{\mathrm{x}}^{\mathrm{mPW}}$ is the modified Perdew-Wang exchange-correlation functional, and E_c^{local} is the local correlation functional contribution.

We have determined the optimal value of α in the above expression that reproduces the first ionization potential of the water dimer (11.21 ± 0.09 eV).[63] DFT calculations were carried out with Woon and Dunning's correlation consistent polarized valence double zeta basis set augmented with diffuse functions (aug-cc-pVDZ).[64] We find that the optimal value of α is 0.375. The MPW1PW91 standard value is $\alpha=0.75$. The results for several properties of the water dimer predicted by the present reparametrization are reported in Table I, where they are compared with experimental data and theoretical results based on Hartree-Fock (HF) calculations, coupled cluster with single and double excitations and perturbative inclusion of triples [CCSD(T)],[65–68] and Møller-Pleset perturbation theory[69] at fourth order (MP4). CCSD(T) and MP4 results for the vertical attachment energies (VAE) and electron binding energies were based on ΔE calculations.

Table I reports (see values in brackets) the electron binding energies relative to the HOMO. For the valence orbitals, these differences are roughly the same for HF calculations

TABLE I. Theoretical and experimental results for the water dimer $(H_2O)_2$. The distances are in angstroms. The binding energies (ΔE_b) are in kJ mol^{-1}. The dipole moments (μ) are in debye. The vertical attachment energies (VAE), HOMO-LUMO energy differences (E_G), and electron binding energies are in eV. The frequencies are in cm^{-1}. For the dimer, [a] and [d] denote the role played (as proton acceptor or donor) by the water molecule for which the contribution from a given orbital is dominant. The numbers in brackets are electron binding energies relative to the HOMO. The calculations were performed with the aug-cc-pVDZ basis set.

		MPW1PW91				
	HF	$\alpha=0.750$[a]	$\alpha=0.375$[b]	CCSD(T)	MP4	Expt.
d(O–O)	3.032	2.892	2.864	2.926	2.917	2.976±0.03[c]
ΔE_b	−16.40	−20.1	−21.8	−22.2	−22.5	−20.9±0.5[d]
μ	2.9	2.6	2.7	2.7	2.7	2.6[e]
VAE	-0.80	0.73	-0.13	0.49	0.50	0.050±0.03[f]
E_G	13.97	7.65	11.33	12.48	12.57	11.16±0.05[g]
$1b_1$ [d]	13.15	8.38	11.20	12.97	13.07	11.21±0.09[h]
$(3a_1,1b_1)$ [a]	14.48[1.3]	9.76[1.4]	12.60[1.4]			
$(3a_1,1b_1)$ [d]	15.12[2.0]	10.51[2.1]	13.34[2.1]			
$3a_1$ [a]	16.67[3.5]	12.05[3.7]	14.91[3.7]			
$1b_2$ [d]	19.22[6.1]	14.36[6.0]	17.34[6.1]			
$1b_2$ [a]	20.47[7.3]	15.75[7.4]	18.72[7.5]			
$2a_1$ [d]	36.34[23.2]	27.68[19.3]	32.53[21.3]			
$2a_1$ [a]	37.72[24.6]	29.28[20.9]	34.15[23.0]			
O($1s$) [d]	559.09[545.9]	522.89[514.5]	541.14(540.20)[i][529.9]			
O($1s$) [a]	560.46[547.3]	524.47[516.1]	542.74(541.48)[i][530.2]			
ν_1		3957	4171			3745[j]
ν_2		3936	4152			3730[j]
ν_3		3849	4062			3600[j]
ν_4		3720	3951			3539[j]
ν_5		1651	1716			1619[j]
ν_6		1629	1693			1601[j]

[a]MPW1PW91 parametrization (Refs. 43–45).
[b]Present parametrization.
[c]From Odutola and Dyke (Ref. 71).
[d]From Feyerisen *et al.* (Ref. 72).
[e]From Dyke *et al.* (Ref. 73).
[f]From Kim *et al.* (Ref. 74).
[g]Estimated from the experimental ionization potential (IP) and vertical attachment energy (VAE) as IP-VAE.
[h]From Ng *et al.* (Ref. 63).
[i]Theoretical results based on CASSCF/aug-cc-pVDZ calculations. From Felicissimo *et al.* (Ref. 70).
[j]From Huang and Miller (Ref. 75).

and for the two MPW1PW91 parametrizations. In a comparative analysis of HF and KS energies, Politzer and Abu-Awwad[54] pointed out that, for a given molecule, different exchange-correlation functionals lead to KS valence orbital energies, which differ from experimental data nearly by a constant value. The present results confirm this behavior. Moreover, they indicate that when the functional is parametrized to reproduce the HOMO energy, the whole set of orbital energies is in good agreement with experiment. For example, our results for the water dimer O($1s$) binding energies (541.14 and 542.74 eV) are very close to theoretical predictions based on complete active space self-consistent field (CASSCF) calculations (540.2 and 541.1 eV).[70] This agreement leads credence to our parametrization for reproducing the core DOS of water aggregates, although our main interest is focused on the valence binding energies and HOMO-LUMO gap.

Although the present reparametrization was oriented to reproduce the first ionization potential, several properties of the water dimer, including the structure,[71] binding energy,[72] dipole moment,[73] vertical attachment energy (VAE),[74] and HOMO-LUMO gap (E_G), are in excellent agreement with experiment and other theoretical approaches. As expected, unscaled harmonic vibrational frequencies are slightly overestimated in comparison with experimental values.[75] We interpret the agreement between our predictions and experimental information for several properties of the water dimer as a strong indication on the reliability of the present approach for investigating the electronic properties of water clusters. The quantum-mechanical calculations were carried out with the GAUSSIAN-98 program.[76]

III. THE ELECTRONIC DENSITY OF STATES IN WATER CLUSTERS

A. Size dependence of electronic properties in free water clusters

The KS orbitals for the optimized structures of the water monomer (w_1), dimer (w_2), and tetramer (w_4) are illustrated in Fig. 1. For the monomer (w_1) they correspond to the $4a_1$, $1b_1$, $3a_1$, and $1b_2$ orbitals. (The $2a_1$ orbital at −33.4 eV is not shown.) $1b_1$ is the highest occupied molecular orbital

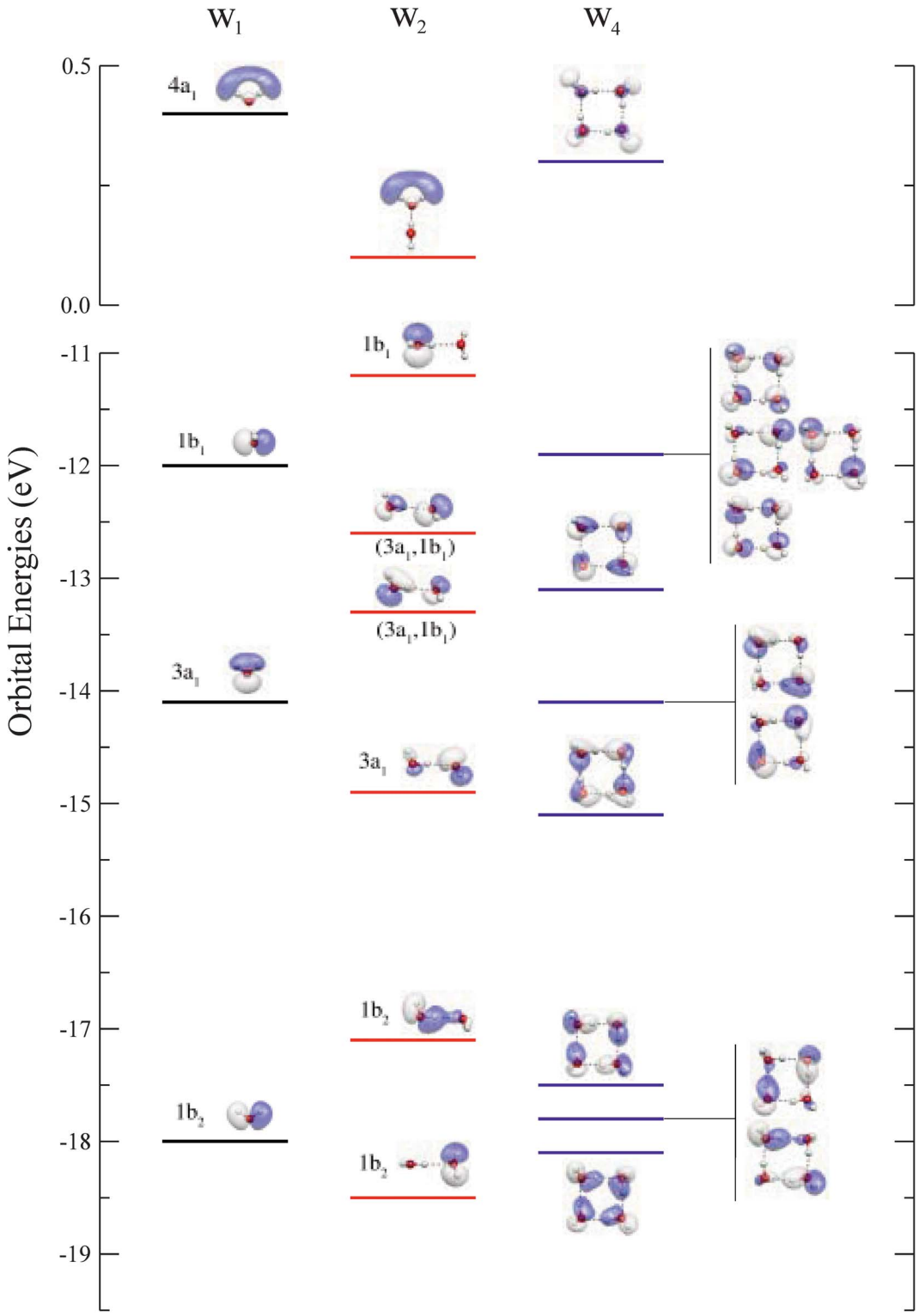

FIG. 1. (Color) Orbital energies (in eV) for the optimized gas-phase structures of the water monomer (w_1), dimer (w_2), and tetramer (w_4).

(HOMO) at the top of the water molecule "valence band." The $1b_1$ orbital has a strong $2p$ character and is centered at the site of the O($1s$) core orbital. For the water dimer (w_2) the HOMO corresponds essentially to the $1b_1$ orbital. The next two lower orbitals involve overlap between $3a_1$ and $1b_1$ orbitals and are represented in Fig. 1 as $(3a_1,1b_1)$. The next-lowest dimer orbital is essentially a $3a_1$ orbital centered at the proton accepting water molecule. The two lowest occupied orbitals of w_2, represented in Fig. 1, are dominated by the contributions from $1b_2$, although the higher one involves some overlap with the $3a_1$ orbital. The most stable $1b_2$ orbital of the dimer correspond essentially to the energetically stabilized monomer orbital upon dimer formation. The splitting of the monomer orbital energies upon dimer formation reflects the feature that each water molecule plays a different role (as a proton donor or proton acceptor). The degeneracy

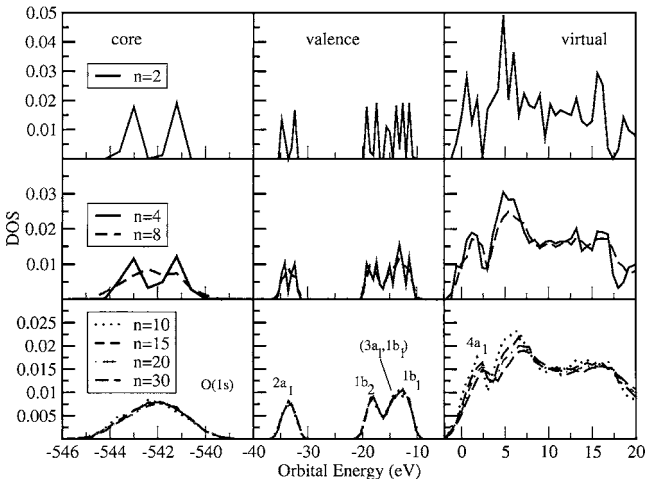

FIG. 2. Dependence of the average density of states (DOS) on the number of water molecules in the cluster (n=2, 4, 8, 10, 15, 20, 30) for free water clusters. MPW1PW91[α=0.375]/aug-cc-pVDZ results. Averages were carried out over 50 uncorrelated MC configurations.

of electron binding energies of the water tetramer (w_4) reflects its symmetrical cyclic structure. The highest occupied orbitals involve the $1b_1$ and $3a_1$ interactions and are related to the orbitals of the water dimer. We stress the specific role played by the $3a_1$ orbital in H bonding. As indicated in Fig. 1, H bonding involves mixing of $3a_1$ and $1b_1$ orbitals. This feature will induce broadening of the $3a_1$ and $1b_1$ bands upon condensation.[37] Also represented in Fig. 1 is the virtual $4a_1$ orbital (LUMO), which plays a central role in the energetic stabilization of an excess electron through the formation of a dipole-bound anion structure.[77,78] The energetical stabilization of the dimer $4a_1$ orbital relative to the monomer illustrates the stabilization of the LUMO (or the increase of the electronic affinity) upon dimer formation. The structure and orbital energies of small water clusters are the departure points to discuss the density of states (DOS) of larger clusters, and the characterization of their respective bands, which will keep a close relationship with the distribution of orbital energies of the small aggregates.

The size dependence of the density of states (DOS) is illustrated in Fig. 2, where the average DOS for water clusters of different sizes is reported. These clusters are supermolecular uncorrelated structures generated by the MC simulations of liquid water. We note that in the case of w_2 and w_4 they do not necessarily correspond to the gas-phase optimized structures of Fig. 1, because the structure of the aggregates taken from the simulations reflects the thermal fluctuations in the liquid phase. Therefore, the DOS of the uncorrelated structures will reflect thermal as well as electronic broadening.[33] The latter effect is basically related to the interactions between the water molecules. On the other hand, thermal fluctuations will be associated with the presence of different configurations at a finite temperature T.

The average DOS for the w_2 cluster associated with the $1b_2$ orbital is bimodal. Their peaks correspond roughly to the orbital energies of Fig. 1. For larger clusters the DOS becomes a broad distribution due to the presence of an increasing number of nearly isoenergetic isomers (thermal broadening). A similar pattern (from peaked to broad DOS) is observed in the formation of the $3a_1$ and $1b_1$ bands. For larger clusters ($n>10$) the $3a_1$ and $1b_1$ bands overlap appearing as a single distribution due to thermal and electronic broadening. The results shown in Fig. 2 indicate that the average DOS of small water aggregates is not dependent on the number of water molecules for $n>15$. The behavior of the core DOS with the cluster size reflects the expected dispersion of the core energies related to different structures and shows that the maxima position of the DOS is not changed for $n>10$.

The DOS of unoccupied orbitals is characterized by two peaks related to the $4a_1$ and $2b_1$ orbitals. For larger clusters ($n>10$) a shoulder (or preedge feature) near the bottom of the conduction band and a broad distribution centered at $\sim$10 eV are observed. Recent x-ray absorption spectroscopy (XAS) experiments[36] provided evidence on significant differences between the XAS spectra of ice and water in liquid and gaseous phases. These differences were related to structural features of the H-bond network and the spectra exhibit a strong dependence of the H-bonding environment.[36,39] Specifically, the presence of a preedge feature at the bottom of the conduction band was associated with broken H bonds. Therefore, a strong preedge is typical of small water clusters where free hydrogen atoms can act as H-bond acceptors. In contrast, only a weak structure is observed in ice, which is an indication of a fully coordinated H-bond network.[36] The behavior of the conduction-band DOS with the cluster size (Fig. 2) shows that the preedge feature is reduced with increasing n, which is an indication of H-bond formation. Moreover, the second broad peak at the high-energy range increases with the cluster size. These findings are in keeping with experimental[36] and theoretical studies[36,39] on x-ray absorption in water and water clusters.

The top of the valence band is related to the nonbonding orbital $1b_1$ (HOMO) and the difference between the HOMO and the bottom of the conduction band (or the average value of the LUMO) defines the optical band gap (E_G). The average energy of the LUMO for a cluster with n water molecules can be associated with the average electron affinity of the aggregates and it is represented as $V_{0,n}$.

The convergence of the DOS or the averaged orbital energies with the number of uncorrelated supermolecular structures (N) is illustrated in Fig. 3, where the cumulative average energies of the LUMO (top) and HOMO (bottom) as a function of N, for clusters of different size (n), are represented. In agreement with previous investigations of the dipole moment of liquid water based on sequential Monte Carlo/quantum mechanics calculations,[10] we observe that N =50 uncorrelated configurations are adequate for a reliable prediction of converged average properties.

Average HOMO energies are redshifted with increasing n. They change from $\sim$−11 (n=2) to $\sim$−9.6 eV (n=30). The dependence of the LUMO energy on the cluster size is also illustrated in Fig. 3. The LUMO energy is shifted to lower energies as the cluster size increases. From the water monomer to the cluster with n=30, the LUMO energy is stabilized by $\sim$1 eV. This tendency may be related to the formation of local structures involving the simultaneous presence of a number of free or dangling hydrogen atoms,

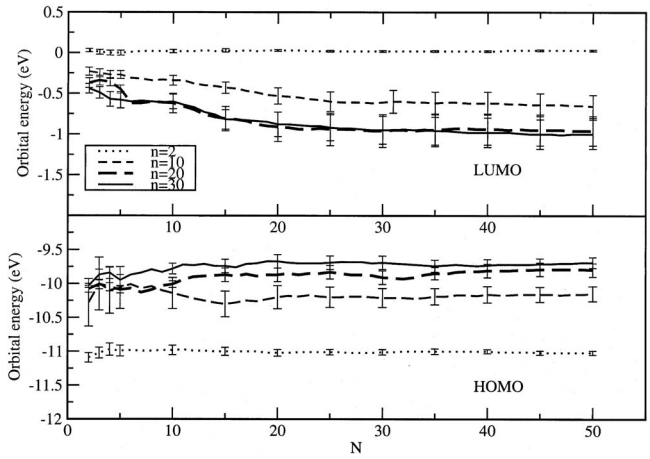

FIG. 3. Dependence of the average HOMO and LUMO energies on the number of uncorrelated configurations (N) for free water clusters of different size n.

mainly at the cluster surface. This number should increase with n because it depends on the number of water molecules close to the surface. Therefore, it seems reasonable to observe that the stabilization of the LUMO or the increase of the clusters electronic affinity with n can be related to surface effects.

B. Introduction of embedding charges: Influence on the water density of states

The uncorrelated supermolecular structures generated by the Monte Carlo simulations are water clusters, where surface effects are certainly significant. Although the calculations for free water clusters indicate the possibility to extrapolate the results for larger clusters, it is of interest to discuss how long-ranged polarization effects can be included and how surface effects can be minimized. Consequently, we have adopted the same strategy used for predicting the average dipole moment of the water molecule in liquid water.[10] Let us consider the larger aggregate ($n=30$). To this supermolecular structure, which has been selected from uncorrelated Monte Carlo simulations with 500 water molecules, the nonpolarizable TIP5P charge distribution of $n_c=200$ surrounding water molecules were added.

We should expect that the introduction of charge distribution mainly affects the water molecules closer to the cluster surface. To illustrate this effect we have calculated the difference of the electronic density in free and embedded clusters. Electronic density differences were calculated with the MOLEKEL visualization package[79] and isosurfaces representing these quantities are shown in Fig. 4. The main changes of the electronic density concern the water molecules close to the surface. No significant changes are observed in the electronic density of the inner molecules. Figure 5 shows the DOS for the free and embedded $\dot{w}_{30}$ aggregates. The core DOS is only slightly modified by the presence of the charges, which lead to a narrower peak centered at ~ -542 eV. This reflects a more homogeneous distribution of the electronic states in the embedded clusters and involves mainly the stabilization of core states for the water molecules close to the charge distribution.

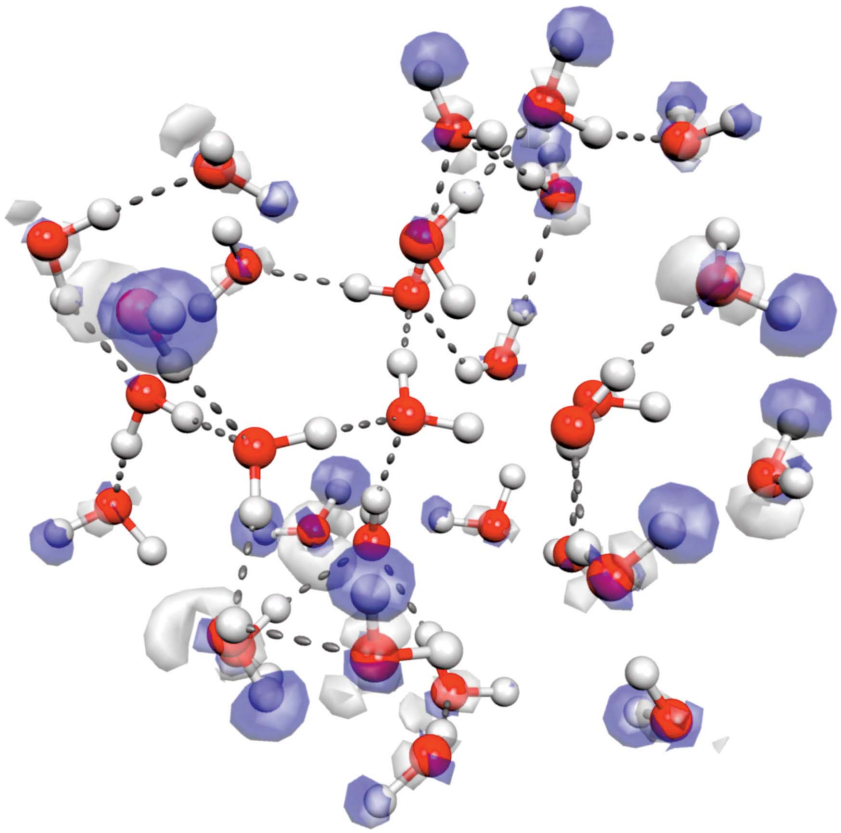

FIG. 4. (Color) Isosurfaces corresponding to the electronic density difference between free and embedded water clusters with $n=30$. The isosurfaces correspond to electronic density differences of -0.0025 (dark) and 0.0025 e Å^{-3} (white). The number of surrounding water molecules (represented by TIP5P charges) is $n_c=200$.

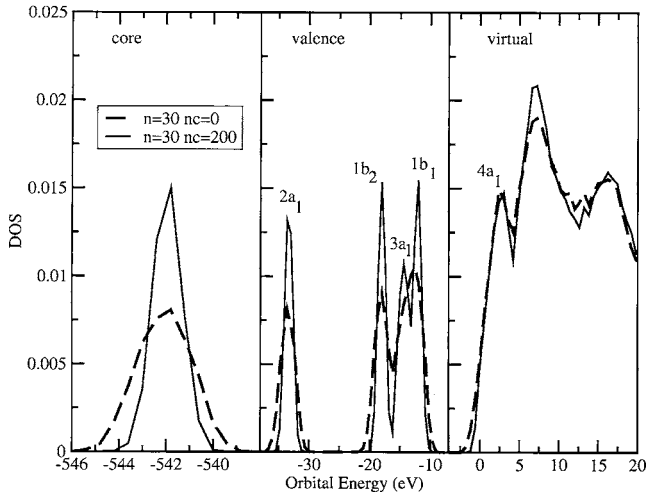

FIG. 5. Dependence of the DOS on the introduction of embedding charges (n_c=200). Results for the w_{30} cluster.

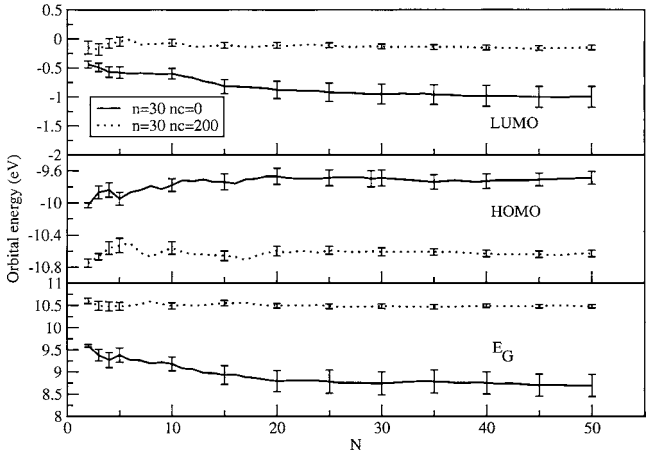

FIG. 6. Dependence of the HOMO and LUMO energies, and optical band gap E_G on the introduction of embedding charges (n_c=200). Results for the w_{30} cluster.

Based on x-ray emission spectra and Hartree-Fock calculations for liquid structures generated by molecular dynamics simulations, Guo *et al.*[37] suggested that the strong involvement of the $3a_1$ valence orbitals in H bonding leads to the broadening of $3a_1$ and $1b_2$ bands from the water monomer to small water clusters.[37] The same behavior of the DOS for free water clusters is presently observed. However, by adding embedding charges, a shoulder at ~ -14 eV, which can be associated to the $3a_1$ band, is observed. In addition, the charges contribute to decrease the mixing of $1b_2$ and $3a_1$ bands. This seems to reflect a significant polarization of the $3a_1$ orbital of the water molecules by the charges. We note that polarization of the $3a_1$ orbital was recently invoked to explain the large increase in the water dipole moment upon condensation.[37] Similar changes are also observed when the aggregates are embedded in a dielectric medium, strongly indicating that the mixing of the $3a_1$ and $1b_2$ bands in the water DOS is mainly related to surface effects. However, it should be observed that in contrast with the continuum dielectric method, thermal fluctuactions related to different charge configurations will characterize long-ranged corrections and thermal broadening in the present approach.

In keeping with the behavior for free water clusters of increasing size, the $1b_1$ conduction band is shifted to lower energies, which indicates that the changes on the DOS for occupied orbitals are similar when the cluster size increases or when an embedding charge distribution is added.

When the clusters are embedded by a charge distribution, the DOS of unoccupied orbitals is also modified. First, the DOS associated with the bottom of the conduction band is slightly shifted to higher energies. Second, the peak of the broad distribution related to the $2b_1$ and Rydberg states increases. The first modification is also illustrated in Fig. 6, where the energies of the HOMO and LUMO, as well as E_G are shown as a function of N (the number of uncorrelated MC configurations) for the w_{30} aggregate with and without embedding charges. By adding charges, the LUMO energy is also shifted upwards. This tendency is opposite to what is observed when the cluster size increases. We note that the LUMO energy is related to the water electron affinity, or to the energy needed to solvate an electron, which depends on the number of nonbonded hydrogen atoms. Therefore, a possible explanation for the behavior of the LUMO energy is that by introducing embedding charges, we simulate the presence of water molecules and the corresponding increase of H bonds. We have verified that a similar effect is observed when self-consistent reaction-field calculations based on the Kirkwood-Onsager model are carried out.

IV. EXTRAPOLATION TO LIQUID WATER AND COMPARISON WITH EXPERIMENT

A. Binding energies and gas-to-condensed-phase energy shifts

Table II reports the experimental[22] and theoretical KS

TABLE II. Electron binding energies and gas-to-condensed-phase energy shifts (δE) for valence orbitals. The data are in eV. The theoretical results are for the w_{30} cluster.

	Expt.			Theor.			
Orbital	Gas[a]	Liquid[b]	δE	Free cluster	δE	Embedded cluster	δE
$1b_1$	12.60	11.16±0.04	1.44	11.57±0.18	1.03(1.05)[c]	11.74±0.02	0.86
$3a_1$	14.80	13.50±0.10	1.30	13.83±0.42	0.97(1.12)[c]	14.10±0.03	0.70
$1b_2$	18.60	17.34±0.04	1.26	17.89±0.05	0.71(1.00)[c]	17.69±0.01	0.91
$2a_1$	32.60	30.90±0.06	1.70	33.16±0.02	−0.56	33.04±0.01	−0.44

[a]Electron binding energies for the water monomer. From Banna *et al.* (Ref. 80).
[b]From Winter *et al.* (Ref. 22).
[c]Experimental results for a cluster with $\langle n \rangle$=250 water molecules. From Björneholm *et al.* (Ref. 21).

TABLE III. HOMO-LUMO gap ($E_{G,n}$) and average LUMO energy ($V_{0,n}$) for water clusters. The results are in eV.

	Free clusters		Embedded clusters	
n	$E_{G,n}$	$V_{0,n}$	$E_{G,n}$	$V_{0,n}$
1	12.31	0.35	12.56±0.08	0.68±0.08
2	11.05±0.04	0.03±0.01	11.97±0.08	0.51±0.08
4	10.60±0.03	−0.19±0.03	11.58±0.08	0.34±0.08
8	9.90±0.16	−0.49±0.05	11.25±0.06	0.19±0.07
10	9.50±0.19	−0.66±0.14	11.10±0.05	0.14±0.07
15	9.15±0.25	−0.85±0.14	10.90±0.04	0.04±0.05
20	8.84±0.27	−0.96±0.18	10.71±0.04	−0.02±0.03
30	8.69±0.25	−1.00±0.18	10.48±0.04	−0.15±0.04
⋮				
∞[a]	8.55±0.08	−1.06±0.03	10.41±0.09	−0.17±0.05

[a]Extrapolated values.

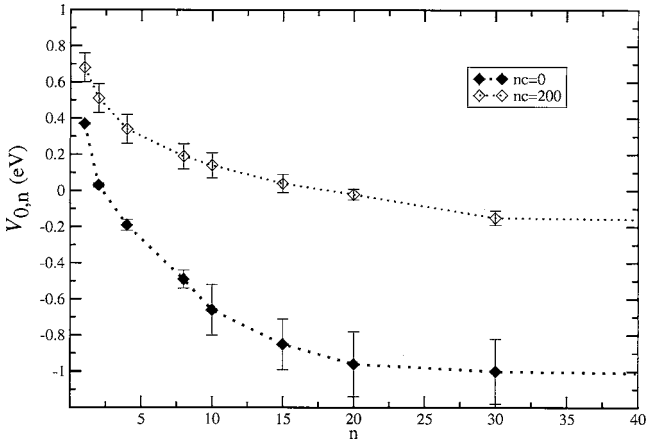

FIG. 7. Size dependence of $V_{0,n}$ for free and embedded water clusters.

electron binding energies, and the gas-to-condensed-phase energy shift (δE) for the valence orbitals. Theoretical values were derived from Gaussian fitting of the DOS, and δE for each orbital is defined as the difference between the experimental electron binding energy for the isolated water molecule[80] and its value in the condensed phase. Theoretical results are for the w_{30} cluster. With the exception of the $2a_1$ orbital, a good agreement between experimental binding energies for liquid water and theoretical results is observed. For the $1b_1$ and $3a_1$ orbitals, experimental binding energies are in better agreement with theoretical results for free water clusters, although the differences are quite small. More important, the redshift of δE, which is a condensed-phase effect, is qualitatively in keeping with experimental information: We find that δE is ~0.9 and 0.7 eV for the $1b_1$ and $3a_1$ orbitals, respectively. The experimental values are ~1.3 eV. The only significant discrepancy relative to experiment concerns the $2a_1$ orbital for which theoretical calculations predict a small blueshift (~0.4 eV), whereas a 1.7-eV redshift is predicted by experiment. Results for free water clusters can be compared with photoemission spectra of water clusters.[21] A good agreement between theoretical and experimental results for the binding energy shift from the molecule to the cluster can be observed, particularly for the $1b_1$ and $3a_1$ orbitals (see Table II).

B. The water electron affinity V_0

V_0 can be defined as the energy to take a zero kinetic-energy gas-phase electron to the bottom of the conduction band of the condensed phase as a delocalized or quasifree electron.[3,18] Several theoretical[23,25] and experimental[3,14] estimates of V_0 were reported. The typical literature value is −1.2 eV.[14] A significantly smaller estimate (−0.12 eV) has been reported.[3] This value is closer to a theoretical prediction by Jortner ($-0.5 < V_0 < 1.0$),[23] and in good agreement with the Henglein's calculation (−0.2 eV).[25]

In the present work $V_{0,n}$ (see Table III) represents V_0 for a cluster with n water molecules. It was estimated as the average LUMO energy of the aggregate. The behavior of $V_{0,n}$ with the number of water molecules (n) is illustrated in Fig. 7. In free water clusters $V_{0,n}$ changes from 0.03 ± 0.01 ($n=2$) to -1.0 ± 0.18 eV ($n=30$). When the electrostatic field of the embedding charges is introduced, significant differences relative to free clusters are observed. In these clusters, $V_{0,n}$ changes from 0.51 ± 0.08 ($n=2$) to -0.15 ± 0.04 eV ($n=30$). It should be expected that non-H-bonded hydrogen atoms at the cluster surface contribute to increase the electron affinity or to lower the LUMO energy. Embedding charges reduce surface effects by simulating the presence of water molecules at the cluster surface and contribute to increase the LUMO energy. Extrapolation of $V_{0,n}$ for $n=\infty$ leads to $V_{0,\infty}=-1.06\pm0.03$ eV (free cluster) and $V_{0,\infty}=-0.17\pm0.05$ eV (embedded cluster). It seems reasonable to assume that the extrapolated average LUMO energy for the embedded water clusters ($V_{0,\infty}$) is a reasonable estimate of the bulk water V_0. Therefore, our result for $V_{0,\infty}$ is in very good agreement with the recent estimate by Coe *et al.*[3] (−0.12 eV) and Henglein[25] (−0.2 eV) but significantly smaller than the value reported by Grand *et al.* (−1.2±0.1 eV).[14]

C. The HOMO-LUMO gap

The HOMO-LUMO gap ($E_{G,n}$) for water clusters of size n is reported in Table III. The values correspond to averages over 50 uncorrelated configurations. The behavior of the average optical gap ($E_{G,n}=\epsilon_{HOMO}-\epsilon_{LUMO}$) with the number of water molecules (n) for free and embedded clusters ($n_c=200$) is illustrated in Fig. 8. In free clusters $E_{G,n}$ changes from 11.05 ± 0.04 ($n=2$) to 8.69 ± 0.25 eV ($n=30$). When embedding charges are introduced $E_{G,n}$ changes from 11.97 ± 0.08 ($n=2$) to 10.48 ± 0.04 eV ($n=30$), indicating a weaker dependence with n in comparison with free clusters. Extrapolated values for the HOMO-LUMO gap ($E_{G,\infty}$) are 8.55 ± 0.08 (free cluster) and 10.41 ± 0.09 eV (embedded cluster). Theoretical informations on the HOMO-LUMO gap of liquid water are relatively scarce. First-principles molecular dynamics of Boero *et al.*[32] estimate the KS HOMO-LUMO gap of liquid water at normal conditions as ~3.6 eV. A previous estimate of 4.65 eV was reported by Laasonen *et al.*[27] The disagreement with the present values illustrates that widely used approximations in density-functional theory lead to gaps that are significantly underestimated. From the theoretical values of $E_{G,\infty}$ and $V_{0,\infty}$ we can estimate the photo-

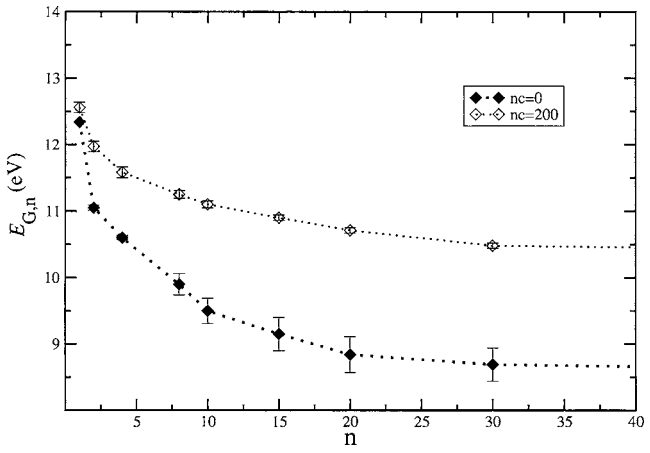

FIG. 8. Size dependence of $E_{G,n}$ for free and embedded water clusters.

electron threshold (PET), which is defined as[17] PET$=E_G+|V_0|$. For free water clusters we find that PET $=9.61\pm0.15$ eV. For embedded water clusters, our extrapolated $E_{G,\infty}$ and $V_{0,\infty}$ leads to PET$=10.58\pm0.10$ eV, which is $\sim$0.5 eV above the experimental values reported by Delahey and Von Burg[15] (10.06 eV) and by Winter *et al.* (9.9 eV).[22] Our theoretical PET is, however, close to an experimental value of $\sim10.5\pm0.5$ eV.[12]

D. The adiabatic band gap of liquid water

The adiabatic band gap of liquid water can be estimated through a thermochemical cycle, which involves several species including H_2O^+, H_3O^+, OH^-, and $OH^\bullet$, and the hydrated electron e^- (aq). A detailed description can be found in Refs. 3 and 4. However, the process can be summarized as follows. Vertical photoionization of liquid water produces an excited H_2O^+ ion and a delocalized e^-(aq). The H_2O^+ formed by ionization reacts quickly by proton transfer to a nearby water molecule leading to the formation of H_3O^+ and of the hydroxide defect OH^-, which can be placed at $\Delta E=0.58$ eV above the valence-band edge. ΔE is the energy of the reaction

$$2H_2O(1) \rightarrow H_3O^+(aq) + OH^-(aq). \quad (2)$$

The conduction-band edge can be associated with

$$H_3O^+(aq) + OH^\bullet(aq) + e^-(cond), \quad (3)$$

where it is assumed that the reorganization of water molecules takes place around the H_3O^+ and $OH^\bullet$ species. By defining a thermochemical cycle[3,4] it is then possible to calculate the water adiabatic band gap by using

$$E_{G,Ad} = \Delta E_{hyd}(OH^\bullet) + V_0 + AEA[OH^\bullet(g)] - \Delta E_{hyd}(OH^-) + \Delta E, \quad (4)$$

where AEA$[OH^\bullet(g)]=1.83$ eV (Ref. 3) is the gas-phase adiabatic electron affinity (AEA) of the OH radical and $\Delta E_{hyd}(OH^-)=-4.97$ eV is the hydration energy of OH^-.[3] The less well-known quantities for predicting $E_{G,Ad}$ are the hydration energy of the OH radical, $\Delta E_{hyd}(OH^\bullet)$, and the water electron affinity V_0. Different works[3,81,82] predicted that $\Delta E_{hyd}(OH^\bullet)$ is close to -0.37 eV. Several electronic properties of liquid water are gathered in Table IV. Based on the Monte Carlo result for $\Delta E_{hyd}(OH^\bullet)=-0.38$ eV (Ref. 82) and the present estimate of V_0, we find that $E_{G,Ad}=6.83\pm0.05$ eV, which is in excellent agreement with the value reported by Coe and co-workers.[3,4]

TABLE IV. Band gap of liquid water. Theoretical and experimental data (in eV).

	This work	Coe *et al.*[a]	Other
$\Delta_{hyd}H(OH^\bullet)$		-0.37	-0.38;[b] -0.37[c]
V_0	-0.17 ± 0.05	-0.12	-1.2 ± 0.1;[d] -0.2[e]
E_G (Theor.)	10.41 ± 0.09		7.8;[f] $\sim3.6\pm0.2$;[g] 4.6 ± 0.05[h]
E_G (Expt.)			7.0;[i] 8.9;[d] 8.7 ± 0.5[j]
$E_{G,Ad}$	6.83 ± 0.05	6.89	
PET	10.58 ± 0.1		10.06;[k] 9.9;[l] 10.5;[m]

[a]From Coe *et al.* (Ref. 3).
[b]From Cabral do Couto *et al.* (Ref. 82).
[c]From Autrey *et al.* (Ref. 81).
[d]From Grand *et al.* (Ref. 14).
[e]From Henglein (Ref. 25).
[f]Band gap for cubic ice. From Parravicini and Resta (Ref. 24).
[g]From Boero *et al.* (Ref. 32).
[h]From Laasonen *et al.* (Ref. 27).
[i]From Goulet *et al.* (Ref. 17).
[j]From Bernas *et al.* (Ref. 19).
[k]From Delahey and Von Burg (Ref. 15).
[l]From Winter *et al.* (Ref. 22).
[m]From Shibaguchi *et al.* (Ref. 12).

V. CONCLUSIONS

Electronic properties of water clusters and liquid water were investigated by sequential Monte Carlo/density-functional theory calculations. DFT calculations were based on the reparametrization of the MPW1PW91 functional that predicts the structural, energetic, and electronic properties of the water dimer in excellent agreement with experimental information. A detailed analysis of the the KS density of states (DOS) and the band gap of water clusters was carried out. Special emphasis was placed on the dependence of the results on the cluster size and surface effects. The behavior of the water DOS with the number of particles and its dependence on surface effects is in keeping with information from x-ray emission and absorption spectra. One relevant conclusion concerns surface effects on the electronic structure of water clusters. It was found that they significantly contribute to the broadening of the water $3a_1$ and $1b_1$ bands that characterize the DOS of water clusters. In addition, surface effects contribute to lower the average LUMO energy in comparison with clusters embedded by a charge distribution, which mimics the presence of water molecules. When the results are extrapolated for larger aggregates embedded in a charge distribution, the results for the water electron affinity (V_0) is in very good agreement with the estimate by Coe *et al.*,[3] and other theoretical calculations. As expected, there is a significant difference between the adiabatic and vertical (HOMO-LUMO) band gap of water. Our result for the adiabatic band gap of liquid water is in excellent agreement with recent predictions.[3,4] The present reparametrization of the MPW1PW91 functional provided reliable information on the

electronic properties of liquid water and indicates that our approach can be of interest for investigating electronic properties of liquids.

ACKNOWLEDGMENTS

This work was partially supported by Fundação para a Ciência e a Tecnologia (FCT), Portugal (Grant No. POCTI/43315/QUI/2001). Two of the authors (S.G.E and P.C.C.) gratefully acknowledge the FCT. (Ph.D. Grants SFRH/BD/10200/2002 and SFRH/XXI/BD/6503/2001.)

[1] *Water a Comprehensive Treatise*, edited by F. Franks (Plenum, New York, 1972), Vol. 1; *Water a Comprehensive Treatise* (Plenum, New York, 1973), Vols. 2 and 3; *Water a Comprehensive Treatise* (Plenum, New York, 1975) Vol. 4.
[2] M. C. R. Symons, Acc. Chem. Res. **14**, 179 (1981).
[3] J. V. Coe, A. D. Earhart, M. H. Cohen, G. J. Hoffman, H. W. Sarkas, and K. H. Bowen, J. Chem. Phys. **107**, 6023 (1997).
[4] J. V. Coe, Int. Rev. Phys. Chem. **20**, 33 (2001).
[5] T. Head-Gordon and G. Hura, Chem. Rev. (Washington, D.C.) **102**, 2651 (2002).
[6] B. Guillot, J. Mol. Liq. **101**, 219 (2002).
[7] R. Rey, K. B. Møller, and J. T. Hynes, Chem. Rev. (Washington, D.C.) **104**, 1915 (2004).
[8] G. Franseze and H. E. Stanley, Physica A **314**, 508 (2002).
[9] Y. Q. Tu and A. Laaksonen, Chem. Phys. Lett. **329**, 283 (2000).
[10] K. Coutinho, R. C. Guedes, B. J. Costa Cabral, and S. Canuto, Chem. Phys. Lett. **369**, 345 (2003).
[11] F. Williams, S. P. Varma, and S. Hillenius, J. Chem. Phys. **64**, 1549 (1976).
[12] T. Shibaguchi, H. Onuki, and R. Onaka, J. Phys. Soc. Jpn. **42**, 152 (1977).
[13] B. Baron, D. Hoover, and F. Williams, J. Chem. Phys. **68**, 1997 (1978).
[14] D. Grand, A. Bernas, and E. Amouyal, Chem. Phys. **44**, 73 (1979).
[15] P. Delahey and K. Von Burg, Chem. Phys. Lett. **83**, 250 (1981).
[16] T. Goulet and J.-P. Jay-Gerin, J. Phys. Chem. **93**, 7532 (1989).
[17] T. Goulet, A. Bernas, C. Ferradini, and J.-P. Jay-Gerin, Chem. Phys. Lett. **170**, 492 (1990).
[18] P. Han and D. M. Bartels, J. Phys. Chem. **94**, 5824 (1990).
[19] A. Bernas, C. Ferradini, and J.-P. Jay-Gerin, Chem. Phys. **222**, 151 (1997).
[20] A. Bernas, C. Ferradini, and J.-P. Jay-Gerin, J. Photochem. Photobiol., A **117**, 171 (1998).
[21] O. Björneholm, F. Federman, S. Kakar, and T. Möller, J. Chem. Phys. **111**, 546 (1999).
[22] B. Winter, R. Weber, W. Widdra, M. Dittmar, M. Faubel, and I. Hertel, J. Phys. Chem. A **108**, 2625 (2004).
[23] J. Jortner, Ber. Bunsenges. Phys. Chem. **75**, 696 (1971).
[24] G. P. Parravicini and L. Resca, Phys. Rev. B **8**, 3009 (1973).
[25] A. Henglein, Can. J. Chem. **55**, 2112 (1977).
[26] P. Cabral do Couto, R. C. Guedes, and B. J. Costa Cabral, Braz. J. Phys. **34**, 42 (2004).
[27] K. Laasonen, M. Sprik, M. Parrinello, and R. Car, J. Chem. Phys. **99**, 9080 (1993).
[28] M. Sprik, J. Hutter, and M. Parrinello, J. Chem. Phys. **105**, 1142 (1996).
[29] P. L. Silvestrelli and M. Parrinello, Phys. Rev. Lett. **82**, 5415 (1999).
[30] P. L. Silvestrelli and M. Parrinello, J. Chem. Phys. **111**, 3572 (1999).
[31] M. Boero, K. Terakura, T. Ikeshoji, C. C. Liew, and M. Parrinello, Phys. Rev. Lett. **85**, 3245 (2000).
[32] M. Boero, K. Terakura, T. Ikeshoji, C. C. Liew, and M. Parrinello, J. Chem. Phys. **115**, 2219 (2001).
[33] P. Hunt, M. Sprik, and R. Vuilleumier, Chem. Phys. Lett. **376**, 68 (2003).
[34] J. VandeVondele, F. Mohamed, M. Krack, J. Hutter, M. Sprik, and M. Parrinello, J. Chem. Phys. **122**, 014515 (2005).
[35] K. R. Wilson, M. Cavalleri, B. S. Rude *et al.*, J. Phys.: Condens. Matter **14**, L221 (2002).
[36] S. Myneni, Y. Luo, L. Å. Näslund *et al.*, J. Phys.: Condens. Matter **14**, L213 (2002).
[37] J.-H. Guo, Y. Luo, A. Augustsson, J.-E. Rubensson, C. Säthe, H. Ågren, H. Siegbahn, and J. Nordgren, Phys. Rev. Lett. **89**, 137402 (2002).
[38] M. Cavalleri, H. Ogasawara, L. G. M. Pettersson, and A. Nilsson, Chem. Phys. Lett. **364**, 363 (2002).
[39] B. Hetényi, F. De Angelis, P. Gianozzi, and R. Car, J. Chem. Phys. **120**, 8632 (2004).
[40] S. Kashtanov, A. Augustsson, Y. Luo *et al.*, Phys. Rev. B **69**, 024201 (2004).
[41] S. Canuto and K. Coutinho, Adv. Quantum Chem. **28**, 89 (1997).
[42] K. Coutinho and S. Canuto, J. Chem. Phys. **113**, 9132 (2000).
[43] C. Adamo and V. Barone, Chem. Phys. Lett. **274**, 242 (1997).
[44] C. Adamo and V. Barone, J. Comput. Chem. **19**, 418 (1998).
[45] C. Adamo and V. Barone, J. Chem. Phys. **108**, 664 (1998).
[46] M. W. Mahoney and W. L. Jorgensen, J. Chem. Phys. **112**, 8910 (2000).
[47] D. Frenkel and B. Smit, *Understanding Molecular Simulation* (Academic, San Diego, 1996).
[48] N. Metropolis, A. W. Rosenbluth, M. N. Rosenbluth, A. H. Teller, and E. Teller, J. Chem. Phys. **21**, 1087 (1953).
[49] J. G. Kirkwood, J. Chem. Phys. **2**, 351 (1934); L. Onsager, J. Am. Chem. Soc. **58**, 1486 (1936).
[50] L. Kleinman, Phys. Rev. B **56**, 16029 (1997).
[51] J. P. Perdew and M. Levy, Phys. Rev. B **56**, 16021 (1997).
[52] X. Hua, X. Chen, and W. A. Goddard III, Phys. Rev. B **55**, 16103 (1997).
[53] P. Politzer and F. Abu-Awwad, Mol. Phys. **95**, 681 (1998).
[54] P. Politzer and F. Abu-Awwad, Theor. Chem. Acc. **99**, 83 (1998).
[55] R. Stowasser and R. Hoffmann, J. Am. Chem. Soc. **121**, 3414 (1999).
[56] F. R. Manby and P. J. Knowles, J. Chem. Phys. **112**, 7002 (2000).
[57] F. Abu-Awwad and P. Politzer, J. Comput. Chem. **21**, 227 (2000).
[58] S. Hamel, P. Duffy, M. E. Casida, and D. R. Salahub, J. Electron Spectrosc. Relat. Phenom. **123**, 345 (2002).
[59] D. P. Chong, O. V. Gritsenko, and E. J. Baerends, J. Chem. Phys. **116**, 1760 (2002).
[60] C.-G. Zhan, J. A. Nichols, and D. A. Dixon, J. Phys. Chem. A **107**, 4184 (2003).
[61] J. Jellinek and P. H. Acioli, J. Chem. Phys. **118**, 7783 (2003).
[62] I. Ciofini, C. Adamo, and H. Chermette, Chem. Phys. **309**, 67 (2005).
[63] C. Y. Ng, D. J. Trevor, P. W. Tiedemann, S. T. Ceyer, P. L. Kronebusch, B. H. Mahan, and Y. T. Lee, J. Chem. Phys. **67**, 4235 (1977).
[64] D. E. Woon and T. H. Dunning, Jr., J. Chem. Phys. **98**, 1358 (1993).
[65] J. Cizek, Adv. Chem. Phys. **14**, 35 (1969).
[66] G. D. Purvis and R. J. Bartlett, J. Chem. Phys. **76**, 1910 (1982).
[67] G. E. Scuseria, C. L. Janssen, and H. F. Schaefer III, J. Chem. Phys. **72**, 4244 (1980).
[68] G. E. Scuseria and H. F. Schaefer III, J. Chem. Phys. **90**, 3700 (1989).
[69] C. Møller and M. S. Pleset, Phys. Rev. **46**, 618 (1934).
[70] V. C. Felic'issimo, I. Minkov, F. F. Guimarães, F. Gel'mukhanov, A. Cesar, and H. Ägren, Chem. Phys. **312**, 311 (2005).
[71] J. A. Odutola and T. R. Dyke, J. Chem. Phys. **75**, 5062 (1980).
[72] M. M. Feyerisen, D. Feller, and D. A. Dixon, J. Phys. Chem. **100**, 2993 (1996).
[73] T. R. Dyke, K. M. Mack, and J. S. Muenter, J. Chem. Phys. **66**, 498 (1977).
[74] J. Kim, I. Becker, O. Cheshnovsky, and M. A. Johnson, Chem. Phys. Lett. **297**, 90 (1998).
[75] Z. S. Huang and R. E. Miller, J. Chem. Phys. **91**, 6613 (1989).
[76] M. J. Frisch, G. W. Trucks, H. B. Schlegel *et al.*, GAUSSIAN-98, Gaussian Inc., Pittsburgh, PA, 1998.
[77] D. M. Chipman, J. Phys. Chem. **83**, 1657 (1979).
[78] K. D. Jordan and F. Wang, Annu. Rev. Phys. Chem. **54**, 367 (2003).
[79] P. F. Flükiger, thèse 2561, Département de Chimie Physique, Université de Genève, Genève, 1992; S. Portmann and H. P. Lüthi, Chimia **54**, 766 (2000).
[80] M. S. Banna, B. H. McQuaide, R. Malutzki, and V. Schmidt, J. Chem. Phys. **84**, 4739 (1986).
[81] T. Autrey, A. K. Brown, D. M. Camaioni, M. Dupuis, N. S. Foster, and A. Getty, J. Am. Chem. Soc. **126**, 3680 (2004).
[82] P. Cabral do Couto, R. C. Guedes, B. J. Costa Cabral, and J. A. Martinho Simões, J. Chem. Phys. **119**, 7344 (2003).

Chapter 5

Paper III: A microscopic view

The adiabatic approach for a definition of a band gap for pure liquid water had only been discussed and defined from a macroscopic perspective, e.g. from hydration energies or adiabatic electron affinities.

Although small neutral [12, 108], cationic [271–274], anionic [275–279], electronically excited [280, 281] water clusters and hydrated hydronium clusters [282, 283] had been the subject of theoretical studies, to our knowledge, no attempt had been made to study small clusters in the context of the electronic structure of liquid water as discussed by Coe et al. [35, 137]. Therefore, the purpose of Paper III was a molecular level verification of the adiabatic picture as discussed by Coe et al [35, 137] trough:

- The study of the energetics and electronic properties of small electronically excited $H_3O^+[OH(H_2O)_{n-2}]^-$ clusters ($n = 2-5$) as finite size analogs of the valence band edge and the hydrated anionic defect.

- The study of the size dependence of analogous finite size properties such as the conduction band edge and the energy gap.

Our estimates for the adiabatic energy gap of the aggregates ranges from 6.01 to 6.55 eV which is in agreement with the experimental value 6.9 eV [35] and theoretical 6.83 eV [131] results. We also report results for a quantity V_0, which is analogous to the conduction band edge of liquid water. Our calculations indicate that this quantity is strongly size dependent, making difficult a comparison with bulk values. However, although the calculation of V_0 illustrates the limitations of a cluster approach, it seems reasonable to conclude that the study of excited water clusters can improve our understanding of the electronic properties of the bulk phase. This work reports, for the first time, an investigation of the electronic properties of small water aggregates that supports the picture proposed by Coe et al. [35] for the adiabatic band gap of pure liquid water.

Electronically excited water aggregates and the adiabatic band gap of water

Paulo Cabral do Couto
Grupo de Física Matemática, Universidade de Lisboa, Avenida Professor Gama Pinto 2, 1649-003 Lisboa, Portugal

Benedito J. Costa Cabral[a)]
Departamento de Química e Bioquímica, Faculdade de Ciências, Universidade de Lisboa, 1749-016 Lisboa, Portugal and Grupo de Física Matemática, Universidade de Lisboa, Avenida Professor Gama Pinto 2, 1649-003 Lisboa, Portugal

(Received 11 September 2006; accepted 22 November 2006; published online 4 January 2007)

The authors report results for the electronic properties of the S_1 singlet excited state of $H_3O^+[OH(H_2O)_{(n-2)}]^-$ aggregates, where $n=2-5$ is the number of water molecules. The energy of the excited state was defined relative to the ground state of neutral water clusters. Results for ionized aggregates are also reported. The results are based on configuration interaction with single excitations geometry optimizations followed by density functional theory and time dependent density functional theory calculations. Emphasis was placed on the relationship between electronic properties of the aggregates and the adiabatic band gap of liquid water. The authors' predictions for the adiabatic energy gap of water clusters are in the 6.01–6.55 eV range. These values are ~0.9–0.4 eV below the experimental adiabatic band gap of liquid water (6.9 eV). Comparison with experimental information for water is reported for several properties of interest including vertical and adiabatic ionization energies, excitation energies, photoemission thresholds, and conduction band edge. The results provide a description, at the molecular level, for the electronic properties of water aggregates that is consistent with the current picture for the band gap of bulk water [J. V. Coe, Int. Rev. Phys. Chem. **20**, 33 (2001)]. © *2007 American Institute of Physics*.
[DOI: 10.1063/1.2423004]

I. INTRODUCTION

Electronic properties of water are not very well understood.[1,2] They are, however, of fundamental importance in investigating the chemical reactivity and dynamics of electronically excited states in aqueous solutions,[3,4] and in explaining several unique properties that characterize the water hydrogen bond (HB) network. A longstanding issue concerns the fact that hydrated electrons in liquid water are produced by photoabsorption at ~6.5 eV.[5–9] This energy is significantly lower than the threshold energy for photoelectron emission (PET) by liquid water (9.9 eV,[2] 10.06 eV,[10,11] and 9.3±0.1 eV[12]) and ~6 eV below the first ionization potential of the gas phase water molecule (12.62 eV).[13] Several works pointed out that the ability of water to reorganize about charged species as well as the reactive nature of electronically excited water molecules should be taken into account in explaining electronic properties of water.[14–16] Moreover, they indicate that an adiabatic route for accessing the conduction band of liquid water can be defined and that the bottom of the conduction band is characterized by the reorganization of the water molecules around the H_3O^+ and OH radical species as well as by the presence of a delocalized or quasi-free electron. The energy associated with this process corresponds to the water adiabatic band gap, and it is estimated as ~6.9 eV.[14,15]

Although some experimental[14–16] and theoretical[17] works on the water adiabatic band gap have been reported, the structure and electronic properties of photoexcited states of water associated with the adiabatic band gap deserve further investigation. On the other hand, it is generally accepted that some of the complex behavior characterizing the water HB network is already present in small water aggregates.[3] Therefore, the study of water clusters can be very useful in understanding, from a microscopic point of view, the electronic properties of bulk water.

In this article we report a theoretical investigation of the electronic properties of small water clusters. Our main interest is to study how the energetic properties of electronically excited water aggregates can be related to the electronic properties of liquid water, such as the photoelectron emission threshold, the conduction band edge, and the adiabatic band gap. The presently adopted procedure relies on *ab initio* configuration interaction with single excitations[18] (CIS) geometry optimizations for the S_1 singlet excited state of water aggregates. The energetic properties of the optimized structures were analyzed by density functional theory (DFT),[19] and excitation energies were calculated by time dependent density functional theory (TDDFT).[20] For the water monomer and dimer, results based on symmetry adapted cluster

[a)]Author to whom correspondence should be addressed. Electronic mail: ben@cii.fc.ul.pt

configuration interaction with single and double excitations[21–23] [SAC-CI(SD)] are also presented. Some recent works on excited water clusters were reported.[24,25] However, they focused, essentially, on vertical excitation processes.

The article is organized as follows. Initially, computational details (Sec. II) are presented. In the same section we introduce the definition and appropriate notation for properties relevant for the discussion. In Sec. III we report results for several electronic properties of water aggregates, including vertical excitation and ionization energies, energetics of the e^- anionic defect, and adiabatic energy gap in water clusters. We conclude by placing emphasis on two aspects: (1) the importance of taking into account the reactive nature of electronically excited water and the structure relaxation of the water molecules upon photoexcitation; (2) the interest in carrying out cluster studies for a better understanding of the electronic properties of bulk water.

II. COMPUTATIONAL DETAILS

Optimized ground state (S_0) and singlet lowest excited (S_1) structures were determined by *ab initio* configuration interaction with single excitations (CIS).[18] A discussion on the reliability of CIS excited state structures has been recently reported.[26] It was concluded that, in general, CIS optimized geometries are usually close to those predicted by equation of motion CCSD (Ref. 27) and are in good agreement with experimental information. The optimizations were carried out with the double augmented *d*-aug-cc-pVDZ basis set.[28] Harmonic frequencies were evaluated at the same level (CIS/*d*-aug-cc-pVDZ).

Different excited conformers corresponding to local minima on the S_1 potential energy surface were identified. They are characterized by the presence of the hydronium (H_3O^+), the OH radical, and a delocalized electronic density that can be associated with the microsolvated electron (see next session for details). Single-point energy DFT calculations were then performed with the BHandHLYP functional[29,30] as implemented in the GAUSSIAN 03 suite of programs.[31] The BHandHLYP exchange-correlation functional is defined as $0.5E_x^{\mathrm{HF}}+0.5E_x^{\mathrm{LSDA}}+0.5\Delta E_x^{\mathrm{Becke88}}+E_c^{\mathrm{LYP}}$, where E_x and E_c are exchange and correlation functionals, respectively. The choice of this functional was oriented by recent works on hydrogen bonding[32,33] and ionized water clusters[34,35] indicating that BHandHLYP provides an adequate description of the structure of water and related systems. This was explained by partial correction of the self-interaction error[19] due to the admixture of "exact Hartree-Fock (HF) exchange."[34] Excitation energies of water clusters were determined by TDDFT (Ref. 20) with Dunning's *d*-aug-cc-pVTZ basis set.[28] Full active SAC-CI(SD) calculations for $n=1,2$ were carried out with the *d*-aug-cc-pVDZ (optimizations) and *d*-aug-cc-pVTZ (single-point energy) basis sets.

We will focus the present discussion on the first excited singlet S_1 states. An extensive search on the potential energy surface (PES) of excited states is not affordable for large water aggregates. Therefore, our procedure to identify local minima on the S_1 excited state potential energy surface was directed to structures characterized by the presence of the three species associated with the conduction band edge for the water adiabatic band gap,[14] namely, H_3O^+, the OH radical, and the hydrated electron. A similar approach was applied by Sobolewski and Domcke to study zwitterionic and biradical forms of the water pentamer.[36] It should be observed that by adopting the present procedure, we can identify the structures of the excited aggregates on the S_1 PES although no information on the dynamics of the microscopic process leading from S_0 to S_1 is provided.

To discuss the importance of structure reorganization upon excitation, we will introduce the following notation. $E(S_i;S_j)$ means that the S_j state energy is calculated in the geometry of the state S_i. For example, $E(S_0;S_0)$ or simply E_0 is the ground state energy calculated in the ground state geometry of the singlet reference state S_0. For a given number of water molecules (n), the ground state reference system was taken as the most energetically stable conformer. In addition, we will represent by $E(S_j;S_j \leftarrow S_i)$ the excitation energy from S_i to S_j in the geometry of the singlet state S_j. Ionization of the S_i state in the S_i geometry will be simply represented as $E(S_i;+)$. The energy of an optimized ionized aggregate $[E(+,+)]$ will be represented as $E(+)$.

The relative (or adiabatic) excitation energy E_R for the $S_1 \leftarrow S_0$ transition can be written as

$$E_R(S_1) = [E(S_1;S_0) - E_0] + E(S_1;S_1 \leftarrow S_0), \tag{1}$$

where E_0 is the ground state reference energy and $E(S_1;S_1 \leftarrow S_0)$ is the $S_1 \leftarrow S_0$ excitation energy calculated at the optimized structure of the excited state S_1. The reorganization (or relaxation) energy associated with the $S_1 \leftarrow S_0$ excitation is $E(S_1;S_0)-E_0$. The relative ionization energy for the S_1 excited state optimized structure will be represented as $E_R(S_1;+)$ and can be written as

$$E_R(S_1;+) = [E(S_1;+) - E_0]. \tag{2}$$

The adiabatic ionization energy can be calculated by $E_R(+;+)=[E(+;+)-E_0]$ and will be simply represented as $E_R(+)=[E(+)-E_0]$.

Energetic properties related to vertical processes, the anionic e^- defect, and the adiabatic energy gap of water clusters are reported and their calculation for the water pentamer is illustrated in Fig. 1. The quantities represented by $V_{0,v}$ and V_0 correspond to the energy to transfer an electron from the vacuum to the lowest unoccupied molecular orbital of the aggregate. For the vertical process (left side of Fig. 1) $V_{0,v}=E(S_0;S_1 \leftarrow S_0)-\mathrm{IP}$, where $\mathrm{IP}=E(S_0;+)-E(S_0)$ is the vertical ionization potential. For the adiabatic process describing the relaxation of the water molecules around the H_3O^+ and OH species (middle of Fig. 1), $V_0=E_R(+;S_1)-E_R(+)$. The last quantity can be considered as analogous to the conduction band edge of liquid water (V_0), which is defined as the energy to take a zero kinetic-energy gas phase electron to the bottom of the conduction band of the condensed phase as a delocalized or quasi-free electron.[14] However, it should be observed that V_0 for liquid water describes the energetic stabilization of a quasi-free electron interacting with the hydrogen bond network. In a small cluster, only a few dangling

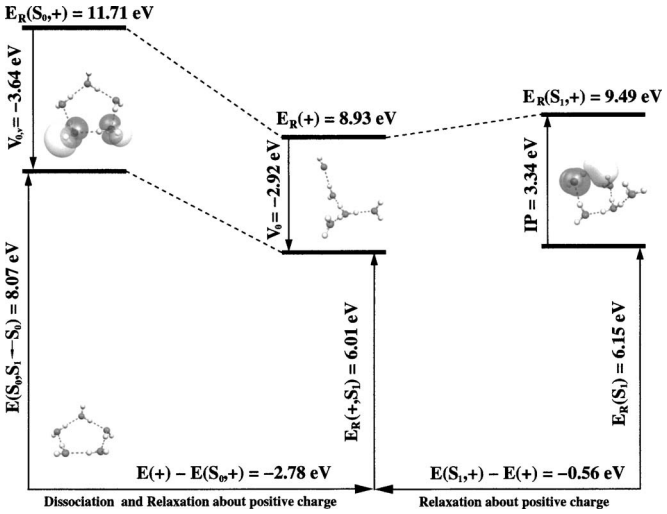

FIG. 1. Electronic properties as a function of the "solvent" coordinate for a water pentamer. (a) The left side arrows indicate vertical excitations (no relaxation). $E(S_0;S_1\leftarrow S_0)=8.07$ eV; IP$=E(S_0;+)-E(S_0)=11.71$ eV; $V_{0,v}=E(S_0;S_1\leftarrow S_0)-\text{IP}=-3.64$ eV. (b) Middle vertical arrows correspond to relaxation around the cationic defect (H_3O^+). $E_R(+;S_1)=[E(+;S_0)-E_0]+E(+;S_1\leftarrow S_0)=6.01$ eV; $V_0=E_R(+;S_1)-E_R(+)=-2.92$ eV; $E_R(+)=E(+)-E_0=8.93$ eV. (c) Right side vertical arrows indicate the energetics of relaxation around the e^- anionic defect. $E_R(S_1)=[E(S_1;S_0)-E_0]+E(S_1;S_1\leftarrow S_0)=6.15$ eV; IP$=E_R(S_1;+)-E_R(S_1)=3.34$ eV; $E_R(S_1;+)=E(S_1;+)-E_0=9.49$ eV. The horizontal arrows correspond to $E_R=E(+)-E(S_0;+)$ (−2.78 eV) and $E_R=E(S_1;+)-E(+)$ (−0.56 eV) relaxation energies.

hydrogen atoms are available and the interaction of the microhydrated electron with the H_3O^+ and OH species cannot be *a priori* discarded.

Optimized structures corresponding to the ground (S_0) and lowest (S_1) singlet states are reported in Figs. 2–4. Ionization of the excited clusters followed by geometry relaxation leads to the ionized structures reported in Figs. 2–4. For $n=3-5$ several isomers (local minima on the S_1 surface) were identified. Electronic density difference isosurfaces, corresponding to the difference between the total CIS unrelaxed density of the excited state and of the HF ground state in the geometry of the S_1 complex, are represented in Figs. 2–4. These isosurfaces provide a qualitative picture of the charge reorganization upon photoexcitation. For a given n, the energies relative to the ground state reference system (most energetically stable conformer) are also reported in Figs. 2–4, where the relative energies in brackets are corrected for $T=298$ K and include zero point vibrational energies (ZPVEs).

III. RESULTS AND DISCUSSION

A. Vertical excitations and the optical energy gap of water clusters

Vertical excitation energy $E(S_0;S_1\leftarrow S_0)$, IP, and $V_{0,v}$ for water clusters are reported in Table I. For a given number of water molecules, these clusters correspond to the most stable structures. Vertical excitation energies can be compared with other results from the literature.[24,37,38] For the water monomer, our result (7.76 eV) is ~0.3 eV above experimental information (7.4–7.5 eV).[38] An excellent agreement between our calculation (7.76 eV) and the semiempirical estimate of Chipman (7.78 eV)[24] is observed. For the water dimer, we predict that $E(S_0;S_1\leftarrow S_0)$ is 7.68 eV, which is also in good agreement with a value reported by Chipman (7.91 eV).[25] A very good agreement between TDDFT and SAC-CI(SD) results for the vertical excitation energies of the water monomer and dimer is observed. In addition, a comparison between SAC-CI(SD)/*d*-aug-cc-pVTZ//CIS/*d*-aug-cc-pVDZ and SAC-CI(SD)/*d*-aug-cc-pVTZ//SAC-CI(SD)/*d*-aug-cc-pVDZ vertical excitation energies indicates that quite similar geometries are predicted by the two methods. From the TD-DFT results for the S_1 vertical excitation energies of water clusters, a 0.44 eV blueshift is observed from the water monomer ($n=1$) to the water pentamer ($n=5$). This value is ~0.5 eV lower than the predicted blueshift of the S_1 vertical excitation energy (~1 eV) observed for bulk water.[39] The

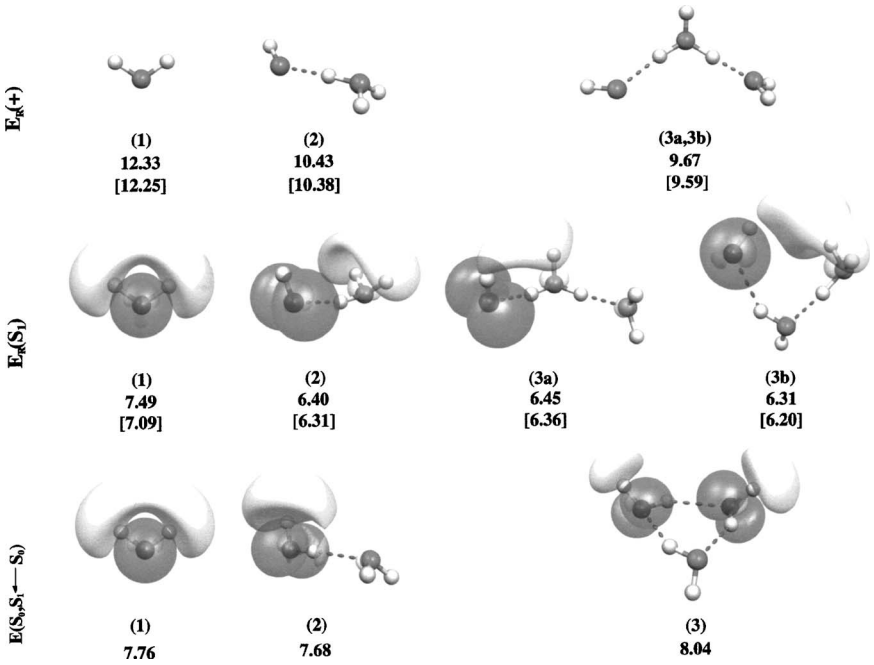

FIG. 2. CIS/*d*-aug-cc-pVDZ optimized structures for the ground state, singlet excited states, and ionized states of water aggregates ($n=1-3$). Values are vertical excitation energies $[E(S_0;S_1\leftarrow S_0)]$ and adiabatic excitation and ionization energies $[E_R(S_1)$ and $E_R(+)]$. Energetic properties were calculated at the BHandHLYP/*d*-aug-cc-pVTZ level. Bracketed values are thermally corrected energy differences (ZPVE included). Data in eV. The isosurfaces correspond to electronic density differences of −0.002 e Å^3 (dark) and +0.002 e Å^3 (white).

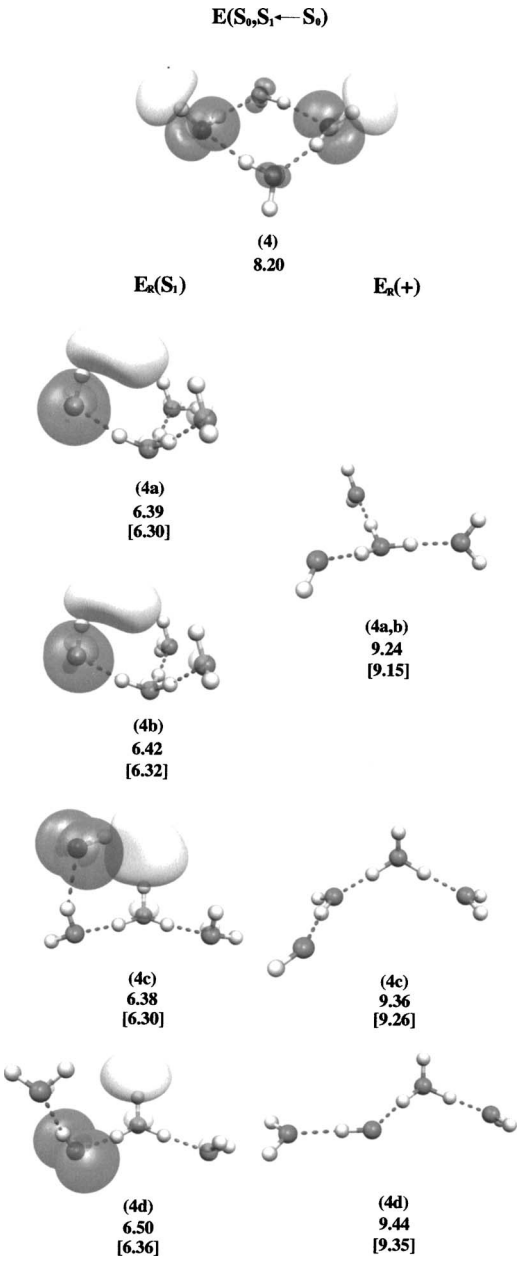

FIG. 3. CIS/*d*-aug-cc-pVDZ optimized structures for the ground state, singlet excited states, and ionized states of water aggregates ($n=4$). Values are vertical excitation energies $[E(S_0;S_1\leftarrow S_0)]$ and relative or adiabatic excitation and ionization energies $[E_R(S_1)$ and $E_R(+)]$. Energetic properties were calculated at the BHandHLYP/*d*-aug-cc-pVTZ level. Bracketed values are thermally corrected energy differences (ZPVE included). Data in eV. The isosurfaces correspond to electronic density differences of $-0.002\ e\ \text{Å}^3$ (dark) and $+0.002\ e\ \text{Å}^3$ (white).

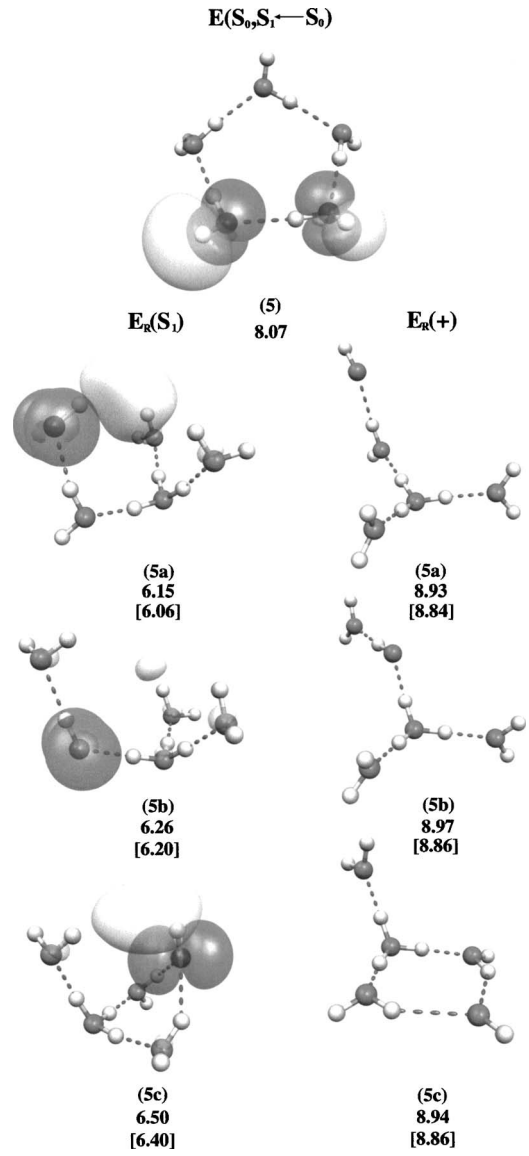

FIG. 4. CIS/*d*-aug-cc-pVDZ optimized structures for the ground state, singlet excited states, and ionized states of water aggregates ($n=5$). Values are vertical excitation energies $[E(S_0;S_1\leftarrow S_0)]$ and relative or adiabatic excitation and adiabatic ionization energies $[E_R(S_1)$ and $E_R(+)]$. Energetic properties were calculated at the BHandHLYP/*d*-aug-cc-pVTZ level. Bracketed values are thermally corrected energy differences (ZPVE included). Data in eV. The isosurfaces correspond to electronic density differences of $-0.002\ e\ \text{Å}^3$ (dark) and $+0.002\ e\ \text{Å}^3$ (white).

~1 eV blueshift of the first absorption band in condensed phases relative to the isolated water molecule has been usually related to Rydbergization effects[40–42] or attributed to excitons of molecular origin.[43,44] The idea behind Rydbergization is that in condensed phases a Rydberg state is energetically destabilized by repulsive interactions of the delocalized electron distribution with the surrounding molecules.[41] It should be expected that this effect is weaker in gas phase water aggregates.

Vertical ionization potentials of the water aggregates are close to 12 eV. The result for the water monomer (12.46 eV) is in good agreement with the experimental value of Dutuit *et al.* (12.62 eV).[13] For the water dimer our prediction (11.64 eV) is 0.46 eV below the experimental value (12.1 eV) reported by Tomoda *et al.*[45] IPs for water clusters ($n=2-5$) are ~1.6 eV above the experimental PET of liquid water (9.9 eV,[2] 10.06 eV,[10] and 9.3 ± 0.1 eV[12]). The reduction of the PET from the clusters to liquid water is related to electronic and thermal broadening. Electronic broadening is associated with the splitting of the orbital energies due to hydrogen bond interactions. Thermal broadening is related to disorder and thermal activation in liquid phase.[46] Therefore, the downward shift of the electron binding energies in liquid water relative to the gas phase clusters can be explained by the presence of liquid configurations with lower (weaker) interaction energies.[47,48]

TABLE I. Vertical excitations and optical energy gap in water clusters. Geometry optimizations were carried out at the CIS/*d*-aug-cc-pVDZ level. DFT energies and TDDFT excitation energies were calculated at the BHandHLYP/*d*-aug-cc-pVTZ//CIS/*d*-aug-cc-pVDZ level. SAC-CI(SD) results for $n=1,2$ are shown in brackets.

n	1	2	3	4	5
E_0	−76.422 007	−152.851 629	−229.289 290	−305.729 222	382.164 651
$E(S_0;+)$	−75.964 020	−152.423 864	−228.850 824	−305.290 051	−381.734 348
$E(S_0;S_1\leftarrow S_0)$[a]	7.76[7.81;[b] 7.74[c]] (7.4–7.5;[d] 7.78;[e] 7.61[f])	7.68[7.88;[b] 7.84[c]] (7.53;[g] 7.91[h])	8.04	8.20	8.07
IP[i]	12.46 [12.61;[b] 12.57[c]] (12.62[j])	11.64 [11.82;[b] 11.79[c]] (12.1)[k]	11.93	11.95	11.71
$V_{0,v}$[l]	−4.70 [−4.80;[b] 4.83[c]]	−3.96 [−3.94;[b] 3.95[c]]	−3.89	−3.75	−3.64

[a] $E(S_0;S_1\leftarrow S_0)$ is the optical energy gap.
[b] SAC-CI(SD)/*d*-aug-cc-pVTZ//*d*-aug-cc-pVDZ.
[c] SAC-CI(SD)/*d*-aug-cc-pVTZ//SAC-CI(SD)/*d*-aug-cc-pVDZ.
[d] Experimental data from Cheng *et al.* (Ref. 38).
[e] Semiempirical estimate from Chipman (Ref. 24).
[f] From Cai *et al.* (Ref. 37).
[g] From Chipman (Ref. 24).
[h] From Chipman (Ref. 25).
[i] $\mathrm{IP}=E(S_0;+)-E_0$.
[j] Experimental value from Dutuit *et al.* (Ref. 13).
[k] Experimental value from Tomoda *et al.* (Ref. 45).
[l] $V_{0,v}=E(S_0;S_1\leftarrow S_0)-\mathrm{IP}$.

For vertical excitations, $V_{0,v}$ range from −4.70 eV (monomer) to −3.64 eV (pentamer). Recent investigations on the electronic structure of liquid water indicate that V_0 should be significantly smaller (−0.17 eV) (Ref. 17) or even close to zero. However, it should be observed that our present estimates indicate that $V_{0,v}$ decreases slowly with increasing cluster size, making difficult a comparison with bulk values. In addition, the definition of V_0 by Coe *et al.*[14] also involves the relaxation of the water molecules around a cationic defect (H_3O^+). Although this feature may not be relevant for bulk water, this seems to be not the case for small water clusters (see also Sec. III C).

B. The e^- anionic defect in water clusters

1. Structure and vibrational frequencies

Several recent studies discussed vertical excited states of water clusters.[24,25] However, the structure reorganization induced by the excitation of water clusters is much less known. Adiabatic excitations of water clusters are relevant for a better understanding of the structure and energetics of anionic defect states, including the microhydrated electron. Starting from a water cluster with n water molecules, photoexcitation may lead to the S_1 excited state structure corresponding to $H_3O^+[OH(H_2O)_{(n-2)}]^-$. The CIS optimized structures (local minima on the S_1 PES) are reported in Figs. 2–4. An analysis of the electronic density differences (also reported in Figs. 2–4) strongly indicates that these aggregates are characterized by the presence of the H_3O^+ cation, the OH radical, as well as by a delocalized electronic distribution which can be associated with a microhydrated electron (e^-). These structures will be associated with the e^- anionic defect in water aggregates. In liquid water, the anionic defect is usually represented as $H_3O^+(aq)+OH(aq)+e^-(aq)$.[14,15,41]

The energetic stabilization of a microhydrated electron is a highly cooperative effect involving the reorganization of the HB network and specific electron-dipole and electron-hydrogen interactions.[49] Different experimental[50,51] and theoretical[49,52–55] investigations on the O–H stretch frequency shift induced by the interaction with an excess electron in water were reported. In comparison with pure water, it was found that the interaction of water molecules with an excess electron leads to a ν_{O-H} redshift distributed over a wide range of values (~0–500 cm^{-1}), depending on the size and structure of the clusters.[52] Although our present interest is mainly oriented to electronic properties, we report (Table II) some information on the structure and vibrational properties of the OH species in the excited (S_1) and ionized (+) aggregates. As shown in Table II, the O–H bond lengths (d_{O-H}) for excited states are not very dependent on the cluster size and their values are scattered in the 0.950–0.965 Å range. For the ionized aggregates, 4d and 5b show slightly increased O–H bond lengths (~0.97 Å) in comparison with the remaining structures. Table II also reports δd_{O-H}, which is the difference between d_{O-H} in the excited and ionized aggregates. With the exception of structures 2, 4d, and 5b, δd_{O-H} is in general quite small. O–H harmonic vibrational frequencies for the excited states exhibit a significant dependence on the cluster size and structure. This dependence reflects specific interactions of the OH species with H_3O^+, H_2O, and the microhydrated electron. Higher frequencies (~4000 cm^{-1}) are observed for the structures where the OH hydrogen atom is free (2) or interacting with water molecules (4d and 5b). Significantly lower O–H frequencies are observed for the structures where the OH species interacts with the charge distribution associated with the microhydrated electron (3a-3b, 4a-4c, 5a, 5c). For ionized clusters, with the exception of conformers 4d and 5b, O–H frequencies are quite similar (~4000 cm^{-1}). This is related to the fact that the OH species is a terminal group in all the ionized structures with the exception of 4d and 5b, where it interacts with one water molecule. Comparison between vibrational frequencies of the excited and ionized clusters shows, again, that the nature (blue or red) or magnitude of the frequency

TABLE II. Data for the O–H bond length (d_{O-H} in angstrom) and harmonic vibrational frequency (ν_{O-H} in cm^{-1}) of the OH species in excited (S_1) and ionized (+) aggregates.

	(S_1)		(+)			
	d_{O-H}	ν_{O-H}	d_{O-H}	ν_{O-H}	δd_{O-H}[a]	$\delta\nu_{O-H}$[b]
2	0.950	4101	0.960	3968	−0.010	133
3a	0.958	3863	0.958	3992	0.000	−129
3b	0.952	3968	0.958	3992	−0.007	−24
4a	0.965	3678	0.957	4005	0.008	−327
4b	0.965	3671	0.957	4005	0.008	−334
4c	0.958	3781	0.956	4020	0.002	−239
4d	0.957	3984	0.975	3634	−0.018	+350
5a	0.959	3738	0.956	4027	0.003	−289
5b	0.956	3976	0.970	3719	−0.014	+257
5c	0.965	3612	0.957	4012	0.008	−400

[a] δd_{O-H} is the difference between d_{O-H} of the OH species in ionized and excited states.
[b] $\delta\nu_{O-H}$ is the difference between the O–H stretch frequencies of OH species in ionized and excited states.

shift is related to specific interactions involving the OH species in the aggregates. For example, only for structures 2, 4d, and 5b, a ν_{O-H} blueshift is observed when we move from the ionized to excited aggregates. For all the other conformers, ν_{O-H} is redshifted. Although strong deviations from harmonic behavior of the PES describing the OH interactions with the microhydrated electron should be expected, the present predictions for the ν_{O-H} redshift from ionized to excited aggregates are in agreement with the trend observed when ν_{O-H} frequencies in negatively charged water clusters are compared with those in neutral water clusters.[53] A specific feature characterizing the ν_{O-H} redshift induced by hydrogen-electron interactions is that the O–H distance is almost constant, indicating that these interactions modify, essentially, the curvature of the PES.

2. Energetics of the e^- anionic defect in water clusters

Data on the energetics of the e^- anionic defect in water clusters are reported in Table III. Quite similar $[E(S_1;S_1 \leftarrow S_0)]$ vertical excitation energies are predicted by TDDFT and SAC-CI(SD) for $n=1,2$. More importantly, a comparison between TDDFT and SAC-CI(SD) results for $n=2$ clearly indicates the reliability of CIS geometries and BHandHLYP excitation energies for the larger aggregates. With the exception of the water monomer, excitation energies $[E(S_1;S_1 \leftarrow S_0)]$ are not very dependent on the number of water molecules in the aggregates, although some dependence on the conformer geometry is observed. For example, $E(S_1;S_1 \leftarrow S_0)$ is 3.73 and 2.56 eV for conformers 4b and 4c, respectively. The smallest value of $E(S_1;S_1 \leftarrow S_0)$ is for the

TABLE III. Energetics of the e^- anionic defect in water clusters. Geometry optimizations were carried out at the CIS/*d*-aug-cc-pVDZ level. DFT energies and TDDFT excitation energies were calculated at the BHandHLYP/*d*-aug-cc-pVTZ//CIS/*d*-aug-cc-pVDZ level. SAC-CI(SD) results for $n=1,2$ are shown in brackets.

n	$E(S_1;S_0)$[a]	$E(S_1;+)$[b]	$E(S_1;S_1 \leftarrow S_0)$[c]	$E_R(S_1)$[d]	$E_R(S_1;+)$[e]	IP[f]
1	−76.408 551	−75.966 295	7.12 [7.10;[g] 7.02[h]]	7.49[7.46[g,h]]	12.40[12.55;[g] 12.60[h]]	4.91 [5.09;[g] 5.14[h]]
2	−152.731 888	−152.459 583	3.14[3.40[g,h]]	6.40[6.58;[g] 6.55[h]]	10.67[10.77;[g] 10.74[h]]	4.27[4.19[g,h]]
3a	−229.186 903	−228.922 231	3.66	6.45	9.99	3.54
3b	−229.139 545	−228.904 991	2.24	6.31	10.46	4.14
4a	−305.629 042	−305.373 112	3.67	6.39	9.69	3.30
4b	−305.630 516	−305.373 828	3.73	6.42	9.67	3.25
4c	−305.588 889	−305.362 184	2.56	6.38	9.99	3.61
4d	−305.597 686	−305.366 126	2.92	6.50	9.88	3.38
5a	−382.036 994	−381.815 862	2.68	6.15	9.48	3.34
5b	−382.037 937	−381.818 521	2.81	6.26	8.42	3.16
5c	−382.065 968	−381.820 666	3.81	6.50	9.36	2.86

[a] $E(S_1;S_0)$ is the electronic energy (in hartree) at the geometry of the S_1 excited state.
[b] $E(S_1;+)$ is the electronic energy (in hartree) of the ionized cluster at the geometry of the S_1 excited state.
[c] $E(S_1;S_1 \leftarrow S_0)$ is the $S_1 \leftarrow S_0$ excitation energy at the S_1 geometry. Data in eV.
[d] $E_R(S_1)=[E(S_1;S_0)-E_0]+E(S_1;S_1 \leftarrow S_0)$. This quantity is the adiabatic excitation energy and places the energy of the anionic defect relative to the ground state energy E_0. Data in eV.
[e] $E_R(S_1;+)=E(S_1;+)-E_0$. This quantity places the energy of the ionized aggregate (at the geometry of the anionic defect) relative to E_0. Data in eV.
[f] $IP=E_R(S_1;+)-E_R(S_1)$ is the vertical ionization potential of the (electron) anionic defect. Data in eV.
[g] SAC-CI(SD)/*d*-aug-cc-pVTZ//CIS/*d*-aug-cc-pVDZ.
[h] SAC-CI(SD)/*d*-aug-cc-pVTZ//SAC-CI(SD)/*d*-aug-cc-pVDZ.

TABLE IV. Adiabatic energy gap in water clusters. Geometry optimizations were carried out at the CIS/*d*-aug-cc-pVDZ level. DFT energies and TDDFT excitation energies were calculated at the BHandHLYP/*d*-aug-cc-pVTZ//CIS/*d*-aug-cc-pVDZ level. SAC-CI(SD) results for $n=1,2$ are shown in brackets.

n	$E(+)$[a]	$E(+;S_0)$[b]	$E(+;S_1\leftarrow S_0)$[c]	$E_R(+)$[d]	$E_R(+;S_1)$[e]	V_0[f]
1	−75.969 033	−76.419 082	7.5[7.5;[g] 7.31[h]]	12.33(12.60)[i]	7.58	−4.75
2	−152.468 202	−152.747 656	3.59	10.43(10.81–10.90;[j] 10.42;[k] 10.7[l])	6.42	−4.02
3	−228.933 942	−229.179 610	3.38	9.67(9.86[k])	6.36	−3.31
4a,4b	−305.389 833	−305.614 711	3.17	9.24	6.29	−2.95
4c	−305.385 186	−305.581 499	2.09	9.36(9.54[k])	6.11	−3.25
4d	−305.382 264	−305.605 961	3.20	9.44	6.55	−2.89
5a	−381.836 483	−382.021 523	2.12	8.93	6.01	−2.92
5b	−381.835 030	−382.037 563	2.91	8.97	6.36	−2.60
5c	−381.836 162	−382.045 135	2.97	8.94	6.22	−2.72

[a] $E(+)$ is the electronic energy (in hartree) of the optimized ionized structure.
[b] $E(+;S_0)$ is the electronic energy (in hartree) of the neutral structure (by electron reattachment) at the geometry of the ionized structure.
[c] $E(+;S_1\leftarrow S_0)$ is the $S_1\leftarrow S_0$ excitation energy of the neutral system calculated at the optimized geometry of the ionized cluster. Data in eV.
[d] $E_R(+)=E(+)-E_0$. This quantity places the energy of the ionized structure relative to E_0 and corresponds to the adiabatic ionization energy. Data in eV.
[e] $E_R(+;S_1)=[E(+;S_0)-E_0]+E(+;S_1\leftarrow S_0)$. This quantity is the adiabatic energy gap. Data in eV.
[f] $V_0=E_R(+;S_1)-E_R(+)$. This quantity is the analogous of the conduction band edge. Data in eV.
[g] SAC-CI(SD)/*d*-aug-cc-pVTZ//CIS/*d*-aug-cc-pVDZ.
[h] SAC-CI(SD)/*d*-aug-cc-pVTZ//SAC-CI(SD)/*d*-aug-cc-pVDZ.
[i] Experimental value from Tomoda *et al.* (Ref. 45).
[j] Experimental value from de Visser *et al.* (Ref. 60).
[k] Theoretical calculations from Barnett and Landman (Ref. 62).
[l] Theoretical calculations from Novakovskaya and Stepanov (Ref. 61).

3b conformer (2.24 eV) and the largest excitation energy is 3.81 eV (5c). This dependence is possibly associated with specific structural features of the excited aggregates. Interestingly, some of the conformers with higher excitation energies (4a, 4b, and 5c) also exhibit lower ν_{O-H} frequencies (see Table II). The ground state electronic density of the optimized S_1 structures should reflect the presence of the OH^- and H_3O^+ species in interaction with water. The electronic density differences isosurfaces (Figs. 2–4) indicate that upon excitation, the promotion of an electron from the *p* orbital of the OH species leads to a diffuse electron density distribution that is stabilized by the interaction with the hydrogen atoms of the aggregate. This excitation energy can be related to charge transfer to solvent (CTTS) precursor states.[56,57] Theoretical results for CTTS energies in hydrated hydroxide anion clusters were reported.[58,59] Random phase approximation B3LYP calculations of Lee *et al.*[59] estimate CTTS energies for clusters of OH^- with one, two, and three water molecules as 3.48, 4.04, and 4.68 eV, respectively. These values are slightly blueshifted in comparison with our results (Table III) for the excitation energies of $H_3O^+[OH(H_2O)_{(n-2)}]^-$ aggregates ($n=3-5$). This tendency is possibly related to the presence of H_3O^+ that will favor electron delocalization and energetical stabilization of the excited state.

The energetics of the adiabatic excitation process can be described by the quantity $E_R(S_1)=[E(S_1;S_0)-E_0]+E(S_1;S_1\leftarrow S_0)$, which places the S_1 excited state relative to the reference state E_0. $E_R(S_1)$ (see Table III) shows a weak dependence on the number of water molecules in the aggregate. The smallest value (6.15 eV) corresponds to the 5a conformer. The largest adiabatic excitation energy is 6.50 eV for the 4d and 5c conformers. The weak dependence of $E_R(S_1)$ on the cluster size (or the number of water molecules) may indicate that the energetics of the adiabatic excitations is mainly controlled by local or short-ranged interactions. The energetics of anionic defects in liquid water was discussed by Coe and collaborators.[14,15] These authors placed the e^- anionic defect in the bulk 5.3 eV above pure water. The same authors also reported a value of ~7 eV for the anionic defect associated with an excited *p* state of e^-(aq).[14] Our results correspond to the lowest $S_1\leftarrow S_0$ excitation and are in agreement with the minimum photon energy required to produce hydrated electrons from pure water (~6.5 eV).[5–9]

Table III also reports results for $E_R(S_1;+)=E(S_1;+)-E_0$. This quantity places the energy of the ionized aggregate (at the geometry of the S_1 state) relative to E_0. From $E_R(S_1;+)$, the vertical ionization potential of the anionic defect (IP) can be estimated as $IP=E_R(S_1;+)-E_R(S_1)$. Values of IP range from 4.27 eV (water dimer) to 2.86 eV (5c pentamer conformer). These IPs correspond to the energy needed to vertically remove the microhydrated electron from the excited aggregate and can be compared with the PET of hydrated electrons in water (PET ~ 2.4 eV).[14]

C. Adiabatic energy gap in water clusters

Ionization of the excited S_1 aggregates followed by geometry optimization leads to the local minima ionized (+) structures also reported in Figs. 2–4. Our results for the energetics of these ionized structures are presented in Table IV.

The relative energies of the ionized structures are given by $E_R(+)=E(+)-E_0$. This quantity places the energy of the optimized ionized structures relative to E_0 and corresponds to the adiabatic ionization energy of the aggregate. With the exception of the structure related to the water dimer, for which $E_R(+)$ is 10.43 eV, $E_R(+)$ exhibits a weak dependence

on the number of water molecules. $E_R(+)$ are 8.93 and 9.67 eV for the 5a and 3b conformers, respectively. For the water monomer and dimer, experimental results for $E_R(+)$ are available.[45,60] Theoretical results were also reported for small water clusters. [61,62] For the water monomer, our prediction (12.33 eV) is ~0.3 eV below experiment.[45] This difference between theory and experiment is quite similar to the one observed for the vertical ionization energy (see Table I) and reflects the fact that, for the water monomer, the vertical and adiabatic ionization energies are very close.[45] Our result for the water dimer (10.43 eV) is in good agreement with experimental information (10.81–10.90 eV) (Ref. 60), and it is quite similar to a theoretical prediction (10.42 eV).[62] A good agreement between our results and the theoretical values reported by Barnett and Landman[62] for the ionized structures 3 and 4c is also observed.

Electron reattachment to the ionized structures provides a route for calculating $E(+;S_1 \leftarrow S_0)$, which is the $S_1 \leftarrow S_0$ excitation energy of the ground state neutral aggregate calculated at the optimized geometry of the ionized cluster. The $E(+;S_1 \leftarrow S_0)$ excitation energy shows some dependence on the geometry of the optimized conformers. For example, it is 3.17 eV for conformers 4a and 4b and 2.09 eV for conformer 4c. A similar dependence of $E(+;S_1 \leftarrow S_0)$ on the geometry is also observed for conformers 5c $[E(+;S_1 \leftarrow S_0)=2.97$ eV] and 5a $[E(+;S_1 \leftarrow S_0)=2.12$ eV]. This trend is the same as that previously observed for $E(S_1;S_1 \leftarrow S_0)$.

A fundamental quantity also reported in Table IV is the adiabatic energy gap for a water cluster, which can be defined as $E_R(+;S_1)=[E(+;S_0)-E_0]+E(+;S_1 \leftarrow S_0)$. A major difference between $E_R(+;S_1)$ and $E_R(S_1)$ (see Sec. III B 2) should be made precise. $E_R(+;S_1)$ only involves the reorganization of the water molecules around the hydronium $(H_3O)^+$ and OH species. However, $E_R(S_1)$ also involves the relaxation of the water molecules around the microhydrated electron. This aspect was stressed by Coe *et al.* in their definition of the adiabatic band gap of water.[14] Our results for $E_R(+;S_1)$ or for the adiabatic energy gap of small water clusters range from 6.01 eV (5a) to 6.55 eV (4d). These values can be compared with experimental (6.9 eV) (Ref. 14) and theoretical (6.83 eV) (Ref. 17) results for the liquid water band gap. The qualitative agreement between our predictions and the results for the liquid phase is an indication of the reliability of the present cluster calculations in describing some basic features characterizing the electronic properties of water.

The quantity (V_0) can now be estimated as $V_0=E_R(+;S_1)-E_R(+)$. In agreement with our previous predictions [Sec. III A], V_0 decreases slowly with increasing cluster size. In comparison with the results reported in Table I, slightly smaller values are predicted by the above expression. For example, when $n=4$, $V_{0,v}=-3.75$ eV from $V_{0,v}=E(S_0;S_1 \leftarrow S_0)-\mathrm{IP}$, whereas it is −3.25 eV (4b) from $V_0=E_R(+;S_1)-E_R(+)$. These differences are possibly related to the feature that in small water clusters, structure and electronic reorganization around the H_3O^+ cation modifies the energetics of electron attachment to the aggregates.

IV. SUMMARY AND CONCLUSIONS

Ab initio CIS/*d*-aug-cc-pVDZ calculations were carried out to investigate the S_1 singlet excited state structures of $H_3O^+[OH(H_2O)_{(n-2)}]^-$ aggregates. The energetics of the excited structures were then investigated by DFT calculations at the BHandHLYP/*d*-aug-cc-pVTZ level. A very good agreement between several electronic properties of water aggregates and experimental information was observed for ionization energies and photoelectron emission thresholds. Further support on the reliability of the present approach to investigate the electronic structure of excited water clusters has been provided by full active SAC-CI(SD) calculations for $n=1,2$.

One important conclusion concerns the relationship between the electronic properties of the aggregates and the adiabatic band gap of water. The importance of taking into account the relaxation of the water molecules for predicting electronic properties of water should be stressed. This is summarized in Fig. 1, where the energetic properties of the excited and ionized aggregates related to the water pentamer are represented as a function of the "solvent" coordinate describing dissociation (bond breaking and formation) and relaxation or structure reorganization around microhydrated species. Therefore, we provide evidence that several relevant quantities characterizing the behavior of water upon photoexcitation can be assessed by the calculation of the electronic properties of small aggregates. Specifically, the adiabatic route to the conduction band of liquid water[14] can be investigated through the analysis of the structure and electronic density reorganization induced by the photoexcitation of water clusters. Our estimates for the adiabatic energy gap of the aggregates (6.01–6.55 eV) are in keeping with experimental (6.9 eV)[14] and theoretical (6.83 eV)[17] results for the band gap of liquid water.

We also report results for a quantity V_0, which is analogous to the conduction band edge of liquid water. Our calculations indicate that this quantity is strongly size dependent, making difficult a comparison with bulk values. However, although the calculation of V_0 illustrates the limitations of a cluster approach, it seems reasonable to conclude that the study of excited water clusters can improve our understanding of the electronic properties of the bulk phase. Finally, we believe that this work reports, for the first time, an investigation of the electronic properties of small water aggregates that supports the picture proposed by Coe *et al.*[14] for the adiabatic band gap of liquid water.

ACKNOWLEDGMENTS

This work was partially supported by Fundação para a Ciência e a Tecnologia (FCT), Portugal (Grant No. POCTI/43315/QUI/2001). One of the authors (P.C.C.) gratefully acknowledges the FCT (Ph.D. Grant No. SFRH/BD/6503/2001).

[1] B. Winter, R. Weber, W. Widdra, M. Dittmar, M. Faubel, and I. Hertel, J. Phys. Chem. A **108**, 2625 (2004).
[2] B. Winter and M. Faubel, Chem. Rev. (Washington, D.C.) **106**, 1176 (2006).

[3] B. C. Garret, D. A. Dixon, D. M. Camaioni *et al.*, Chem. Rev. (Washington, D.C.) **105**, 355 (2005).
[4] R. Laenen, T. Roth, and A. Laubereau, Phys. Rev. Lett. **85**, 50 (2000).
[5] J. W. Boyle, J. A. Ghormley, C. J. Hochanadel, and J. F. Riley, J. Phys. Chem. **73**, 2886 (1969).
[6] E. J. Hart and M. Anbar, *The Hydrated Electron* (Wiley-Interscience, New York, 1970).
[7] D. N. Nikogosyan, A. A. Oraevsky, and V. I. Rupasov, Chem. Phys. **77**, 131 (1983).
[8] A. Bernas, C. Ferradini, and J.-P. Jay-Gerin, J. Photochem. Photobiol., A **117**, 171 (1998).
[9] D. M. Bartels and R. A. Crowell, J. Phys. Chem. A **104**, 3349 (2000).
[10] P. Delahay and K. Von Burg, Chem. Phys. Lett. **83**, 250 (1981).
[11] P. Delahay, Acc. Chem. Res. **15**, 40 (1982).
[12] T. Watanabe and H. Gerischer, J. Electroanal. Chem. Interfacial Electrochem. **122**, 73 (1981).
[13] O. Dutuit, A. Tabche-Fouhaile, I. Nenner, H. Frolich, and P. M. Guyon, J. Chem. Phys. **83**, 584 (1985).
[14] J. V. Coe, A. D. Earhart, M. C. Cohen, G. J. Hoffman, H. W. Sarkas, and K. H. Bowen, J. Chem. Phys. **107**, 6023 (1997).
[15] J. V. Coe, Int. Rev. Phys. Chem. **20**, 33 (2001).
[16] C. G. Elles, A. E. Jailaubekov, R. A. Crowell, and S. E. Bradforth, J. Chem. Phys. **125**, 044515 (2006).
[17] P. Cabral do Couto, S. G. Estácio, and B. J. Costa Cabral, J. Chem. Phys. **123**, 054510 (2005).
[18] J. B. Foresman, M. Head-Gordon, J. A. Pople, and M. J. Frisch, J. Phys. Chem. **96**, 135 (1992).
[19] R. G. Parr and W. Yang, *Density Functional Theory of Atoms and Molecules* (Oxford University Press, Oxford, 1989).
[20] M. A. L. Marques and E. K. U. Gross, in *A Primer in Density Functional Theory*, edited by C. Fiolhais, F. Nogueira, and M. Marques (Springer, Berlin, 2002), Chap. 4.
[21] H. Nakatsuji and K. Hirao, J. Chem. Phys. **68**, 2053 (1978).
[22] M. Ishida, K. Toyota, M. Ehara, and H. Nakatsuji, Chem. Phys. Lett. **350**, 351 (2001).
[23] K. Toyota, M. Ehara, and H. Nakatsuji, Chem. Phys. Lett. **356**, 1 (2002).
[24] D. M. Chipman, J. Chem. Phys. **122**, 044111 (2005).
[25] D. M. Chipman, J. Chem. Phys. **124**, 044305 (2006).
[26] K. B. Wiberg, Y.-G. Wang, A. E. de Oliveira, S. A. Perera, and P. H. Vaccaro, J. Phys. Chem. A **109**, 466 (2005).
[27] J. F. Stanton and R. J. Bartlett, J. Chem. Phys. **98**, 7029 (1993).
[28] T. H. Dunning, Jr., J. Chem. Phys. **90**, 1007 (1989).
[29] A. D. Becke, J. Chem. Phys. **98**, 1372 (1993).
[30] C. Lee, W. Yang, and R. G. Parr, Phys. Rev. B **37**, 785 (1988).
[31] M. J. Frisch, G. W. Trucks, H. B. Schlegel *et al.*, GAUSSIAN 03, Revision C.02, Gaussian Inc., Pittsburgh, PA, 2003.
[32] Y. Zhao and D. G. Truhlar, J. Chem. Theory Comput. **1**, 415 (2005).
[33] J. A. Anderson and G. S. Tschumper, J. Phys. Chem. A **110**, 7268 (2006).
[34] M. Sodupe, J. Bertran, L. Rodríguez-Santiago, and E. J. Baerends, J. Phys. Chem. A **103**, 166 (1999).
[35] M. Grüning, O. V. Gritsenko, S. J. A. van Gisbergen, and E. J. Baerends, J. Phys. Chem. A **105**, 9211 (2001).
[36] A. L. Sobolewski and W. Domcke, J. Chem. Phys. **122**, 184320 (2005).
[37] Z.-L. Cai, D. J. Tozer, and J. R. Reimers, J. Chem. Phys. **113**, 7084 (2000).
[38] B.-M. Cheng, E. P. Chew, C.-P. Liu, M. Bahou, Y.-P. Lee, Y. L. Yung, and M. F. Grestell, Geophys. Res. Lett. **26**, 3657 (1999).
[39] K. Kobayashi, J. Phys. Chem. **87**, 4317 (1983).
[40] R. S. Mulliken, Chem. Phys. Lett. **46**, 197 (1977).
[41] P. Han and D. M. Bartels, J. Phys. Chem. **94**, 5824 (1990).
[42] B. D. Bursulaya, J. Jeon, C.-N. Yang, and H. J. Kim, J. Phys. Chem. A **104**, 45 (2000).
[43] G. P. Parravicini and L. Resca, Phys. Rev. B **8**, 3009 (1973).
[44] P. H. Hahn, W. G. Schmidt, K. Seino, M. Preuss, F. Bechstedt, and J. Bernholc, Phys. Rev. Lett. **94**, 037404 (2005).
[45] S. Tomoda, Y. Achiba, and K. Kimura, Chem. Phys. Lett. **87**, 197 (1982).
[46] P. Hunt, M. Sprik, and R. Vuilleumier, Chem. Phys. Lett. **376**, 68 (2003).
[47] T. Malaspina, K. Coutinho, and S. Canuto, J. Chem. Phys. **117**, 1692 (2002).
[48] P. Cabral do Couto, B. J. Costa Cabral, and S. Canuto, Chem. Phys. Lett. **429**, 129 (2006).
[49] S. Lee, J. Kim, S. J. Lee, and K. S. Kim, Phys. Rev. Lett. **79**, 2038 (1997).
[50] C. G. Bailey, J. Kim, and M. A. Johnson, J. Phys. Chem. **100**, 16782 (1996).
[51] P. Ayotte and M. A. Johnson, J. Chem. Phys. **106**, 811 (1997).
[52] J. Kim, J. Y. Lee, K. S. Oh, J. M. Park, S. Lee, and K. S. Kim, Phys. Rev. A **59**, R930 (1999).
[53] J. Kim, S. B. Suh, and K. S. Kim, J. Chem. Phys. **111**, 10077 (1999).
[54] A. L. Sobolewski and W. Domcke, Phys. Chem. Chem. Phys. **4**, 4 (2002).
[55] A. L. Sobolewski and W. Domcke, J. Phys. Chem. A **106**, 4158 (2002).
[56] M. J. Blandamer and M. F. Fox, Chem. Rev. (Washington, D.C.) **70**, 59 (1970).
[57] R. A. Crowell, R. Lian, I. A. Shkrob, and D. M. Bartels, J. Chem. Phys. **120**, 11712 (2004).
[58] M. Masamura, J. Chem. Phys. **117**, 5257 (2002).
[59] H. M. Lee, P. Tarkeshwar, and K. S. Kim, J. Chem. Phys. **121**, 4657 (2004).
[60] S. P. de Visser, L. J. de Koning, and N. M. M. Nibbering, J. Phys. Chem. **99**, 15444 (1995).
[61] Y. V. Novakovskaya and N. F. Stepanov, J. Phys. Chem. A **103**, 3285 (1999).
[62] R. N. Barnett and U. Landman, J. Phys. Chem. **101**, 164 (1997).

Chapter 6

Conclusions and future perspectives

The most stable $OH(H_2O)_{n=2-5}$ minimum energy geometries correspond to cyclic single donor-acceptor hydrogen bonding patterns. As these geometries were derived from $(H_2O)_n$ minimum energy clusters by the removal of a dangling hydrogen, the present results suggest that this might constitute a possible route for a systematic search for minimum energy geometries of larger clusters. Although hydrogen bonding in water and small water clusters has been the subject of numerous studies, radical-water interactions are comparatively less studied. In future work the geometry and relative stability of $OH(H_2O)_n$ clusters will be studied by means of many-body decomposition of the full interaction energy for minimum energy geometries. A many-body decomposition of the $OH\cdots(H_2O)_n$ interaction as function of cluster size can also provide qualitative information on the importance of many-body effects in $OH\cdots$water interactions in the condensed phase. A realistic estimate for the latter can be obtained trough a sequential Quantum Chemical / Monte Carlo methodology, trough the study of the size-converged many-body decomposition of the $OH\cdots(H_2O)_n$ interaction energy for configurations sampled from molecular simulation. This approach can be generally applied as means of insight into solute-solvent interactions and cooperative behaviour in the condensed phase.

Agreement between sequential Quantum Mechanical / Monte Carlo methodology theoretical results and experimental electron binding energies for liquid water was observed. Extrapolation of V_0 to bulk yields -0.17$\pm$0.05 eV, in good agreement with the recent estimate by Coe et al. (-0.12 eV). Our estimate for the photoemission threshold is 10.58$\pm$0.1 eV. The current approach overestimates the experimental photoemission threshold of pure liquid water by $\sim$0.5 eV, which leads to a 10.41$\pm$0.09 eV optical gap. This constitutes a considerable improvement over previous density functional results, which range from 3.6 to 6.5 eV. A sequential Quantum Chemical / Monte Carlo methodology can be of interest for the study of the electronic properties of liquid water. In future work, further improvement can be achieved by the determination of the optimal amount of Hartree-Fock exchange required for the reproduction of the electronic properties of both global

and local minimum energy geometries for the water dimer and also larger clusters. Other possible improvements include a self-consistent determination of polarization charges for the correction of surface effects and also the use of a flexible potential in order to account for one-body effects.

The hydration enthalpy of the hydroxyl radical estimated from Monte Carlo simulation is ΔH_{hyd}[OH] =-39.1±3.9 kJ mol^{-1}. This result was later found to be in agreement with experiment (-38.1±6.3 kJ mol^{-1}) [264]. Both ΔE_{hyd}[OH] and V_0, are in agreement with the values proposed by Coe et al.. Consequently, our calculation for the adiabatic band gap, E_gap =6.83±0.05, does not differ from Coe's estimate (6.9 eV). A similar value was also obtained trough the study of the relative energetics and electronic properties of neutral, ionized and electronically excited water clusters. For the first time, these results provide a molecular level verification of an adiabatic route for the definition of an adiabatic ionization potential for liquid water.

The study of the system size convergence of the electronic properties for clusters sampled from molecular simulation constitutes an affordable alternative to much more expensive ab-initio based molecular simulation methods. This approach can be viewed as a complement to minimum enegy cluster studies which only provide partial information on condensed phase interactions and electronic properties. One promissing perspective is the study of the relation between the local hydrogen bonding environment and the many-body decomposition of the interaction energy with the remainig molecules, the molecular dipole moment as well as the electronic density of states and excitation energies. This can provide a molecular level understanding of interactions, cooperative behaviour and structure in liquid water as well as the observed photoemission and absorption spectrum.

Bibliography

[1] G.R. Desiraju. Chemistry beyond the molecule. *Nature*, 412:397–400, 2001.

[2] G.R. Desiraju. Chemistry - The middle kingdom. *Current Science*, 88:374–380, 2005.

[3] P.L. Luisi. Emergence in chemistry: Chemistry as the embodiment of emergence. *Foundations of Chemistry*, 4:183–200, 2002.

[4] S. Schweber and M. Wächter. Complex systems, modelling and simulation. *Studies in History and Philosophy of Modern Physics*, 31:583–609, 2000.

[5] M.J. Elrod and R.J. Saykally. Many-body effects in intermolecular forces. *Chemical Reviews*, 94:1975–1997, 1994.

[6] I.G. Kaplan. *Intermolecular interactions: Physical picture, computational methods and model potentials*. John Wiley & Sons, 2006.

[7] P. Ball. *A Biography of water*. Phoenix, Orion Books Ltd, London, 2000.

[8] D. Eisenberg and W. Kauzmann. *The structure and properties of water*. Clarendon Press, Oxford, 1969.

[9] F. Franks, editor. *Water, a comprehensive treatise. Vol.1: The physics and physical chemistry of water*. Plenum Press, New York, 1972.

[10] Y. Maréchal. *The hydrogen bond and the water molecule: The physics and chemistry of water, aqueous and bio media*. Elsevier, 2007.

[11] F.H. Stillinger. Water revisited. *Science*, 209:451–457, 1980.

[12] R. Ludwig. Water: From clusters to the bulk. *Angewandte Chemie International Edition*, 40:1808–1827, 2001.

[13] J.L. Finney. Water? What's so special about it? *Philosophical Transactions of The Royal Society London B*, 359:1145–1165, 2004.

[14] B. Guillot. A reappraisal of what we have learned during three decades of computer simulations on water. *Journal of Molecular Liquids*, 101:219–260, 2002.

[15] J.L. Finney. The water molecule and its interactions: The interaction between theory, modelling, and experiment. *Journal of Molecular Liquids*, 90:303–312, 2001.

[16] S.R. Billeter, P.M. King, and W.F. van Gunsteren. Can the density maximum of water be found by computer simulation? *The Journal of Chemical Physics*, 100:6692–6699, 1994.

[17] A. Brodsky. Is there predictive value in water computer simulations? *Chemical Physics Letters*, 261:563–568, 1996.

[18] C. Vega, J.L.F. Abascal, E. Sanz, L.G. MacDowell, and C. McBride. Can simple models describe the phase diagram of water? *Journal of Physics: Condensed Matter*, 17:S3283–S3288, 2005.

[19] A. Baranyai, A. Bartók, and A.A. Chialvo. Limitations of the rigid planar nonpolarizable models for water. *Journal of Chemical Physics*, 124:074507, 2006.

[20] T.J. Giese and D.M. York. Many-body force field models based solely on pairwise coulomb screening do not simultaneously reproduce correct gas-phase and condensed-phase polarizability limits. *Journal of Chemical Physics*, 120:9903–9906, 2004.

[21] R. Chelli, V. Schettino, and P. Procacci. Comparing polarizable force fields to ab initio calculations reveals nonclassical effects in condensed phases. *Journal of Chemical Physics*, 122:234107, 2005.

[22] J. Jortner. *Physics and chemistry of finite systems: From clusters to crystals*, chapter Clusters as a key to the understanding of properties as a function of size and dimensionality, pages 1–17. Dortrecht, 1992.

[23] J. Jortner. Cluster size effects. *Zeitschrift für Physik D Atoms, Molecules and Clusters*, 24:247–275, 1992.

[24] J. Jortner. Cluster size effects revisited. *Journal de Chimie Physique et de Physico-Chimie Biologique*, 92:205–225, 1995.

[25] B. Hartke. Structural transition in clusters. *Angewandte Chemie International Edition*, 41:1468–1487, 2002.

[26] G. Torchet, J. Farges, M.F. de Feraudy, and B. Raoult. Structural study of CH_4, CO_2 and H_2O clusters containing from several tens to several thousands of molecules. *Annales de Physique*, 14:245–260, 1989.

[27] B.W. van de Waal, G. Torchet, and M.F. de Feraudy. Structure of large argon clusters Ar_N,10^3<N<10^5: Experiments and simulations. *Chemical Physics Letters*, 331:57–63, 2000.

[28] J.K. Gregory, D.C. Clary, K. Liu, M.G. Brown, and R.J. Saykally. The water dipole moment in water clusters. *Science*, 275:814–817, 1997.

[29] B. Winter, E.F. Aziz, U. Hergenhahn, M. Faubel, and I.V. Hertel. Hydrogen bonds in liquid water studied by photoelectron spectroscopy. *Journal of Chemical Physics*, 126:124504, 2007.

[30] J.-H. Guo, Y. Luo, A. Augustsson, J.-E. Rubensson, C. Såthe, H. Ågren, H. Siegbahn, and J. Nordgren. X-ray emission spectroscopy of hydrogen bonding and electronic structure of liquid water. *Physical Review Letters*, 89:137402, 2002.

[31] Ph. Wernet, D. Nordlund, U. Bergmann, M. Cavalleri, M. Odelius, H. Ogasawara, L.Å. Näslund, T. K. Hirsch, L. Ojamäe, P. Glatzel, L.G.M. Pettersson, and A. Nilsson. The structure of the first coordination shell in liquid water. *Science*, 304:995–999, 2004.

[32] B. Winter, R. Weber, W. Widdra, M. Dittmar, Faubel, and I.V. Hertel. Full valence band photoemission from liquid water using EUV synchrotron radiation. *Journal of Physical Chemistry A*, 108:2625–2632, 2004.

[33] B. Winter and M. Faubel. Photoemission from liquid aqueous solutions. *Chemical Reviews*, 106:1176–1211, 2006.

[34] F. Williams, S.P. Varma, and S. Hillenius. Liquid water as a lone-pair amorphous semiconductor. *Journal of Chemical Physics*, 64:1549–1554, 1976.

[35] J.V. Coe, A.D. Earhart, M.H. Cohen, G.J. Hoffman, H.W. Sarkas, and K.H. Bowen. Using cluster studies to approach the electronic structure of bulk water: Reassessing the vacuum level, conduction band edge, and band gap of water. *Journal of Chemical Physics*, 107:6023–6031, 1997.

[36] B.C. Garrett, D.A. Dixon, D.M. Camaioni, D.M. Chipman, M.A. Johnson, C.D. Jonah, G.A. Kimmel, J.H. Miller, T.N. Rescigno, P.J. Rossky, et al. Role of water in electron-initiated processes and radical chemistry: Issues and scientific advances. *Chemical Reviews*, 105:355–389, 2005.

[37] D. Marx. Proton transfer 200 years after von Grotthuss: Insights from ab initio simulations. *ChemPhysChem*, 7:1848–1870, 2006.

[38] M.L. Huggins. PhD thesis, University of California, 1919.

[39] M.L. Huggins. Hydrogen bridges in organic compounds. *Journal of Organic Chemistry*, 1:407–456, 1936.

[40] G.N. Lewis. *Valence and the structure of atoms and molecules*. The Chemical Catalog Co., New York, 1923.

[41] W.M. Latimer and W.H. Rodebush. Polarity and ionization from the standpoint of the Lewis theory of valence. *Journal of the American Chemical Society*, 42:1419–1433, 1920.

[42] L. Pauling. *The nature of the chemical bond*. Cornell University Press: Ithaca, New York, 1939.

[43] T. Steiner. The hydrogen bond in the solid state. *Angewandte Chemie International Edition*, 41:48–76, 2002.

[44] G.R. Desiraju and T. Steiner. *The weak hydrogen bond: In structural chemistry and biology*. Oxford University Press, Oxford, 1999.

[45] G.A. Jeffrey and W. Saenger. *Hydrogen bonding in biological structures*. Springer-Verlag, New York, 1991.

[46] C. Reichardt. *Solvents and solvent effecs in organic chemistry*. John Wiley & Sons, 2003.

[47] G.C. Pimentel and A.L. McClellan. *The hydrogen bond*. W.H. Freeman and Co., San Francisco, 1960.

[48] G.A. Jeffrey. *An introduction to hydrogen bonding*. Oxford University Press, Oxford, 1997.

[49] D. Hadži, editor. *Theoretical treatments of hydrogen bonding*. John Wiley & Sons, 1997.

[50] S. Scheiner. *Hydrogen bonding - A theoretical perspective*. Oxford University Press, Oxford, 1997.

[51] S.J. Grabowski, editor. *Hydrogen bonding - New insights*. Springer, 2006.

[52] V.I. Minkin. Glossary of terms used in theoretical organic chemistry (IUPAC recommendations 1999). *Pure and Applied Chemistry*, 71:1919–1981, 1999.

[53] P. Lipkowski, A. Koll, A. Karpfen, and P. Wolschann. An approach to estimate the energy of the intramolecular hydrogen bond. *Chemical Physics Letters*, 360:256–263, 2002.

[54] S.G. Estácio, P.C. do Couto, B.J. Costa Cabral, M.E. Minas da Piedade, and J.A. Martinho Simões. Energetics of intramolecular hydrogen bonding in di-substituted benzenes by the *ortho-para* method. *Journal of Physical Chemistry A*, 108:10834–10843, 2004.

[55] V.V. Gromak. Ab initio study of intra- and intermolecular H-bond energies in π-conjugated molecular systems. *Journal of Molecular Structure - Theochem*, 726:213–224, 2005.

[56] G. Buemi. *Hydrogen bonding - New insights*, chapter Intramolecular hydrogen bonds. Methodologies and strategies for their strenght evaluation, pages 51–107. Springer, 2006.

[57] J. Marco, J.M. Orza, R. Notario, and J.-L.M. Abboud. Hydrogen bonding of neutral species in the gas phase: The missing link. *Journal of the American Chemical Society*, 116:8841–8842, 1994.

[58] G. Chalasinski. State of the art and challenges of the ab initio theory of intermolecular interactions. *Chemical Reviews*, 100:4227–4252, 2000.

[59] A.D. Buckingham. *Theoretical treatments of hydrogen bonding*, chapter The hydrogen bond: An electrostatic interaction?, pages 1–12. John Wiley & Sons, 1997.

[60] F. Weinhold. Nature of H-bonding in clusters, liquids, and enzimes: an ab initio natural bond orbital perspective. *Journal of Molecular Structure - Theochem*, 398-399:181–197, 1997.

[61] G.R. Desiraju. Hydrogen bridges in crystal engeneering: interactions without borders. *Accounts of Chemical Research*, 35:565–573, 2002.

[62] G.R. Desiraju. C$-$H$\cdots$O and other weak hydrogen bonds. From crystal engeneering to virtual screening. *Chemical Communications*, pages 2995–3001, 2005.

[63] I. Alkorta, D.C. Clary, R.H. Crabtree, J.J. Dannenberg, G.R. Desiraju, H.G. Kjaergaard, R.A. Klein, K. Kleinermanns, A.C. Legon, B. Mennucci, D.J. Nesbitt, and J. Sadlej. Categorizing hydrogen bonding and other intermolecular interactions. Project 2004-026-2-100, Physical and Biophysical Chemistry Division (I), International Union of Pure and Applied Chemistry, 2004.

[64] J.J. Novoa, I. Nobeli, F. Grepioni, and D. Braga. Are all short O−H···O contacts hydrogen bonds? A quantitative look at the nature of O−H···O intermolecular hydrogen bonds. *New Journal of Chemistry*, 24:5–8, 2000.

[65] V. Aquilanti, E. Cornicchi, M.M. Teixidor, N. Saendig, F. Pirani, and D. Cappelletti. Glory-scattering measurement of water-noble-gas interactions: The birth of the hydrogen bond. *Angewandte Chemie International Edition*, 44:2356–2360, 2005.

[66] N.V. Belkova, E.S. Shubina, and L.M. Epstein. Diverse world of unconventional hydrogen bonds. *Accounts of Chemical Research*, 38:624–631, 2005.

[67] K. Kitaura and K. Morokuma. New energy decomposition scheme for molecular-interactions within hartree-fock approximation. *International Journal of Quantum Chemistry*, 10:325–340, 1976.

[68] W.J. Stevens and W.H. Fink. Frozen fragment reduced variational space analysys of hydrogen-bonding interactions - Application to the water dimer. *Chemical Physics Letters*, 139:15–22, 1987.

[69] E.D. Glendening and A.J. Streitwieser. Natural energy decomposition analysis - An energy partitioning procedure for molecular interactions with application to weak hydrogen-bonding, strong ionic, and moderate donor-acceptor interactions. *Journal of Chemical Physics*, 100:2900–2909, 1994.

[70] J. Korchowiec and T. Uchimaru. New energy partitioning scheme based on the self-consistent charge and configuration method for subsystems: Application to water dimer. *Journal of Chemical Physics*, 112:1623–1633, 2000.

[71] G. Gilli and P. Gilli. Towards a unified hydrogen bond theory. *Journal of Molecular Structure*, 552:1–15, 2000.

[72] P. Gilli, V. Bertolasi, L. Pretto, V. Ferretti, and G. Gilli. Covalent versus electrostatic nature of the strong hydrogen bond: Discrimination among single, double, and asymmetric single-well hydrogen bonds by variable-temperature X-ray crystallographic methods in β-diketone enol RAHB systems. *Journal of the American Chemical Society*, 126:3845–3855, 2004.

[73] K. Morokuma. Why do molecules interact? The origin of electron donor-acceptor complexes, hydrogen bonding and proton affinity. *Accounts of Chemical research*, 10:294–300, 1977.

[74] T. Steiner and G.R. Desiraju. Distinction between the weak hydrogen bond and the van der Waals interaction. *Chemical Communications*, pages 891–892, 1998.

[75] J.J. Dannenberg, L. Haskamp, and A. Matsunov. Are hydrogen bonds covalent or electrostatic? A molecular orbital comparison of molecules in electric fields and H-bonding environments. *Journal of Physical Chemistry A*, 103:7083–7086, 1999.

[76] W.H. Thompson and J.T. Hynes. Frequency shifts in the hydrogen-bonded OH strech in halide-water clusters. The importance of charge transfer. *Journal of The American Chemical Society*, 122:6278–6286, 2000.

[77] R. Parthasarathi and V. Subramanian. *Hydrogen bonding - New insights*, chapter Characterization of hydrogen bonding: From van der Waals interactions to covalency, pages 1–50. Springer, 2006.

[78] A.J. Dingley and S. Grzesiek. Direct observation of hydrogen bonds in nucleic acid base pairs by internucleotide $^2J_{NN}$ couplings. *Journal of the American Chemical Society*, 120:8293–8297, 1998.

[79] F. Cordier and S. Grzesiek. Direct observation of hydrogen bonds in proteins by interresidue $^{3h}J_{NC'}$ scalar couplings. *Journal of the American Chemical Society*, 121:1601–1602, 1999.

[80] G. Cornilescu, J-S. Hu, and A. Bax. Identification of the hydrogen bonding network in a protein by scalar couplings. *Journal of the American Chemical Society*, 121:2949–2950, 1999.

[81] E.D. Isaacs, A. Shukla, P.M . Platzman, D.R. Hamman, B. Barbiellini, and C.A. Tulk. Covalency of the hydrogen bond in ice: A direct X-ray measurement. *Physical Review Letters*, 82:600–603, 1999.

[82] E.D. Isaacs, A. Shukla, P.M . Platzman, D.R. Hamman, B. Barbiellini, and C.A. Tulk. Compton scattering evidence for covalency of the hydrogen bond in ice. *Journal of Physics and Chemistry of Solids*, 61:403–406, 2000.

[83] A. Karpfen. Cooperative effects in hydrogen bonding. *Advances in Chemical Physics*, 123:469–510, 2002.

[84] W.H.E. Schwarz, K. Ruedenberg, and L. Mensching. Chemical deformation Densities 1. Principles and formulation of quantitative determination. *Journal of the American Chemical Society*, 111:6926–6932, 1989.

[85] L. Mensching, W. Von Niessen, P. Valtazanos, K. Ruedenberg, and W.H.E. Schwarz. Chemical deformation densities. 2. Small molecules. *Journal of the American Chemical Society*, 111:6932–6941, 1989.

[86] H.S. Frank and W.-Y Wen. Structural aspects of ion-solvent interaction in aqueous solutions: A suggested picture of water structure. *Faraday Discussions of the Chemical Society*, 24:133–410, 1957.

[87] L. Rincón, R. Almeida, and D.G. Aldea. Many-body energy decomposition analysis of cooperativity in hydrogen fluoride clusters. *International Journal of Quantum Chemistry*, 102:443–453, 2005.

[88] S.L. Shostak, W.L. Ebenstein, and J.S. Muenter. The dipole moment of water. I. Dipole moments and hyperfine properties of H_2O and HDO in the ground and excited vibrational states. *Journal of Chemical Physics*, 94:5875–5882, 1991.

[89] K. Ichikawa, Y. Kameda, T. Yamaguchi, H. Wakita, and M. Misawa. Neutron-diffraction investigation of the intramolecular structure of a water molecule in the liquid-phase at high-temperatures. *Molecular Physics*, 73:79–86, 1991.

[90] Y.S. Badyal, M.-L. Saboungi, D.L. Price, S.D. Shastri, and D.R. Haeffner. Electron distribution in water. *Journal of Chemical Physics*, 112:9206–9208, 2000.

[91] K. Laasonen, M. Sprik, and M. Parinello. "Ab initio" liquid water. *Journal of Chemical Physics*, 99:9080–9089, 1993.

[92] L. Delle Site, A. Alavi, and R.M. Lynden-Bell. The electrostatic properties of water molecules in condensed phases: An ab initio study. *Molecular Physics*, 96:1683–1693, 1999.

[93] P.L. Silvestrelli and M. Parrinello. Structural, electronic, and bonding properties of liquid water from first principles. *Journal of Chemical Physics*, 111:3572–3580, 1999.

[94] Y. Tu and A. Laaksonen. The electronic properties of water molecules in water clusters and liquid water. *Chemical Physics Letters*, 329:283–288, 2000.

[95] K. Coutinho, R.C. Guedes, B.J.C. Cabral, and S. Canuto. Electronic polarization of liquid water: converged monte carlo - quantum mechanics results for the multipole moments. *Chemical Physics Letters*, 369:345–353, 2003.

[96] T. Todorova, A.P. Seitsonen J., Hutter, I.F.W. Kuo, and C.J. Mundy. Molecular dynamics simulation of liquid water: Hybrid density functionals. *Journal of Physical Chemistry B*, 110:3685–3691, 2006.

[97] D.C. Ghosh and A. Chakraborty. Dipole correlation of the electronic structures of the conformations of water molecule evolving through the normal modes of vibrations between angular (C_2v) to linear ($D_{\infty h}$) shapes. *International Journal of Molecular Sciences*, 7:71–96, 2006.

[98] Y.A. Mantz, B. Chen, and G.J. Martyna. Structural correlations and motifs in liquid water at selected temperatures: Ab Initio and empirical model predictions. *Journal of Physical Chemistry B*, 110:3540–3554, 2006.

[99] W.F. Kuhs and M.S. Lehman. The structure of ice-Ih. *Water Science Reviews*, 2:1–65, 1986.

[100] T. Head-Gordon and G. Hura. Water structure from scattering experiments and simulation. *Chemical Reviews*, 102:2651–2670, 2002.

[101] T. Head-Gordon and M.E. Johnson. Tetrahedral structure or chains for liquid water. *Proceedings of the National Academy od Sciences of the United States*, 103:7973–7977, 2006.

[102] S. Myneni, Y. Luo, L.Å. Näslund, M. Cavalleri, L. Ojamäe, H. Ogasawara, A. Pelmenschikov, Ph. Wernet, P. Väterlein, C. Heske, Z. Hussain, L.G.M. Pettersson, and A. Nilsson. Spectroscopic probing of local hydrogen-bonding structures in liquid water. *Journal of Physics: Condensed Matter*, 14:L213–L219, 2002.

[103] M. Cavalleri, H. Ogasawara, L. G. M. Pettersson, and A. Nilsson. The interpretation of X-ray absorption spectra of water and ice. *Chemical Physics Letters*, 364:363–370, 2002.

[104] J.D. Smith, C.D. Cappa, B.M. Messer, W.S. Drisdell, R.C. Cohen, and R.J. Saykally. Probing the local structure of liquid water by X-ray absorption spectroscopy. *Journal of Physical Chemistry B*, 110:20038–20045, 2006.

[105] D. Prendergast and G. Galli. X-ray absorption spectra of water from first principles calculations. *Physical Review Letters*, 96:215502, 2006.

[106] R.L.C. Wang, H.J. Kreuzera, and M. Grunze. Theoretical modeling and interpretation of X-ray absorption spectra of liquid water. *Physical Chemistry Chemical Physics*, 8:4744–4751, 2006.

[107] J.T. Su, X. Xu, and W.A. Goddard III. Accurate energies and structures for large water clusters using the X3LYP hybrid density functional. *Journal of Physical Chemistry A*, 108:10518–10526, 2004.

[108] X. Xu and W.A. Goddart III. Bonding properties of the water dimer: A comparative study of density functional theories. *Journal of Physical Chemistry A*, 108:2305–2313, 2004.

[109] G.I. Csonka, A. Ruzsinszky, and J.P. Perdew. Proper gaussian gasis sets for density functional studies of water dimers and trimers. *Journal of physical chemistry. B*, 109:21471–21475, 2005.

[110] E.E. Dahlke and D.G. Truhlar. Improved density functionals for water. *Journal of Physical Chemistry B*, 109:15677–15683, 2005.

[111] M.P. Hodges, A.J. Stone, and S.S. Xantheas. Contribution of many-body terms to the energy for small water clusters: A comparison of ab initio calculations and accurate model potentials. *Journal of Physical Chemistry A*, 101:9163–9168, 1997.

[112] T. James, D.J. Wales, and J. Hernández-Rojas. Global minima for water clusters $(H_2O)_n$, $n \leq 21$, described by a five site emprical potential. *Chemical Physics Letters*, 415:302–307, 2005.

[113] S.S. Xantheas. Interaction potentials for water from accurate cluster calculations. *Structure and Bonding*, 116:119–148, 2005.

[114] D. Hankins, J.W. Moskowitz, and F.H. Stillinger. Water molecule interactions. *Journal of Chemical Physics*, 53:4544–4554, 1970.

[115] L. Ojamäe and K. Hermansson. Ab initio study of cooperativity in water chains: Binding energies and anharmonic frequencies. *Journal of Physical Chemistry*, 098:4271–4282, 1994.

[116] S.S. Xantheas. Cooperativity and hydrogen bonding network in water clusters. *Chemical Physics*, 258:225–231, 2000.

[117] W. Chen and M.S. Gordon. Energy decomposition analyses for many-body interaction and applications to water complexes. *Journal of Physical Chemistry*, 100:14316–14328, 1996.

[118] E.D. Glendening. Natural energy decomposition analysis: Extension to density functional methods and analysis of cooperative effects in water clusters. *Journal of Physical Chemistry A*, 109:11936–11940, 2005.

[119] K. Hermansson. Many-body effects in tetrahedral water clusters. *Journal of Chemical Physics*, 89:2149–2159, 1988.

[120] A. Lenz and L. Ojamäe. A theoretical study of water clusters: the relation between hydrogen-bond topology and interaction energy from quantum-chemical computations for clusters with up to 22 molecules. *Physical Chemistry Chemical Physics*, 7:1905–1911, 2005.

[121] E.E. Dahlke and D.G. Truhlar. Assessment of the pairwise additive approximation and evaluation of many-body terms for water clusters. *Journal of Physical Chemistry B*, 110:10595–10601, 2006.

[122] C.L. Perrin and J.B. Nielson. "Strong" hydrogen bonds in chemistry and biology. *Annual Reviews in Physical Chemistry*, 48:511–544, 1997.

[123] T. Malaspina, K. Coutinho, and S. Canuto. Ab initio calculation of hydrogen bonds in liquids: A sequential monte carlo quantum mechanics study of pyridine in water. *Journal of Chemical Physics*, 117:1692–1699, 2002.

[124] E.E. Fileti, K. Coutinho, T. Malaspina, and S. Canuto. Electronic changes due to thermal disorder of hydrogen bonds in liquids: pyridine in an aqueous environment. *Physical Review E*, 67:61504, 2003.

[125] R.A. Christie and K.D. Jordan. *Theory and applications of Computational Chemistry: The first forty years*, chapter Monte Carlo simulations of the finite temperature properties of $(H_2O)_6$, pages 1006–1009. Elsevier, 2005.

[126] S.P. Ju, S.H. Yang, and M.L. Liao. Study of molecular behavior in a water nanocluster: Size and temperature effect. *Journal of Physical Chemistry B*, 110:9286–9290, 2006.

[127] S. Kashtanov, A. Augustsson, Y. Luo, J.-H. Guo, C. Såthe, J.-E. Rubensson, and H. Siegbahn. Local structures of liquid water studied by X-ray emission spectroscopy. *Physical Review B*, 69:024201, 2004.

[128] A. Nillson, H. Ogasawara, M. Cavallieri, D. Nordlund, M. Nyberg, Ph. Wernet, and L.G.M. Pertterson. The hydrogen bond in ice probed by soft X-ray spectroscopy and density functional theory. *Journal of Chemical Physics*, 122:154505, 2005.

[129] P. Hunt, M. Sprik, and R. Vuilleumier. Thermal versus electronic broadening in the density of states of liquid water. *Chemical Physics Letters*, 376:68–74, 2003.

[130] P. Cabral do Couto, R.C. Guedes, and B.J. Costa Cabral. The density of states and band gap of liquid water by sequential monte carlo / quantum mechanics calculations. *Brazilian Jounal of Physics*, 34:42–47, 2004.

[131] P. Cabral do Couto, S.G. Estácio, and B.J. Costa Cabral. The kohn-sham density of states and band gap of water: From small clusters to liquid water. *Journal of Chemical Physics*, 123:054510, 2005.

[132] D. Prendergast, J.C. Grossman, and G. Galli. The electronic structure of liquid water within density-functional theory. *Journal of Chemical Physics*, 123:14501, 2005.

[133] D. Grand, A. Bernas, and E. Amouyal. Photo-ionization of aqueous indole - Conduction-band edge and energy-gap in liquid water. *Chemical Physics*, 44:73–79, 1979.

[134] T. Goulet, A. Bernas, C. Ferradini, and J.-P. Jay-Gerin. On the electronic-structure of liquid water - Conduction-band tail revealed by photoionization data. *Chemical Physics Letters*, 170:492–496, 1990.

[135] P. Delahay and K. von Burg. Photoelectron emission spectroscopy of liquid water. *Chemical Physics Letters*, 83:250–254, 1981.

[136] A. Bernas, D. Grand, and E. Amouyal. Photoionization of solutes and conduction band edge of solvents. Indole in water and alcohols. *Journal of Physical Chemistry*, 84:1259–1262, 1980.

[137] J.V. Coe. Fundamental properties of bulk water from cluster ion data. *International Reviews in Physical Chemistry*, 20:33–58, 2001.

[138] A. Bernas, C. Ferradini, and J.P. Jay-Gerin. On the electronic structure of liquid water: Facts and reflections. *Chemical Physics*, 222:151–160, 1997.

[139] E.J. Hart and M. Anbar. *The hydrated electron*. John Wiley & Sons, 1970.

[140] R.C. Weast. *CRC Handbook of chemistry and physics*. CRC Press, 1985.

[141] J.V. Coe. Connecting cluster ions and bulk aqueous solvation. A new determination of bulk single ion solvation enthalpies. *Chemical Physics Letters*, 229:161–168, 1994.

[142] P. Delahay. Photoelectron emission spectroscopy of aqueous solutions. *Accounts of Chemical Research*, 15:40–45, 1982.

[143] J. Jortner and R.M. Noyes. Some thermodynamic properties of the hydrated electron. *Journal of Physical Chemistry*, 70:770–774, 1966.

[144] D.N. Nikogosyan, A.A. Oraevsky, and V.I. Rupasov. 2-Photon ionization and dissociation of liquid water by powerful laser UV radiation. *Chemical Physics*, 77:131–143.

[145] P. Han and D.M. Bartels. Hydrogen/deuterium isotope effects in water radiolysis. 2. Dissociation of electronically excited water. *Journal of Physical Chemistry*, 94:5824–5833, 1990.

[146] A. Bernas and D. Grand. On the so-called ionization potential of water and associated liquids. *Journal of Physical Chemistry*, 98:3440–3443, 1994.

[147] A. Bernas, C. Ferradini, and J.P. Jay-Gerin. On apparent contradictions in some photophysical properties of liquid water. *Journal of Photochemistry and Photobiology A: Chemistry*, 117:171–173, 1998.

[148] P. Politzer and F. Abu-Awwad. A comparative analysis of Hartree-Fock and Kohn-Sham orbital energies. *Theoretical Chemistry Accounts*, 99:83–87, 1998.

[149] F. Abu-Awwad and P. Politzer. Variation of parameters in Becke-3 hybrid exchange-correlation functional. *Journal of Computational Chemistry*, 21:227–238, 2000.

[150] H.D. Cochran Jr., P.T. Cummings, D.A. Dixon, J.T. Golab, G.S. Heffelfinger, B.K. Peterson, A. Redondo, T.B. Thompson, and P.R. Westmoreland. Chemical industry of the future: Technology roadmap for computational chemistry. Technical report, available from the Chemical Industry Vision2020 Technology Partnership at: http://www.chemicalvision2020.org, 1999.

[151] V. I. Minkin. Glossary of terms used in theoretical organic chemistry. *Pure and Applied Chemistry*, 71:1919–1981, 1999.

[152] J.A. Pople. Nobel lecture: Quantum chemical models. *Angewandte Chemie International Edition*, 38:1894–1902, 1999.

[153] M.J. Frisch, G.W. Trucks, H.B. Schlegel, G.E. Scuseria, M.A. Robb, J.R. Cheeseman, Jr. J.A. Montgomery, T. Vreven, K.N. Kudin, J.C. Burant, J.M. Millam, S.S. Iyengar, J. Tomasi, V. Barone, B. Mennucci, M. Cossi, G. Scalmani, N. Rega, G. A. Petersson, H. Nakatsuji, M. Hada, M. Ehara, K. Toyota, R. Fukuda, J. Hasegawa, M. Ishida, T. Nakajima, Y. Honda, O. Kitao, H. Nakai, M. Klene, X. Li, J.E. Knox, H.P. Hratchian, J.B. Cross, V. Bakken, C. Adamo, J. Jaramillo, R. Gomperts, R.E. Stratmann, O. Yazyev, A.J. Austin, R. Cammi, C. Pomelli, J.W. Ochterski, P.Y. Ayala, K. Morokuma, G.A. Voth, P. Salvador, J.J. Dannenberg, V.G. Zakrzewski, S. Dapprich, A.D. Daniels, M.C. Strain, O. Farkas, D.K. Malick, A.D. Rabuck, K. Raghavachari, J.B. Foresman, J.V. Ortiz, Q. Cui, A.G. Baboul,

S. Clifford, J. Cioslowski, B.B. Stefanov, G. Liu, A. Liashenko, P. Piskorz, I. Komaromi, R.L. Martin, D.J. Fox, T. Keith, M.A. Al-Laham, C.Y. Peng, A. Nanayakkara, M. Challacombe, P.M.W. Gill, B. Johnson, W. Chen, M.W. Wong, C. Gonzalez, and J.A. Pople. Gaussian 03, Revision C.03. Gaussian, Inc., Wallingford, CT, 2004.

[154] K. Coutinho and S. Canuto. Dice (version 2.8): A general monte carlo program for liquid simulation. University of Sã̃o Paulo, Sã̃o Paulo, Brazil, 2002.

[155] F. Jensen. *Introduction to computational chemistry.* John Wiley & Sons, 1999.

[156] E.G. Lewars. *Computational chemistry: Introduction to the theory and applications of molecular and quantum mechanics.* Springer, 2003.

[157] C.J. Cramer. *Essentials of computational chemistry: Theories and models.* John Wiley & Sons, 2004.

[158] D.C. Young. *Computational chemistry: a practical guide for applying techniques to real world problems.* John Wiley & Sons, 2001.

[159] A. Szabó and N.S. Ostlund. *Modern quantum chemistry: Introduction to advanced electronic structure theory.* Dover, 1996.

[160] T. Helgaker, P. Jørgensen, and J. Olsen. *Molecular electronic-structure theory.* Wiley, 2000.

[161] R.G. Parr and W. Yang. *Density-Functional theory of atoms and molecules.* Oxford University Press, 1989.

[162] W. Koch and M.C. Holthausen. *A chemist's guide to density functional theory.* John Wiley & Sons, 2001.

[163] D. Frenkel and B. Smit. *Understanding molecular simulation: From algorithms to applications.* Academic Press, 2002.

[164] M.P. Allen and D.J. Tildesley. *Computer simulation of liquids.* Oxford University Press, 1987.

[165] C.E. Dykstra, G. Frenking, K.S. Kim, and G.E. Scuseria, editors. *Theory and applications of Computational Chemistry: The first forty years.* Elsevier, 2005.

[166] M. Alcamí, O. Mó, and M. Yanez. Computational chemistry: A useful (sometimes mandatory) tool in mass spectrometry studies. *Mass Spectrometry Reviews*, 20:195–245, 2001.

[167] Y. Feng, L. Liu, J.T. Wang, H. Huang, and Q.X. Guo. Assessment of experimental bond dissociation energies using composite ab initio methods and evaluation of the performances of density functional methods in the calculation of bond dissociation energies. *Journal of Chemical Information and Computer Sciences*, 43:2005–2013, 2003.

[168] W. Kohn. Nobel Lecture: Electronic structure of matter - wave functions and density functionals. *Reviews of Modern Physics*, 71:1253–1266, 1999.

[169] M. Born and R. Oppenheimer. Zur Quantentheorie der Molekeln. *Annalen der Physik*, 84:457–484, 1927.

[170] J.C. Tully. Perspective on "Zur Quantentheorie der Molekeln". *Theoretical Chemistry Accounts*, 103:173–176, 2000.

[171] H.P. Hratchian and H.B. Schlegel. *Theory and applications of computational chemistry: The first forty years*, chapter Finding minima, transition states, and following reaction pathways on ab initio potential energy surfaces, pages 195–249. Elsevier, 2005.

[172] F. Jensen. An introduction to the state of the art in quantum chemistry. *Annual Reports in Computational Chemistry*, 1:3–17, 2005.

[173] J.C. Slater. The theory of complex spectra. *Physical Review*, 34:1293–1322, 1929.

[174] J.C. Slater. Molecular energy levels and valence bonds. *Physical Review*, 38:1109–1144, 1931.

[175] P.A.M. Dirac. *Principles of quantum mechanics*. Clarendon Press, 1958.

[176] J.K.L. MacDonald. Successive approximations by the Rayleigh-Ritz variation method. *Physical Review*, 43:830–833, 1933.

[177] D.R. Hartree. The wave mechanics of an atom with a non-Coulomb central field. Part I. Theory and methods. *Proceedings Cambridge Philosophical Society*, 24:89–110, 1928.

[178] D.R. Hartree. The wave mechanics of an atom with a non-Coulomb central field. Part II. Some results and discussion. *Proceedings Cambridge Philosophical Society*, 24:111–132, 1928.

[179] V.A. Fock. Näherungsmethode zur Lösung des quantenmechanischen Mehrkörperproblems. *Zeitschrift für Physik A Hadrons and Nuclei*, 61:126–148, 1930.

[180] J.C. Slater. Note on Hartree's method. *Physical Review*, 35:210–211, 1930.

[181] T. Koopmans. The distribution of wave function and characteristic value among the individual electrons of an atom. *Physica*, 1:104–113, 1933.

[182] Z.B. Maksic and R. Vianello. How good Is Koopmans' approximation? G2 (MP2) Study of the vertical and adiabatic ionization potentials of some small molecules. *Journal of Physical Chemistry A*, 106:6515–6520, 2002.

[183] J. Kobus. Diatomic molecules: Exact solutions of HF equations. *Advances in Quantum Chemistry*, 28:1–14, 1997.

[184] C. Zener. Analytic atomic wave functions. *Physical Review*, 36:51–56, 1930.

[185] J.C. Slater. Atomic shielding constants. *Physical Review*, 36:57–64, 1930.

[186] S.F. Boys. Electronic wave functions. I. A general method of calculation for the stationary states of any molecular system. *Proceedings of the Royal Society of London A*, 200:542–554, 1950.

[187] T. H. Dunning Jr. Gaussian basis functions for use in molecular calculations. I. Contraction of (9s5p) atomic basis sets for the first-row atoms. *The Journal of Chemical Physics*, 53:2823–2833, 1970.

[188] R. Krishnan, J.S. Binkley, R. Seeger, and J.A. Pople. Self-consistent molecular-orbital methods 20 Basis set for correlated wave-functions. *The Journal of Chemical Physics*, 72:650–654, 1980.

[189] T.H. Dunning Jr. Gaussian basis sets for use in correlated molecular calculations. I. The atoms boron through neon and hydrogen. *The Journal of Chemical Physics*, 90:1007–1023, 1989.

[190] M.J. Frisch, J.A. Pople, and J.S. Binkley. Self-consistent molecular orbital methods 25. Supplementary functions for Gaussian basis sets. *The Journal of Chemical Physics*, 80:3265–3269, 1984.

[191] R.A. Kendall, T.H. Dunning Jr, and R.J. Harrison. Electron affinities of the first-row atoms revisited. Systematic basis sets and wave functions. *The Journal of Chemical Physics*, 96:6796–6806, 1992.

[192] T. Clark, J. Chandrasekhar, G.W. Spitznagel, and P.V. Schleyer. Efficient diffuse function - augmented basis-sets for anion calculations .3. The 3-21+G basis set for 1st-row elements, Li-F. *Journal of Computational Chemistry*, 4:294–301, 1983.

[193] E.R. Davidson and D. Feller. Basis set selection for molecular calculations. *Chemical Reviews*, 86:681–696, 1986.

[194] J. Almlof, T. Helgaker, and P.R. Taylor. Gaussian basis sets for high-quality ab initio calculations. *The Journal of Physical Chemistry*, 92:3029–3033, 1988.

[195] K.L. Schuchardt, B.T. Didier, T. Elsethagen, L. Sun, V. Gurumoorthi, J. Chase, J. Li, and T.L. Windus. Basis set exchange: A community database for computational sciences. *Journal of Chemical Information and Modelling*, 47:1045–1052, 2007. Basis Set Exchange: v1.0 beta, available at https://bse.pnl.gov/bse/portal.

[196] C.C.J. Roothaan. New developments in molecular orbital theory. *Reviews of Modern Physics*, 23:69–89, 1951.

[197] G.G. Hall. The molecular orbital theory of chemical valency. VIII. A method of calculating ionization potentials. *Proceedings of the Royal Society of London A*, 205:541–552, 1951.

[198] M.C. Zerner. Perspective on "New developments in molecular orbital theory". *Theoretical Chemistry Accounts*, 103:217–218, 2000.

[199] J.A. Pople. Self-Consistent orbitals for radicals. *Journal of Chemical Physics*, 22:571–572, 1954.

[200] F. Jensen. Estimating the Hartree-Fock limit from finite basis set calculations. *Theoretical Chemistry Accounts*, 113:267–273, 2005.

[201] P.O. Löwdin. Correlation problem in many-electron quantum mechanics .1. Review of different approaches and discussion of some current ideas. *Advances in Chemical Physics*, 2:207–322, 1959.

[202] P.E.M. Siegbahn. *Methods in computational molecular physics*, chapter The direct CI method, pages 189–207. Dordrecht, 1983.

[203] B.O. Roos. *Theory and applications of computational chemistry: The first forty years*, chapter Multiconfigurational quantum chemistry, pages 725–764. Elsevier, 2005.

[204] C.D. Sherrill. Bond breaking in quantum chemistry. *Annual Reports in Computational Chemistry*, 1:45–56, 2005.

[205] S.F. Boys. Electronic wave functions. II. A calculation for the ground state of the beryllium atom. *Proceedings of the Royal Society of London A*, 201:125–137, 1950.

[206] J.A. Pople, J.S. Binkley, and R. Seeger. Theoretical models incorporating electron correlation. *International Journal of Quantum Chemistry*, Suppl Y-10:1–19, 1976.

[207] K. Raghavachari and J.A. Pople. Calculation of one-electron properties using limited configuration interaction techniques. *International Journal of Quantum Chemistry*, 20:1067–1071, 1981.

[208] J.A. Pople, M. Head-Gordon, and K. Raghavachari. Quadratic configuration interaction. A general technique for determining electron correlation energies. *The Journal of Chemical Physics*, 87:5968–5975, 1987.

[209] I. Shavitt. The history and evolution of configuration interaction. *Molecular Physics*, 94:3–17, 1998.

[210] J. Čížek. On the correlation problem in atomic and molecular systems. Calculation of wavefunction components in Ursell-type expansion using quantum-field theoretical methods. *The Journal of Chemical Physics*, 45:4256–4266, 1966.

[211] G.D. Purvis and R.J. Bartlett. A full coupled-cluster singles and doubles model: The inclusion of disconnected triples. *The Journal of Chemical Physics*, 76:1910–1918, 1982.

[212] J. Paldus. *Theory and applications of computational chemistry: The first forty years*, chapter The beginnings of coupled-cluster theory: An eyewitness account, pages 115–147. Elsevier, 2005.

[213] R.J. Bartlett. *Theory and applications of computational chemistry: The first forty years*, chapter How and why coupled-cluster theory became the preeminent method in an ab into quantum chemistry, pages 1191–1221. Elsevier, 2005.

[214] C. Møller and M.S. Plesset. Note on an approximation treatment for many-electron systems. *Physical Review*, 46:618–622, 1934.

[215] J.S. Binkley and J.A. Pople. Møller-Plesset theory for atomic ground-state energies. *International Journal of Quantum Chemistry*, 9:229–236, 1975.

[216] J. Olsen, O. Christiansen, H. Koch, and P. Jørgensen. Surprising cases of divergent behavior in Møller–Plesset perturbation theory. *The Journal of Chemical Physics*, 105:5082–5090, 1996.

[217] M.L. Leininger, W.D. Allen, and H.F. Schaefer III. Is Møller-Plesset perturbation theory a convergent ab initio method? *The Journal of Chemical Physics*, 112:9213–9222, 2000.

[218] T. Müller. Basis sets, accuracy, and calibration in quantum chemistry. In *Computational NanoScience: Do it Yourself!*, volume 31 of *NIC Series*, pages 19–43. John von Neumann Institute for Computing, Jülich, 2006.

[219] P. Hohenberg and W. Kohn. Inhomogeneous Electron Gas. *Physical Review*, 136:B864–B871, 1964.

[220] W. Kohn and L.J. Sham. Self-Consistent equations including exchange and correlation effects. *Physical Review*, 140:1133–1138, 1965.

[221] J.P. Perdew, R.G. Parr, M. Levy, and J.L. Balduz Jr. Density-Functional theory for fractional particle number: Derivative discontinuities of the energy. *Physical Review Letters*, 49:1691–1694, 1982.

[222] J.C. Slater. A simplification of the Hartree-Fock method. *Physical Review*, 81:385–390, 1951.

[223] S.H Vosko, L. Wilk, and M. Nusair. Accurate spin-dependent electron liquid correlation energies for local spin density calculations: a critical analysis. *Canadian Journal of Physics*, Canadian Journal of Physics:1200–1211, 1980.

[224] A.D. Becke. Density-functional exchange-energy approximation with correct asymptotic behavior. *Physical Review A*, 38:3098–3100, 1988.

[225] J.P. Perdew. Density-functional approximation for the correlation energy of the inhomogeneous electron gas. *Physical Review B*, 33:8822–8824, 1986.

[226] J.P. Perdew and Y. Wang. Accurate and simple analytic representation of the electron-gas correlation energy. *Physical Review B*, 45:13244–13249, 1992.

[227] C. Lee, W. Yang R.G., and Parr. Development of the Colle-Salvetti correlation-energy formula into a functional of the electron density. *Physical Review B*, 37:785–789, 1988.

[228] J. Harris. Adiabatic-connection approach to Kohn-Sham theory. *Physical Review A*, 29:1648–1659, 1984.

[229] A.D. Becke. A new mixing of Hartree–Fock and local density-functional theories. *The Journal of Chemical Physics*, 98:1372–1377, 1993.

[230] A.D. Becke. Density-functional thermochemistry. III. The role of exact exchange. *The Journal of Chemical Physics*, 98:1993–, 1993.

[231] K. Rhaghavachari. Perspective on "Density functional thermochemistry. III. The role of exact exchange". *Theoretical Chemistry Accounts*, 103:361–363, 2000.

[232] K. Burke, M. Ernzerhof, and J.P. Perdew. The adiabatic connection Mmethod: A non-empirical hybrid. *Chemical Physics Letters*, 265:115–120, 1997.

[233] C. Adamo and V. Barone. Exchange functionals with improved long-range behavior and adiabatic connection methods without adjustable parameters: The mPW and mPW1PW models. *The Journal of Chemical Physics*, 108:664–675, 1998.

[234] M. Sodupe, J. Bertran, L. Rodríguez-Satiago, and E.J. Baerends. Ground State of the $(H_2O)_2^+$ Radical Cation: DFT versus Post-Hartree-Fock Methods. *Journal of Physical Chemistry A*, 105:166–170, 1999.

[235] J. Poater, M. Duran, and M. Solà. Parametrization of the Becke3-LYP hybrid functional for a series of small molecules using quantum molecular similarity techniques. *Journal of Computational Chemistry*, 22:1666–1678, 2001.

[236] R.D. Johnson III Editor. NIST Computational Chemistry Comparison and Benchmark Database, NIST standard reference database number 101. http://srdata.nist.gov/cccbdb, August 2005.

[237] J.B. Foresman, M. Head-Gordon, J.A. Pople, and M.J. Frisch. Toward a systematic molecular orbital theory for excited states. *The Journal of Physical Chemistry*, 96:135–149, 1992.

[238] M. Head-Gordon, M. Oumi, and D. Maurice. Quasidegenerate second-order perturbation corrections to single excitation configuration interaction. *Molecular Physics*, 96:593–602, 1999.

[239] A. Dreuw M. and Head-Gordon. Single-reference ab initio methods for the calculation of excited states of large molecules. *Chemical Reviews*, 105:4009–4037, 2005.

[240] S. Hirata, M. Head-Gordon, and R.J. Bartlett. Configuration interaction singles, time-dependent Hartree-Fock, and time-dependent density functional theory for the electronic excited states of extended systems. *Journal of Chemical Physics*, 108:10774–10786, 1999.

[241] K.B. Wiberg, Y. Wang, A.E. de Oliveira, S.A. Perera, and P.H. Vaccaro. Comparison of CIS-and EOM-CCSD-calculated adiabatic excited-state structures. Changes in charge density on going to adiabatic excited states. *Journal of Physical Chemistry A*, 109:466–477, 2005.

[242] E. Runge and E.K.U. Gross. Density-Functional theory for time-dependent systems. *Physical Review Letters*, 52:999–1000, 1984.

[243] M.E. Casida, C. Jamorski, K.C. Casida, and D.R. Salahub. Molecular excitation energies to high-lying bound states from time-dependent density-functional response theory: Characterization and correction of the time-dependent local density approximation ionization threshold. *Journal of Chemical Physics*, 108:4439–4449, 1998.

[244] A. Dreuw, J.L Weisman, and M. Head-Gordon. Long-range charge-transfer excited states in time-dependent density functional theory require non-local exchange. *The Journal of Chemical Physics*, 119:2943–2946, 2003.

[245] M.W. Mahoney and W.L. Jorgensen. A five-site model for liquid water and the reproduction of the density anomaly by rigid, nonpolarizable potential functions. *Journal of Chemical Physics*, 112:8910–8922, 2000.

[246] M.J. McGrath, J.I. Siepmann, I-F.W. Kuo, C.J. Mundy, J. VandeVondele, J. Hutter, F. Mohamed, and M. Krack. Isobaric-isothermal monte carlo simulations from first-principles: Application to liquid water at ambient conditions. *ChemPhysChem*, 6:1849–1901, 2005.

[247] H. J. C. Berendsen, J. R. Grigera, and T. P. Straatsma. The Missing Term in Effective Pair Potentials. *Journal of Physical Chemistry*, 91:6269–6271, 1987.

[248] G. S. Fanourgakis and S. S. Xantheas. The bend angle of Water in Ice Ih and Liquid Water: The significance of implementing the nonlinear monomer dipole moment surface in classical interaction potentials. *Journal of Chemical Physics*, 124:174504, 2006.

[249] T. A. Halgren and W. Damm. Polarizable Force Fields. *Current Opinion in Structural Biology*, 11:236–242, 2001.

[250] H. Yu and W. F. van Gunsteren. Accounting for Polarization in Molecular Simulation. *Computer Physics Communications*, 172:69–85, 2005.

[251] A. Wallqvist and B. J. Berne. Effective Potentials for Liquid Water Using Polarizable and Nonpolarizable Models. *Journal of Physical Chemistry*, 97:13841–13851, 1993.

[252] T. M. Nymand, P. Linse, and P.-O. Åstrand. A comparison of Effective and Polarizable Intermolecular Potentials in Simulations: Liquid Water as a Test Case. *Molecular Physics*, 99:335–348, 2001.

[253] M. W. Mahoney and W. L. Jorgensen. Quantum, Intramolecular Flexibility, and Polarizability Effects on the Reproduction of the Density Anomaly of Liquid Water by Simple Potential Functions. *Journal of Chemical Physics*, 115:10758–10768, 2001.

[254] J. Zielkiewicz. Structural Properties of Water: Comparison of the SPC, SPCE, TIP4P, and TIP5P Models of Water. *Journal of Chemical Physics*, 123:104501, 2005.

[255] K. Coutinho and S. Canuto. Solvent effects from a sequential monte-carlo - quantum mechanical approach. *Advances in Quantum Chemistry*, 28:89–105, 1997.

[256] K. Coutinho, M.J. de Oliveira, and S. Canuto. Sampling configurations in monte carlo simulations for quantum mechanical studies of solvent effects. *International Journal of Quantum Chemistry*, 66:249–253, 1998.

[257] K.S. Kim, H.S. Kim, J.H. Jang, H.S. Kim, B.-J. Mhin, Y. Xie, and H.F. Schaefer III. Hydrogen bonding between the water molecule and the hydroxyl radical ($H_2O{\cdot}OH$): The $^2A''$ and $^2A'$ minima. *Journal of Chemical Physics*, 94:2057–2062, 1991.

[258] Y. Xie and H.F. Schaefer III. Hydrogen bonding between the water molecule and the hydroxyl radical ($H_2O{\cdot}HO$): The global minimum. *Journal of Chemical Physics*, 98:8829–8834, 1993.

[259] B. Wang, H. Hou, and Y. Gu. Density functional study of the hydrogen bonding: $H_2O{\cdot}HO$. *Chemical Physics Letters*, 303:96–100, 1999.

[260] Z. Zhou, Y. Qu, A. Fu, B. Du, F. He, and H. Gao. Density functional complete study of hydrogen bonding between the water molecule and the hydroxyl radical ($H_2O{\cdot}HO$). *International Journal of Quantum Chemistry*, 89:550–558, 2002.

[261] S. Hamad, S. Lago, and J.A. Mejías. A computational study of the hydration of the OH radical. *Journal of Physical Chemistry A*, 106:9104–9113, 2002.

[262] H.J.C. Berendsen, J.P.M. Postma, W.F. van Gunsteren, and J. Hermans. *Intermolecular forces*, page 133. Dordrecht, 1981.

[263] S.D Belair, J.S. Francisco, and S.J. Singer. Hydrogen bonding in cubic $(H_2O)_8$ and $OH(H_2O)_7$ clusters. *Physical Review A*, 71:13204, 2005.

[264] T. Autrey, A.K. Brown, D.M. Camaioni, M. Dupuis, N.S. Foster, and A. Getty. Thermochemistry of aqueous hydroxyl radical from advances in photoacoustic calorimetry and ab initio continuum solvation theory. *Journal of the American Chemical Society*, 126:3680–3681, 2004.

[265] M.G. Campo and J.R. Grigera. Classical molecular-dynamics simulation of the hydroxyl radical in water. *The Journal of Chemical Physics*, 123:084507, 2005.

[266] P. Vassilev, M.J. Louwerse, and E.J. Baerends. Ab initio molecular dynamics simulation of the OH radical dot radical in liquid water. *Chemical Physics Letters*, 398:212–216, 2004.

[267] J.M Khalack and A.P. Lyubartsev. Solvation structure of hydroxyl radical by Car-Parrinello molecular dynamics. *Journal of Physical Chemistry A*, 109:378–386, 2005.

[268] J. VandeVondele, M. Sprik, and S. Matter. A molecular dynamics study of the hydroxyl radical in solution applying self-interaction-corrected density functional methods. *Physical Chemistry Chemical Physics*, 7:1363–1367, 2005.

[269] P. Vassilev, M.J. Louwerse, and E.J. Baerends. Hydroxyl radical and hydroxide ion in liquid Water: A comparative electron density functional theory study. *Journal of Physical Chemistry B*, 109:23605–23610, 2005.

[270] M. Boero, K Terakura, T. Ikeshoji, C.C. Liew, and M. Parrinello. Water at supercritical conditions: A first principles study. *Journal of Chemical Physics*, 115:2219–2227, 2001.

[271] Y.V. Novakovskaya and N.F. Stepanov. Structure and energy of the positively ionized water clusters. *International Journal of Quantum Chemistry*, 61:981–990, 1997.

[272] Y.V. Novakovskaya and N.F. Stepanov. Small charged water clusters: Cations. *Journal of Physical Chemistry A*, 103:3285–3288, 1999.

[273] R.N. Barnett and U. Landman. Structure and energetics of ionized water clusters: $(H_2O)_n^+$, $n = 2 - 5$. *Journal of Physical Chemistry A*, 101:164–169, 1997.

[274] H. Tachikawa. Ionization dynamics of the small-sized water clusters: A direct ab initio trajectory study. *Journal of Physical Chemistry A*, 108:7853–7862, 2004.

[275] J. Kim, S.B. Suh, and K.S. Kim. Water dimer to pentamer with an excess electron: Ab initio study. *The Journal of Chemical Physics*, 111:10077–10087, 1999.

[276] T. Tsurusawa and S. Iwata. Theoretical studies of the water-cluster anions containing the OH {e} HO structure: energies and harmonic frequencies. *Chemical Physics Letters*, 315:433–440, 2000.

[277] J.M. Herbert and M. Head-Gordon. Charge penetration and the origin of large O−H vibrational red-shifts in hydrated-electron clusters,$(H_2O)_n^-$. *Journal of the American Chemical Society*, 128:13932–13939, 2006.

[278] J.M. Herbert and M. Head-Gordon. First-principles, quantum-mechanical simulations of electron solvation by a water cluster. *Proceedings of the National Academy of Sciences*, 103:14282–14287, 2006.

[279] H. Tachikawa. Electron hydration dynamics in water clusters: A direct ab initio molecular dynamics approach. *The Journal of Chemical Physics*, 125:144307, 2006.

[280] D.M. Chipman. Excited electronic states of small water clusters. *The Journal of Chemical Physics*, 122:044111, 2005.

[281] D.M. Chipman. Stretching of hydrogen-bonded OH in the lowest singlet excited electronic state of water dimer. *The Journal of Chemical Physics*, 124:044305, 2006.

[282] A.L. Sobolewski, W. Domcke, and S. Matter. Hydrated hydronium: a cluster model of the solvated electron? *Physical Chemistry Chemical Physics*, 4:4–10, 2002.

[283] A.L. Sobolewski and W. Domcke. Ab initio investigation of the structure and spectroscopy of hydronium-water clusters. *Journal of Physical Chemistry A*, 106:4158–4167, 2002.